ISTANBUL TECHNICAL UNIVERSITY ★ GRADUATE SCHOOL OF SCIENCE ENGINEERING AND TECHNOLOGY

INTEGRATION OF NAVIGATION SYSTEMS AND IDENTIFICATION OF NONLINEAR MODEL PARAMETERS FOR AUTONOMOUS UNDERWATER VEHICLES IN THE PRESENCE OF MEASUREMENT BIASES

Ph.D. THESIS

Mustafa DİNÇ

Department of Aeronautical and Astronautical Engineering

Aeronautical and Astronautical Engineering Programme

JANUARY 2013

ISTANBUL TECHNICAL UNIVERSITY ★ GRADUATE SCHOOL OF SCIENCE ENGINEERING AND TECHNOLOGY

INTEGRATION OF NAVIGATION SYSTEMS AND IDENTIFICATION OF NONLINEAR MODEL PARAMETERS FOR AUTONOMOUS UNDERWATER VEHICLES IN THE PRESENCE OF MEASUREMENT BIASES

Ph.D. THESIS

Mustafa DİNÇ
(511052011)

Department of Aeronautical and Astronautical Engineering

Aeronautical and Astronautical Engineering Programme

Thesis Advisor: Prof. Dr. Çingiz HACIYEV

JANUARY 2013

İSTANBUL TEKNİK ÜNİVERSİTESİ ★ FEN BİLİMLERİ ENSTİTÜSÜ

İNSANSIZ SUALTI ARAÇLARI İÇİN SEYRÜSEFER SİSTEMLERİNİN TÜMLEŞTİRİLMESİ VE ÖLÇÜM KAYNAKLI KAYMA HATALARININ OLDUĞU DURUMDA NONLİNEER HAREKET MODELİN PARAMETRELERİNİN TANILAMASI

DOKTORA TEZİ

Mustafa DİNÇ
(511052011)

Uçak ve Uzay Mühendisliği Anabilim Dalı

Uçak ve Uzay Mühendisliği Programı

Tez Danışmanı: Prof. Dr. Çingiz HACIYEV

OCAK 2013

Mustafa DİNÇ, a **Ph.D.** student of ITU **Graduate School of Science, Engineering and Technology** student ID 511052011**,** successfully defended the **thesis** entitled "**Integration of Navigation Systems and Identification of Nonlinear Model Parameters for Autonomous Underwater Vehicles in the Presence of Measurement Biases**", which he prepared after fulfilling the requirements specified in the associated legislations, before the jury whose signatures are below.

Thesis Advisor :	**Prof. Dr. Çingiz HACİYEV** İstanbul Technical University	....
Jury Members :	**Prof.Dr. İbrahim ÖZKOL** İstanbul Technical University	....
	Prof.Dr. Muammer KALYON İstanbul Commerce University	....
	Prof.Dr. Ömer GÖREN İstanbul Technical University	....
	Doç.Dr. Ali Can TAKİNACI İstanbul Technical University	....

Date of Submission : October 12, 2012
Date of Defense : January 18, 2013

To my family,

FOREWORD

I would like to express my deepest appreciation to my supervisor, Prof. Chingiz HACIYEV, Ph.D., who gave me valuable advices and support in this Ph.D. program.

Additionally, I would like to thank to my thesis committee: Prof. İbrahim ÖZKOL, Ph.D., and Prof. Muammer KALYON, Ph.D., for their valuable comments and guidance. This work is supported by ITU Institute of Science and Technology.

I would like to express my special thanks to my family: my wife and daughter, for their valuable support and patience.

Finally, I sincerely commemorate the memory of Prof. Yücel ODABAŞI, Ph.D., whom I would like to express my special thanks for giving me the opportunity to share his deep knowledge and the best available information regarding Autonomous Underwater Vehicle (AUV) modeling.

October 2012

Mustafa DİNÇ
(Computer Engineer, M.Sc.)

TABLE OF CONTENTS

Page

ABBREVIATIONS

App	**:** Appendix
AUV	**:** Autonomous Underwater Vehicle
CB	**:** Center of Buoyancy
CFD	**:** Computational Fluid Dynamics
CG	**:** Center of Gravity
DOF	**:** Degree of Freedom
DVL	**:** Doppler Velocity Log
EOM	**:** Equations of Motion
EKF	**:** Extended Kalman Filter
FOG	**:** Fiber-Optic Gyro
GPS	**:** Global Positioning System
GRV	**:** Gaussian Random Variable
IMU	**:** Inertial Measurement Unit
INS	**:** Inertial Navigation System
KF	**:** Kalman Filter
LSE	**:** Least Square Estimation
MEMS	**:** Micro Electro-Mechanical System
PLBL	**:** Pseudo Long Base Line
PPM	**:** Part Per Million
ROV	**:** Remotely Operated Vehicle
RLG	**:** Ring Laser Gyro
SINS	**:** Strap-down INS
SMC	**:** Sliding Mode Control
UAV	**:** Unmanned Air Vehicle
UUV	**:** Unmanned Underwater Vehicle
WGS-84	**:** World Geodetic System 1984

LIST OF TABLES

Page

LIST OF FIGURES

Page

INTEGRATION OF NAVIGATION SYSTEMS AND IDENTIFICATION OF NONLINEAR MODEL PARAMETERS FOR AUTONOMOUS UNDERWATER VEHICLES IN THE PRESENCE OF MEASUREMENT BIASES

SUMMARY

The research on underwater systems has gained enormous attention during the last two decades because of applications taking place in many fields. Therefore, the significant number of Unmanned Underwater Vehicles (UUVs) has been developed for solving the wide range of scientific and applied tasks of ocean research and development in the world. Guidance, navigation, and control techniques are key research and development areas for the success of those sophisticated UUV missions.

Autonomous Underwater Vehicle (AUV), a type of UUV, requires a precise navigational system for localization, positioning, path tracking, guidance, and control. In order to develop a robust and precise AUV navigation system, we need to know an overall modeling of an AUV, which is a complex problem and involves interdisciplinary studies of kinematic, hydrostatics, and hydrodynamics.

One of the main objective of this thesis is to provides detailed explanations on the theory behind the main concepts that directly influence the design of the dynamic mathematical model of AUV and then to accomplish dynamic mathematical modeling of an AUV in MATLAB Simulink environment under different swimming conditions. Based on this model we develop three different types of low-cost Integrated Navigation System based on error models of Inertial Navigation System (INS) and its aiding devices such as Doppler Velocity Log (DVL), compass, and a Pressure Depth Sensor. An INS error model and the corresponding measurement models of those aiding sources will be derived for the Kalman Filter (KF). The simulation results confirmed that low-cost IMU sensors produce a notable amount of noisy measurements but our Integrated Navigation System models for AUV based on KF can effectively mitigate those drawbacks.

Another main focus of this thesis is to accomplish the parameter identification of hydrodynamic coefficients of AUV based on a Least Square Estimation (LSE) algorithm in the presence of measurement biases. Parameter Identification is very important to have the estimated values of these coefficients in order to accurately simulate the AUV's dynamic performance. The estimated hydrodynamic coefficients can be used as inputs not only for a mathematical model to analyze the maneuvering performance but also for a controller model to design AUVs under development.

İNSANSIZ SUALTI ARAÇLARI İÇİN SEYRÜSEFER SİSTEMLERİNİN TÜMLEŞTİRİLMESİ VE ÖLÇÜM KAYNAKLI KAYMA HATALARININ OLDUĞU DURUMDA NONLİNEER MODELİN PARAMETRELERİNİN TANILAMASI

ÖZET

Dünyada son yirmi yıllık gelişmeler dikkate alındığında, sualtı sistemlerinin farklı uygulamalarına yönelik araştırmalar muazzam şekilde artış göstermiştir. Bu kapsamda, geniş çaplı kullanım alanı olan, okyanus ve deniz tabanı araştırma/geliştirme faaliyetlerine yönelik çok sayıda İnsansız Sualtı Aracı (İSA) tasarlanarak, hizmete sunulmuştur. İSA'ların gerçekleştirdiği görevler dikkate alındığında, askerî ve sivil uygulamaları ön plana çıkmaktadır.

Tipik olarak sualtı araçları üç ana grupta incelenmektedir;

1. İnsanlı Sualtı Sistemleri (Denizaltılar, İnsanlı Sualtı Robotları, vb.),
2. Uzaktan Kumandalı Sualtı Robotları (ROV'lar) ve
3. Otonom Sualtı Araçları (OSA -AUV).

Yukarıda adı geçen her bir tip sualtı aracının kendine has özellikleri olmasının yanında, birbirleriyle kıyaslandığında kullanım alanlarına bağlı olarak üstünlükleri ve zafiyetleri mevcuttur. Bu tez kapsamında sadece insansız sualtı araçlarının özellikleri hakkında bilgi verilmiştir. Kavram olarak, insansız sistemler olan ROV'lar ile İSA'lar arasındaki temel fark kısaca ifade etmek gerekirse, ROV'lar bir suüstü gemisine veya denizaltıya bir kablo yardımıyla bağlı olup, bu platformlar üzerinden kumanda edilebilen genellikle dikdörtgenler prizması veya küp şeklinde tasarlanmış düşük süratli, hantal sualtı araçlardır. Diğer taraftan OSA'lar, genellikle bir platformdan tamamen bağımsız kendi başına hareket edebilen, silindirik yapılı, askeri ve sivil kullanım alanlarına bağlı olarak farklı süratlere sahip, otonom sualtı araçlarıdır. İSA'ların dünyadaki farklı uygulama alanlarını aşağıdaki şekilde sıralayabiliriz.

- Mayın avlama,
- Keşif,
- Sualtı kablolarının döşenmesi,
- Sualtı hedeflerine ekipman taşınması,
- Deniz ve okyanus suyu incelemeleri,
- Petrol ve doğalgaz boruları gözlem ve bakımı,
- Sualtı arkeoloji çalışmaları,

- Deprem araştırmaları,
- Torpido sistemleri.

Türkiye'de mevcut olan insansız araçları incelendiğinde, çalışmaların büyük bir çoğunluğunu insansız kara araçlarını kapsamaktadır. Kara araçlarından sonra, ikinci seviyede araştırmalar hava araçları üzerine yoğunlaşmaktadır. Ülkemizin üç tarafı denizlerle çevrili olmasına ve halâ bir denizci millet olamamamızın bir sonucu olarak, Türkiye'de İnsansız Sualtı Araçları (İSA'lar) birkaç istisna proje dışında, bir inceleme konusu olarak istenilen rağbeti ve ilgiyi görmemektedir. Çok farklı kullanım alanları olan bu araçlar, dünyada son yirmi yıldır başta ABD olmak üzere gelişmiş ülkeler tarafından okyanus araştırmalarında yoğun olarak kullanılmaktadır.

OSA`lar, sualtında gerçekleştirdikleri uzun süreli seyirleri boyunca güdüm, kontrol, yol takibi, konumlandırma ve mevkilendirme açısından yüksek doğruluğa sahip bir seyrüsefer sistemine ihtiyaç duyarlar. OSA'lara yönelik sağlam, güvenilir ve doğru bir seyrüsefer sistemi tasarlamak için ise İSA'nın tüm gövde modeline ihtiyaç duyulmaktadır. Ancak OSA modellemesi çok karmaşık ve zor bir işlem olup, hidrodinamik ve hidrostatik bilim dallarının birlikte kullanılmasını gerektirir.

Bir OSA'nın sualtı modellemesi, katı bir cisim olarak ele alınsa bile oldukça karmaşık süreçleri içermektedir. Bir OSA sistemi sualtı ortamında hareket ederken doğrusal olmayan (nonlinear) etkilere maruz kalır. Bu etkiler arasında serbest yüzey etkisi, kavitasyon, dalgalar, zamanla değişen kütle ve pervane sürati, rijid olmayan gövde dinamiği, düzensiz akışlar ile hareketli kanatların etkisi sayılabilir. Bütün bu etkilerin modellemeye katılması, modelleme sürecini içinden çıkılmaz bir duruma itmektedir ve bu etkilerin büyük bir çoğunlu çekme tanklarında dikkate alınmaktadır.

Hidrodinamik etkiler OSA'nın su ortamındaki hareketinden kaynaklanmaktadır. Bir İSA sisteminin hidrodinamik parametrelerinin belirlenmesinde tamamen kendi şekil ve formuna bağlı olarak deney ve teoriye dayalı yöntemler kullanılır. Genel olarak, bir İSA'nın hidrodinamik parametreleri üç faklı yöntemle belirlenir. Bunlar:

1. Hesaplamalı Yöntemler (Navier Stokes Denklemleri, Hesaplamalı Akışkanlar Dinamiği, vb.),
2. Çekme tankı (towing tank) testleri,
3. Gerçek Ortamında Testler.

Bu tezin ana amaçlarından biri, bir OSA sisteminin dinamik hareket modelinin oluşturulması ve MATLAB yazılım ortamı kullanılarak oluşturulan hareket modeli üzerinde, Ataletsel Seyrüsefer Sistemi (ASS)'den elde edilen seyrüsefer çözümünü düzeltmek için Dopler Hız Kaydedici, Manyetik Pusula ve Derinlik Ölçer yardımcı sensörleri kullanarak Kalman Süzgeci tabanlı oluşturulan tümleşik seyrüsefer sistemi tasarımını gerçekleştirmektir.

Tez kapsamında, OSA'lar için geliştirilmiş tümleşik seyrüsefer sistemi için üç farklı yaklaşım kullanılmıştır. Birinci yaklaşımda, Dopler Hız Kaydedici, Manyetik Pusula ve Derinlik Ölçer yardımcı sensörlerin kalibrasyonlarının mükemmel yapıldığı farz ve kabul edilerek, sadece ASS'nin hatalarının Kalman Süzgeci kullanılarak kestirimleri hesaplanmış ve yardımcı sensörlerin düzeltmeleri Kalman ölçüm vektörü yardımıyla girdi yapılmıştır. Bu yaklaşımda Kalman durum vektörü boyutu 9'dur. İkinci yaklaşımda, yine yardımcı sensörlerin kalibrasyonlarının mükemmel yapıldığı farz ve kabul edilerek, ASS ile ASS sensörleri olan gyro ve ivmeölçerlerin hatalarının Kalman Süzgeci kullanılarak kestirimleri hesaplanmış ve yardımcı sensörlerin düzeltmeleri Kalman ölçüm vektörü yardımıyla girdi yapılmıştır. Bu yaklaşımda Kalman durum vektörü boyutu 15'dir. Üçüncü ve son yaklaşımda ise, ASS sensörlerinin kalibrasyonlarının mükemmel yapıldığı farz ve kabul edilerek,ASS ile yardımcı sensörlerin hataları Kalman Süzgeci kullanılarak kestirimleri hesaplanmıştır. Bu yaklaşımda Kalman durum vektörü boyutu 14'tür. Daha sonra bu üç tümleşik seyrüsefer sistem yaklaşımı grafiksel ve nümerik yaklaşımla kıyaslanarak üstünlükleri ortaya konmuştur.

Simülasyon sonuçları göstermiştir ki, düşük maliyetli ASS sistemi zamanla dikkate değer oranda ölçüm hatası üretmesine rağmen, farklı boyutlu durum vektörlerine sahip Kalman Süzgeci tabanlı geliştirdiğimiz Tümleşik Seyrüsefer Sistemi bu hataların azaltılmasında etkin bir rol oynamıştır.

Bu tezin diğer ana hedefi ise, en küçük kareler yöntemi yardımıyla İSA'nın mevcut doğrusal olmayan (nonlineer) hareket modeline ait hidrodinamik parametrelerin, seyrüsefer sistemlerinden kaynaklanan kayma hatalarının mevcut olduğu durumda tanılanmasıdır. Bu hidrodinamik parametrelerin doğru olarak belirlenmesi, İSA sisteminin dinamik performansının gerçeğe yakın bir şekilde simüle edilmesinde önemli rol oynar. Ayrıca kestirimi yapılan bu parametreler sadece dinamik modelin manevra performansının analizinde kullanılmaz aynı zamanda geliştirme aşamasında olan İSA'ların kontrolcü tasarımında da etkin olarak kullanılır.

Tanılama yöntemi olarak en küçük kareler yöntemi basit ve kısa zamanda çözüm ürettiği için tercih edilmiştir. En küçük kareler yöntemi kullanılarak bulunan hidrodinamik parametreler, *Hottling's* T^2 istatiksel yöntemi kullanılarak doğrulanmaya çalışılmıştır. Tümleşik seyrüsefer sistemi ile büyük oranda düzeltilen seyrüsefer bilgileri kullanılarak, elde edilen Hidrodinamik parametreler gerçek değerine yakın istatiksel olarak doğrulanmış, elde edilen simülasyon sonuçları nümerik ve grafiksel olarak gösterilmiştir.

1. INTRODUCTION

The researches on Unmanned Underwater Vehicles (UUVs) began in the 1960s, with the first prototypes emerging in the 1980s. Nevertheless, the research on underwater systems has gained immense interest during the last two decades with applications taking place in multiple fields of marine systems. Therefore, the significant numbers of UUVs have been developed for solving a wide range of scientific and applied tasks of ocean and seabed research and development in the world [29]. The military as well as civilian industaries can see great potential uses of UUVs in the underwater environment.

UUVs by definition are small submersible vehicles that contain independent propulsion systems and are capable of carrying sensors such as side-scan sonar, video cameras, depth sensor, and other oceanographic measuring devices [29]. UUVs are highly desirable as they can at least limit the level of human life risk and direct physical human involvement in a mission.

Typically, UUVs can be classified into two unmanned underwater systems that are Remotely Operated Vehicles (ROVs) and Autonomous Underwater Vehicles (AUVs): Each branch has its own pros and cons due to the mission type. ROVs, characterized by direct human assistance, is remotely operated through the presence of a tether cable; the other group is known as the AUVs, which is the topic of this thesis, characterized by their autonomous behavior, having cylindrical geometric shape and absence of a tether cable. This classification is of course not precise given the varying degrees of autonomy in both groups which can differ according to the requirements of the designed mission. In addition, the presence of a tether cable does not necessarily mean that the vehicle cannot perform autonomous tasks. The basic difference between AUVs and ROVs is that AUVs use “intelligence”, such as sensing and automatic decision-making. They have predefined plan of operations in its “mind” allowing them to perform tasks autonomously [29]. ROVs are remotely controlled by a human with the help of communication links based on tether cable (such as cupper, fiber optic, etc.).

The AUVs have shown efficiency at performing complex search and inspection missions, and opening a number of new important application areas which include environmental monitoring, surveillance, underwater inspection of harbors and pipelines, geological and biological surveys, mine countermeasures, etc. [29].

The key element of the AUV navigation system is the Inertial Navigation System (INS), which integrates the output of a set of sensors (gyros and accelerometers) to compute position, velocity, and attitude. Among these sensors, gyros measure angular rate, and accelerometers measure linear acceleration with respect to an inertial frame. Integration is a simple process; complexities arise due to the various coordinate frames encountered, sensor measurement errors, and noise in the system. During the last 70 years, INS has progressed from the crude electromechanical devices that guided the early V-2 rockets to the current solid-state devices that are in many modern vehicles. The impetus for this significant progress came during the ballistic missile programs of the 1960s, in which the need for high accuracy at ranges of thousands of kilometers using autonomous navigation systems was made apparent [48]. Today, INS is used in all types of commercial and military UUVs and ships, submarines, torpedoes, and missiles of all sizes.

Although INS is autonomous and provides good short-term accuracy, its usage as a stand-alone navigational system is limited due to the time-dependent growth of the inertial sensor errors that is the main disadvantage of using the INS. Therefore, the accuracy of the INS is highly dependent on the sensor quality, navigational system mechanization and dynamics of the vehicle [25]. Thus, the major error sources of the INS are due to gyro and accelerometer inertial sensor imperfections, incorrect navigational system initialization, and imperfections in the gravity model used in the computations [3].

Additionally, the challenge in an AUV navigational system is maintaining the accuracy of an AUV's position over the course of a long mission time. An initial accurate position can quickly become uncertain through variations in the AUV's motion. This effect can be reduced by using accurate heading, position, and velocity sensors, but these sensors cannot be made arbitrarily accurate. During long mission periods, these inaccuracies become significant. Strong sea currents and other underwater phenomena that affect the motion of the AUV cannot be precisely modeled which leads to greater inaccuracies [52].

1.1 Purpose of Thesis

One of the main purposes of this thesis is to develop of dynamic model of an AUV under different swimming conditions, and then to apply Integrated AUV Navigational System based on the Kalman Filter (KF) to this model. This thesis also addresses the issue of providing low cost, high integrity, and small size aided INS based on each sensor error model and filter structure for a generic AUV system. In order to achieve this, it is important to develop an INS fitting into the AUV dynamic model. Because the key element of AUV navigation system is INS, which is accomplished by integrating the output of a set of sensors (including, Doppler Velocity Log (DVL), compass, depth sensor, gyros and accelerometers) to compute position, velocity and attitude.

Another main focus of this thesis is to realize the parameter identification of hydrodynamic coefficients based on the Least Square Estiomation (LSE) algorithm for a nonlinear mathematical modeling of AUV. It is important to have the estimated values of these coefficients in order to accurately simulate the AUV's dynamic performance. The estimated coefficients can be used as inputs not only for a mathematical model to analyze the maneuvering performance but also for a controller model to design AUVs under development.

1.2 Literature Review

Autonomous guidance, navigation, and control techniques are key research & development areas for the success of AUV specific missions. However, further work is needed for in precision navigation, sensor development and integration, and improving the realiability and robustness of long term and complex mission completion [48].

This thesis is primarily focused on integrated AUV navigation system, which is a complex problem that has been the subject of a great amount of research efforts in recent years. For AUVs, precise navigation solution is one of the key issues that require accurate navigation system for localization, positioning, path tracking, guidance and control. In order to develop an accurate and robust navigation system, we need to know an overall mathematical modeling of AUV, which involves the interdisciplinary study of kinematics, hydrostatics, and hydrodynamics. Hydrostatics is concerned with the equilibrium of underwater bodies at rest or moving with constant velocity, whereas hydrodynamics is concerned with bodies having accelerated motion [8]. In this thesis, we develop nonlineer dynamic model of an AUV for different swimming conditions, and then to apply Integrated AUV Navigation System based on KF to this model. In many literature, authors employ parameter specific nonlineer AUV model for only one swimming condition.

In real world applications, an AUV does not have continuous position updates; hence, a navigational system based on INS has an unacceptable position error drift without sufficient aiding. The navigational system of AUVs play a crucial role together with the sensor architecture in the degree of system autonomy that can be achieved. A typical navigation sensor outfitted for an AUV may consist of standard components such as compass, pressure depth sensor, and some class of Inertial Measurement Unit (IMU). In addition, some aiding devices may be available, for instance acoustic sonar, pressure depth sensor, compass, DVL, terrain-based techniques, and surface Global Positioning System (GPS) [53].

Navigational accuracy depends not only on the initialization and on drift errors of the low cost IMU and the aiding sensors, but also on the performance of the sensor fusion filter (i.e. KF) used in the navigation algorithm. In the design of an integrated navigational system, KF plays a key role for which KF, resident in the INS, performs real-time integration of the sensor measurements to provide accurate position, velocity, and attitude information in all axes of the vehicle [7].

The KF is a set of mathematical equations that provides an efficient computational (recursive) mean to estimate the state of a process in a way that minimizes the mean of the squared error. The filter is very powerful in several aspects: it supports estimations of past, present, and even future states, and it can do so even when the precise nature of the modeled system is unknown [58].

In reference [12], Geng, Martins and Sousa focused on the performance analysis of the bias of inertial sensors and the error of position using different level IMU. An extended KF is employed to estimate the bias of the inertial sensors and then give the ultimate error of position in about one hour campaign. In another reference [25], Hegrenæs, Berglund, and Hallingstad made a study on the implementation and experimental evaluation of a complete model-aided INS for underwater vehicle navigation. The proposed approach showed promise to improve underwater navigation capabilities both for systems lacking disparate velocity measurements, typically from a DVL, and for systems where the need for redundancy and integrity is important, e.g. during sensor dropouts or failures, or in case of emergency navigation. In another study (reference [64]), Zhao and Gao proposed a KF method working in the GPS/INS/DVL integrated mode, which combines output of INS, DVL and GPS (when available). They acknowledged that the test results show that the system is able to achieve high precision, which is one meter approximately, with GPS and DVL working properly. Similarly, in reference [36], Lee, Jun, Kim, Lee, Aoki and Hyakudome made a study on an integrated navigation system for underwater vehicles to improve the performance of a conventional inertial acoustic navigation system by introducing range measurement. The integrated navigation system is based on a strapdown inertial navigation system (SINS) accompanying range sensor, DVL, magnetic compass, and depth sensor.

On the other hand, in reference [36], Lee and Jun presented an integrated navigational algorithm for UUV using two acoustic range transducers and strap-down inertial measurement unit (S-IMU). The proposed algorithm, called pseudo long base line (PLBL), estimates the position of the vehicle integrating the S-IMU signals corrected with the two range measurements. Extended KF was applied to propagate error covariance, to update measurement errors and to correct state equation whenever the external measurements are available. Additionally, in reference [28], Li, Tang, and Yuan proposed the navigation equipments of Synthetic Aperture Sonar (SAS) comprise SINS and DVL. For the large attitude error, the nonlinear error models of SINS/DVL based on quaternion error are presented. Overall, we develop nonlineer dynamic model of an AUV for different swimming conditions, and then to apply this model to Integrated AUV Navigation System model based on KF that we developed.

Another main focus of this thesis is to realize the parameter identification of hydrodynamic coefficients based on Least Square Estiomation (LSE) algorithm for a nonlinear mathematical modeling of AUV. The hydrodynamic coefficients of AUV can be estimated based on the calculations of the first principle of dynamics of AUVs and from statistical LSE of experimental data, or a combination of the two [7]. The identification of the parameters of the item being tracked can be approached in many different ways. The parameters can be determined once, from a model of the expected input signal. It could also be done adaptively utilizing a recursive method to identify the parameters of the incoming signal.

Another approach that estimates the hydrodynamic coefficients of AUVs is the observer method, in which a model-based estimation algorithm is used. A representative method amongst observer methods is the KF, which has been widely used to estimate state variables and parameters [7]. Hwang [29] estimated the maneuvering coefficients of a ship and identified the dynamic system of a maneuvering ship using an EKF technique. Additionally, referencing [44], Meng & Veras, they concentrated on the application and comparison of EKF and iterated EKF for aerodynamic parameter estimation of a fixed wing UAV. In another reference [4], Chowdhary compared the performance of three recursive parameter estimation algorithms for aerodynamic parameter estimation of two aircrafts derived from real flight data. These algorithms are the EKF -the simplified version of the Unscented Kalman Filter (UKF) and the augmented version of the UKF.

On the other hand, the report [47] compares responses obtained by the KF, the least squares estimation, and the linear model for the NPS Phoenix AUV. The LSE provided results similar to those obtained by the KF, but the latter produced a more accurate model.

Referencing [58] Vandersteen, Rolain, Schoukens & Pintelon, they proposed a robust estimation algorithm for the estimation of static and nonlinear systems which can be described as a nonlinear function corrected with a rational form. The errors-in-variables-based algorithm solves the starting-value problem using an iterative, weighted least-squares procedure, which constructs the rational form such that the set of normal equations becomes best conditioned, and uses a maximum-likelihood estimation step to increase the efficiency of the estimates.

2. DYNAMIC MATHEMATICAL MODELING OF AN AUV

2.1 Purpose

This section provides detailed explanations on the theory behind the main concepts that directly influence the design of the dynamic mathematical model of AUV. AUV modeling is fairly complicated, and even when considered as a rigid body, an exact analysis is only possible by including the underlying infinite dimensional dynamics of the surrounding fluid [62], which is seawater. This can be done using partial differential equations, which are solved by Computational Fluid Dynamics (CFD), but it still involves a formidable computational burden, which is infeasible for most practical applications [8]. As a result, the conventional approach has been to use finite-dimensional approximations.

On the other hand, AUV modeling involves the interdisciplinary study of kinematics, hydrostatics, and hydrodynamics. The study of hydrostatics is concerned with the equilibrium of underwater bodies at rest or moving with constant velocity, whereas hydrodynamics is concerned with bodies having accelerated motion [8]. An increased knowledge of hydrodynamic parameters then leads to a better navigational system design and performance on AUVs.

The aim of this thesis does not directly involve the modeling of AUV systems from scratch since this is a different area of research interest alltogether. However, in this study we try to develop nonlineer mathematical modeling of an AUV for different swimming conditions and then, directly use the mathematical model of REMUS AUV that is designed to perform hydrographic analysis in the very shallow water. In Figure 2.1, a picture of REMUS is shown. REMUS is used for missions such as hydrographic surveys, mine counter-measure operations, harbor security operations, environmental monitoring debris field mapping, search and resque operations, fishery operations, and scientific sampling and mapping.

Figure 2.1 : REMUS AUV [46].

2.2 Modeling Assumptions

2.2.1 Environmental assumptions

The corresponding assumptions are made about the vehicle with respect to its environment [44]:

- The AUV is deeply submerged in a homogeneous and unbounded fluid. In other words, the AUV is located far from the free surface (no surface effects, i.e. no sea wave or vehicle wave-making loads), walls and bottom.
- The AUV does not experience underwater currents.

2.2.2 Dynamics assumptions

In dynamic modeling of AUV, the following assumptions are used [22]:

- The AUV behaves as a rigid body of a constant mass.
- The earth's rotation is negligible for acceleration components of the vehicle's center of mass
- The primary forces that act on the AUV are inertial and gravitational in the center of buoyancy and are derived from hydrostatic, propulsion, thruster, and hydrodynamic lift and drag forces.
- The thruster assumption is that it uses an extremely simple propulsion model, which treats the vehicle propeller as a source of constant thrust and torque.

2.3 6-DOF Rigid-Body Equations of Motion

AUVs move in six degrees of freedom (6-DOF) since six independent coordinates are necessary to determine the position and orientation of a rigid body dynamics. The first three coordinates and their time derivatives are based off of translational motion along the *x, y* and *z*-axes, while the last three coordinates (ϕ, θ, ψ) and their time derivatives are used to describe orientation and rotational motion [26]. Velocity and angular velocity components of the AUV relative to the body axes (x, y, z) are denoted by the velocity of surge, sway, heave motion, (u, v, w) and angular velocity of roll, pitch, and yaw motion (p, q, r), respectively. *X, Y, Z, K, M,* and *N* represent the resultant forces and moments with respect to the ***x, y,*** and ***z*** axis. For AUVs, it is common to use the SNAME notation. In Table 2.1 below, the six different translational and rotational motion components are defined as: *surge, sway, heave, roll, pitch* and *yaw* respectively [8].

Table 2.1 : AUV dynamic components.

Motion Components	*Forces and Moments*	*Linear and Angular Velocities*	*Position and Euler Angles*
Surge	***X***	*u*	*X*
Sway	***Y***	*v*	*Y*
Heave	***Z***	*w*	*Z*
Roll	***K***	*p*	*Φ*
Pitch	***M***	*q*	*θ*
Yaw	***N***	*r*	*Ψ*

2.3.1 Coordinate frames

Typically, three different right-handed and rectangular coordinate frames are used for defining AUV motion. First, the body axes (x, y, z) have their origin at the center of buoyancy (CB) with *x* directed toward the bow along the hull centerline axis, *y* directed to the starboard side, and *z* toward the keel (see Figure 2.3). The axes fixed in the earth are (x_e, y_e, z_e) with the x_e, y_e plane in the water surface and z_e directed downward into the ocean. Second, the Earth-fixed coordinates frame is also measured to CB of AUV. If roll, pitch and yaw orientation angles ϕ, θ, ψ of the AUV are zero, the (x, y, z) axes will be parallel to the (x_e, y_e, z_e) axes, respectively.

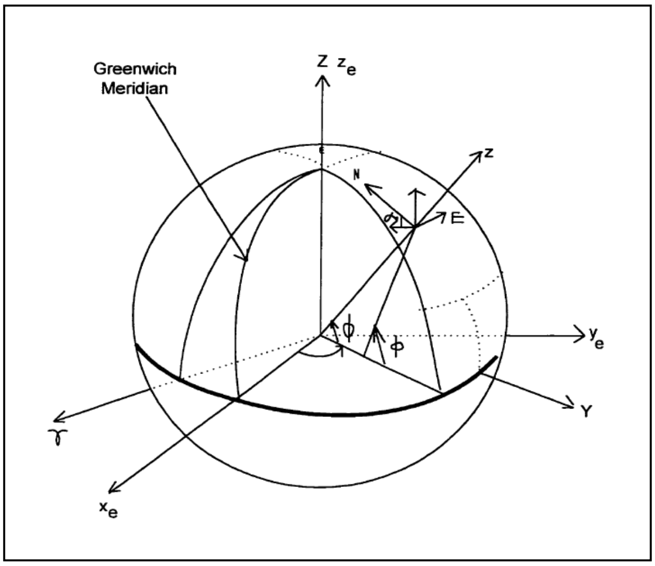

Figure 2.2 : 6-DOF navigational frame [22].

The third coordinate frame (x_f, y_f, z_f) is fixed in the fluid, which can move with a constant velocity (u_f, v_f, w_f) relative to the earth-fixed frame. The x_f, y_f, z_f axes are always parallel to the x_e, y_e, z_e axes, respectively [3]. In Figure 2.3, it is shown 6-DOF AUV angular and transaltion motions in body frame.

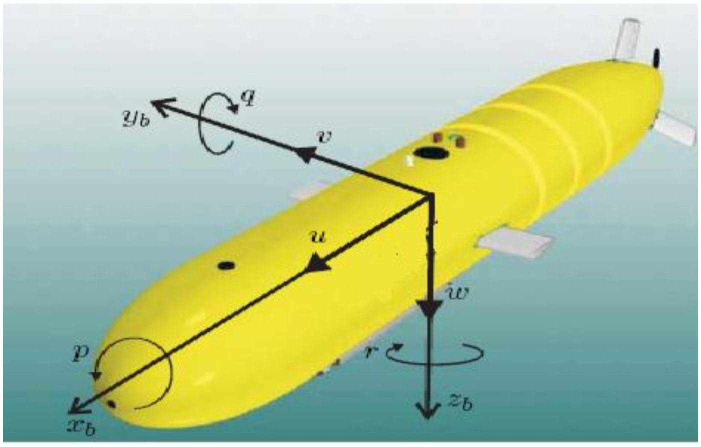

Figure 2.3 : 6-DOF AUV angular and translational motions [46].

A set of axes commonly used with the Earth-fixed axis system is shown in Figure 2.4 :, where X_e axis is chosen to point north, Y_e axis points east with the orthogonal triad being completed when Z_e axis pointing down.

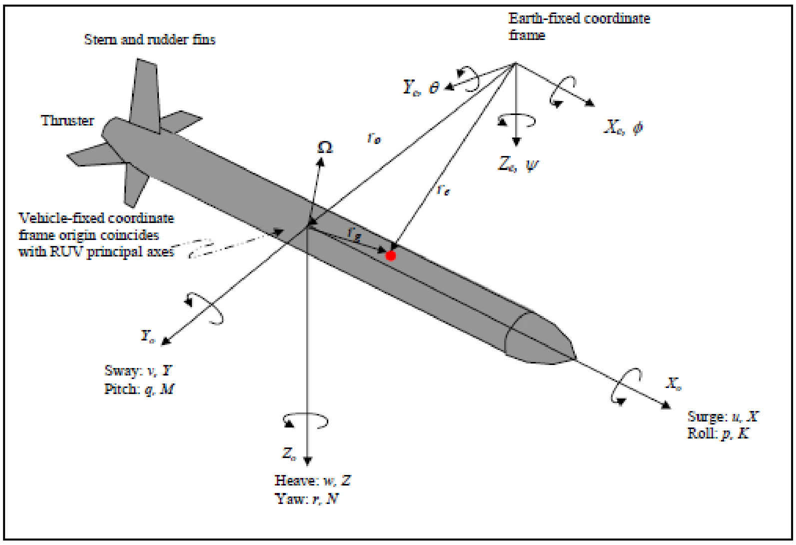

Figure 2.4 : AUV body-fixed and earth-fixed coordinate system [29].

A transformation matrix containing '*Euler*' angles ϕ, θ, ψ, where ϕ is roll, θ is pitch, and ψ is yaw, must be defined. The transformation order from the earth-fixed frame ($\Im_e$) to the body-fixed frame ($\Im_b$) is given by

$$\Im_e \xrightarrow[\psi]{u_3} \Im_1 \xrightarrow[\theta]{u_2} \Im_2 \xrightarrow[\phi]{u_1} \Im_b \qquad \textbf{(2.1)}$$

Transformation matrix is defined in the following equation (2.2):

$$T(\varphi,\theta,\psi) = \begin{bmatrix} \cos\psi\cos\theta & \sin\psi\cos\theta & -\sin\theta \\ \cos\psi\sin\theta\sin\varphi - \sin\psi\cos\varphi & \sin\psi\sin\theta\sin\varphi + \cos\psi\cos\varphi & \cos\theta\sin\varphi \\ \cos\psi\sin\theta\cos\varphi + \sin\psi\sin\varphi & \sin\psi\sin\theta\cos\varphi - \cos\psi\sin\varphi & \cos\theta\cos\varphi \end{bmatrix} \qquad \textbf{(2.2)}$$

The Simulink model of direction cosine matrix is shown in Figure 2.5.

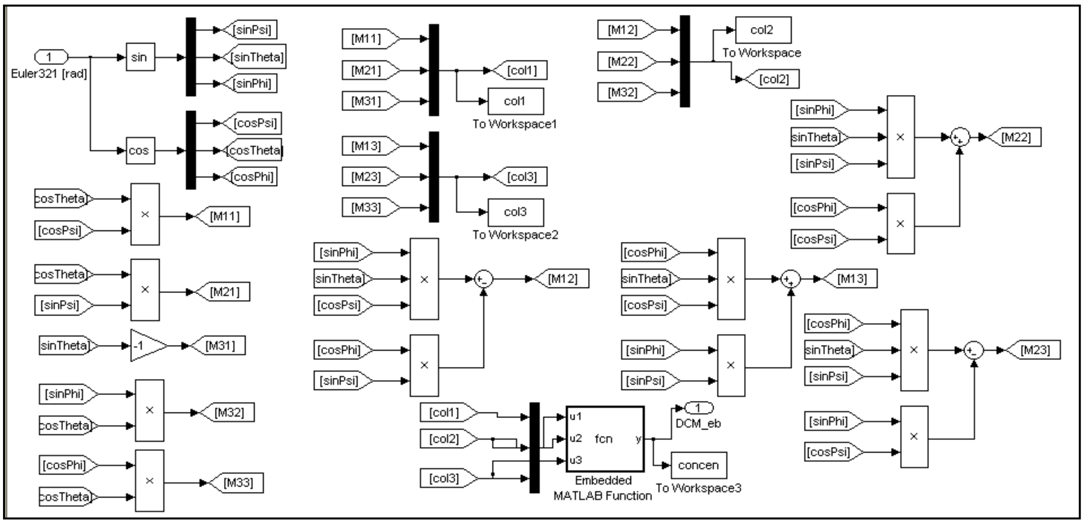

Figure 2.5 : Direction cosine matrix.

Transformation from a global velocity vector to the local velocity vector is given by

$$\begin{bmatrix} u \\ v \\ w \end{bmatrix} = T\left(\varphi,\theta,\psi\right) \bullet \begin{bmatrix} \dot{X} \\ \dot{Y} \\ \dot{Z} \end{bmatrix} \qquad \textbf{(2.3)}$$

On the other hand, transformation from a local velocity vector to a global velocity vector is derived in equation (2.4):

$$\begin{bmatrix} \dot{X} \\ \dot{Y} \\ \dot{Z} \end{bmatrix} = T^{-1}\left(\varphi,\theta,\psi\right) \bullet \begin{bmatrix} u \\ v \\ w \end{bmatrix} \qquad \textbf{(2.4)}$$

The global angular velocity vector $[p,q,r]$ can be transformed into the rates of change of the *Euler* angles as given by:

$$\begin{bmatrix} \dot{\varphi} \\ \dot{\theta} \\ \dot{\psi} \end{bmatrix} = \begin{bmatrix} 1 & sin\varphi tan\theta & cos\varphi tan\theta \\ 0 & cos\varphi & -sin\varphi \\ 0 & sin\varphi/cos\theta & cos\varphi/cos\theta \end{bmatrix} \begin{bmatrix} p \\ q \\ r \end{bmatrix} \qquad \textbf{(2.5)}$$

The Simulink model of transformation of Euler angles is shown in Figure 2.6.

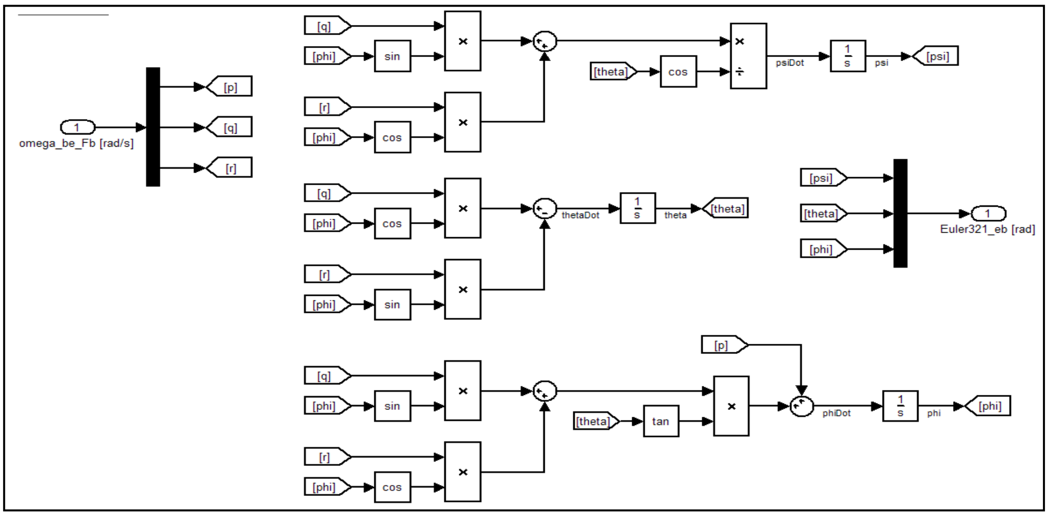

Figure 2.6 : Transformation of Euler angles.

Three dimensional (3D) spatial rotations can be parametrized using both *Euler* angles and unit quaternions. Unit quaternion provides a convenient mathematical notation for representing orientations and rotations of vehicle in three dimensions. Compared to *Euler* angles, unit quaternions are simpler to compose and avoid the problem of the gimbal lock. Additionally, compared to rotation matrices, they are more numerically stable and may be more efficient [15]. Nevertheless, *Euler* angles are preferred in this study for simplification reasons.

After a general model structure for AUV is derived, we look further into the modeling aspects in terms of environmental disturbance models, in which waves (wind generated), wind, and sea currents will be considered. In general, these environmental disturbances will both be additive and multiplicative to dynamic EOM [3]. Transformation order from body-fixed frame ($\Im_b$) to sea current frame ($\Im_w$) using orientation angles of $\boldsymbol{\alpha}$ and $\boldsymbol{\beta}$ are given in equation 2.6.

$$\Im_b \xrightarrow[-\alpha]{u_2} \Im_1 \xrightarrow[\beta]{u_3} \Im_w \tag{2.6}$$

The transformation matrix from body-fixed frame ($\Im_b$) to the sea current frame ($\Im_w$):

$$\begin{gathered}\hat{C}^{(b,w)} = R_2(-\alpha) \times R_3(\beta) \\ R_2(-\alpha) = \begin{bmatrix} cos\alpha & 0 & -sin\alpha \\ 0 & 1 & 0 \\ sin\alpha & 0 & cos\alpha \end{bmatrix} \quad , \quad R_3(\beta) = \begin{bmatrix} cos\beta & -sin\beta & 0 \\ sin\beta & cos\beta & 0 \\ 0 & 0 & 1 \end{bmatrix}\end{gathered} \tag{2.7}$$

After mathematical calculations, the transformation matrix from the body-fixed coordinate to the sea coordinate axes including sea current can be expressed as

$$\hat{C}^{(b,w)} = \begin{bmatrix} \cos\alpha\cos\beta & -\cos\alpha\sin\beta & -\sin\alpha \\ \sin\beta & \cos\beta & 0 \\ \sin\alpha\cos\beta & -\sin\alpha\sin\beta & \cos\alpha \end{bmatrix} \tag{2. 8}$$

The sea current velocity components are assumed constant relative to axes fixed in the earth. This permits the use of axes fixed in the fluid as an inertial frame of reference. AUV velocity with respect to the sea is expressed as

$$\vec{V}_{b/w} = \vec{V}_{b/e} - \vec{V}_{w/e} \tag{2.9}$$

Then, dynamic pressure is calculated as

$$Q_d = \frac{1}{2}\rho V_{b/w}^2 \tag{2.10}$$

In this study, however, we ignore the sea currents, which normally effects the AUV motion. Additionally, wind and wind generated waves phenomena will not be discussed since the attention is focused on AUVs performing a motion or manipulation task in an underwater environment.

2.3.2 Newtonian and Lagrangian mechanics

The EOM of AUVs are highly nonlinear, time-varying and coupled due to hydrodynamic added mass, lift, drag, coriolis and centripetal forces, which are acting on the vehicle and generally include uncertainties [8]. Overall 6-DOF nonlinear dynamic EOM can be expressed in the matrix form as

$$M(v)\dot{v} + C(v)v + D(v)v + g(\eta) = \tau \tag{2.11}$$

Where:

M(v) = inertia matrix (including added mass),
C(v) = matrix of Coriolis and centripetal terms (including added mass),
D(v) = damping matrix,
$g(\eta)$ = vector of gravitational forces and moments,
τ = vector of control inputs,
$v = [u, v, w, p, q, r]^T$,
$\eta = [x, y, z, \phi, \theta, \psi]^T$.

The coupled EOM of AUV are derived from two possible modeling approaches; one is a *Lagrangian* method and the other is a *Newtonian-Euler* formulation. Basically, the *Lagrangian* approach consists of three main steps: first, to formulate a suitable expression for the vehicle's kinetic (***T***) and potential energy (***P***), second, to compute the *Lagrangian L* (*L=T-P*), and finally to apply the *Lagrangian* (***L)*** to the *Lagrangian* formulation [2].

$$\frac{d}{dt}\left(\frac{\partial L}{\partial \dot{\eta}}\right) - \frac{\partial L}{\partial \eta} = J^{-T}(\eta)\,\tau \tag{2.12}$$

Another modeling approach is the *Newtonian-Euler* formulation, which is based on Newton’s Second Law that relates mass (***m***), acceleration (***a***) and force (***F***). *Euler* suggested expressing Newton's Second Law in terms of conservation of both linear and angular momentum. The forces (***F***) and moments (***M***) refers to the body's center of gravity [8].

In this study, the dynamic behavior of an AUV is described through *Newton's laws* of linear and angular momentum.

Newton's Second Law is expressed as:

$$\mathbf{F} = \frac{d}{dt}\{m\mathbf{V}\} \tag{2.13}$$

$$\mathbf{M} = \frac{d}{dt}\{\mathbf{H}\} \tag{2.14}$$

where ***F*** represents the sum of all externally applied forces, ***M*** represents the sum of all applied torques, and ***H*** is the angular momentum.

It is convenient to regard the sums of applied torque (***M***) and force (***F***) as consisting of an equilibrium point and a perturbational component. Thus, assuming constant AUV mass

$$\mathbf{F} = \mathbf{F}_0 + \Delta\mathbf{F} = m\frac{d}{dt}\{\mathbf{V}\} \tag{2.15}$$

$$\mathbf{M} = \mathbf{M}_0 + \Delta\mathbf{M} = \frac{d}{dt}\{\mathbf{H}\} \tag{2.16}$$

The subscript "$_0$" denotes the equilibrium condition, and "Δ" the component of perturbation. Equilibrium of AUV by definition must be an unaccelerated motion along a straight path; during this motion the linear velocity vector relative to fixed space is invariant, and the angular velocity is zero. Therefore, $\mathbf{M}_0$ are zero, but . $\mathbf{F}_0$ is not zero due to drag. Furthermore, since the axis system being used as an inertial reference system is the Earth-fixed coordinate system, Equation (2.15) and (2.16) can be expressed as

$$\Delta \mathbf{F} = m \frac{d}{dt} \{\mathbf{V}_T\}_E \tag{2.17}$$

$$\Delta \mathbf{M} = \frac{d}{dt} \{\mathbf{H}\}_E \tag{2.18}$$

The force equation based on the rate of change of velocity ***V*** relative to the Earth's fixed axis frame is given by

$$\vec{F} = D_e\left(m\vec{V}\right) = D_b\left(m\vec{V}\right) + \vec{\omega}_{b/e} \times m\vec{V} \tag{2.19}$$

where $\boldsymbol{\omega}_{b/e}$ is the angular velocity of the AUV with respect to the Earth fixed coordinate frame. The open form of Equation 2.19 is given by

$$F \Rightarrow \begin{cases} F_x = X = m\left(\dot{u} + qw - rv\right) \\ F_y = Y = m\left(\dot{v} + ru - pw\right) \\ F_z = Z = m\left(\dot{w} + pv - qu\right) \end{cases} \tag{2.20}$$

After the rearrangement of ***F***, translational accelerations become:

$$\begin{aligned} \dot{u} &= \frac{F_x}{m} - qw + rv \\ \dot{v} &= \frac{F_y}{m} - ru + pw \\ \dot{w} &= \frac{F_z}{m} - pv + qu \end{aligned} \tag{2.21}$$

In Figure 2.7, the Simulink model of translational transformation is shown.

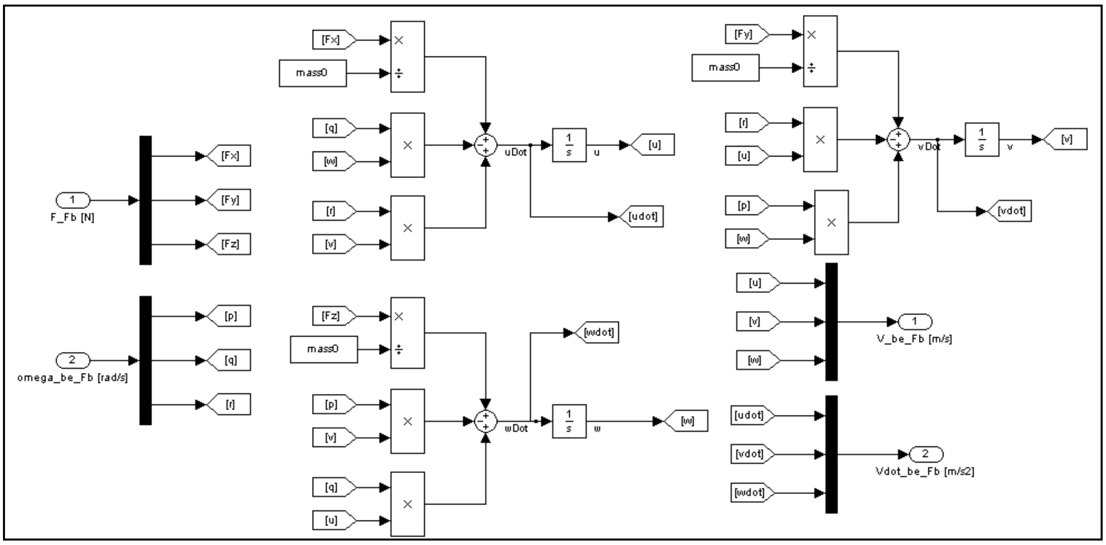

Figure 2.7 : Translational transformation matrix.

Similarly, after transforming from the body-fixed frame to the Earth-fixed frame the moment equation and its open form becomes

$$\vec{M} = D_e\left(\hat{I}\,\vec{\omega}_{b/e}\right) = D_b\left(\hat{I}\,\vec{\omega}_{b/e}\right) + \vec{\omega}_{b/e} \times \left(\hat{I}\,\vec{\omega}_{b/e}\right)$$

$$\vec{M} \Rightarrow \begin{cases} M_x = K = I_x\dot{p} - I_{yz}\left(q^2 - r^2\right) - I_{zx}\left(\dot{r} + pq\right) - I_{xy}\left(\dot{q} - rp\right) - \left(I_y - I_z\right)qr \\ M_y = M = I_y\dot{q} - I_{zx}\left(r^2 - p^2\right) - I_{xy}\left(\dot{p} + qr\right) - I_{yz}\left(\dot{r} - pq\right) - \left(I_z - I_x\right)rp \\ M_z = N = I_z\dot{r} - I_{xy}\left(p^2 - q^2\right) - I_{yz}\left(\dot{q} + rp\right) - I_{zx}\left(\dot{p} - qr\right) - \left(I_x - I_y\right)pq \end{cases} \quad \textbf{(2.22)}$$

For a rigid body, angular momentum can be defined as

$$\mathbf{H} = I\boldsymbol{\omega} \quad \textbf{(2.23)}$$

where the inertia matrix is defined as

$$I = \begin{bmatrix} I_{xx} & -I_{xy} & -I_{xz} \\ -I_{xy} & I_{yy} & -I_{yz} \\ -I_{xz} & -I_{yz} & I_{zz} \end{bmatrix} \quad \textbf{(2.24)}$$

where, I_{ii} denotes a moment of inertia, and I_{ij} a product of inertia $j \neq i$.

In this thesis, we assume that the AUV is symmetrical along the *XY* and *XZ* planes, therefore cross inertia parameters become

$$I_{xy} = I_{yz} = I_{xz} = 0 \text{ and } I_y = I_z \quad \textbf{(2.25)}$$

As a result of this symmetry, the rotational EOM of AUV in particular, becomes:

$$
\begin{aligned}
M_x &= I_x\,\dot{p} \\
M_y &= I_y\,\dot{q} - \left(I_z - I_x\right) r\,p \\
M_z &= I_z\,\dot{r} - \left(I_x - I_y\right) p\,q
\end{aligned}
\qquad \textbf{(2.26)}
$$

After rearrangement, Equation 2.26 is expressed as:

$$
\begin{aligned}
\dot{p} &= \frac{M_x}{I_x} \\
\dot{q} &= \frac{1}{I_y}\left[M_y + \left(I_z - I_x\right) r\,p\right] \\
\dot{r} &= \frac{1}{I_z}\left[M_z + \left(I_x - I_y\right) p\,q\right]
\end{aligned}
\qquad \textbf{(2.27)}
$$

In Figure 2.8, AUV rotational transformation is implemented in Simulink.

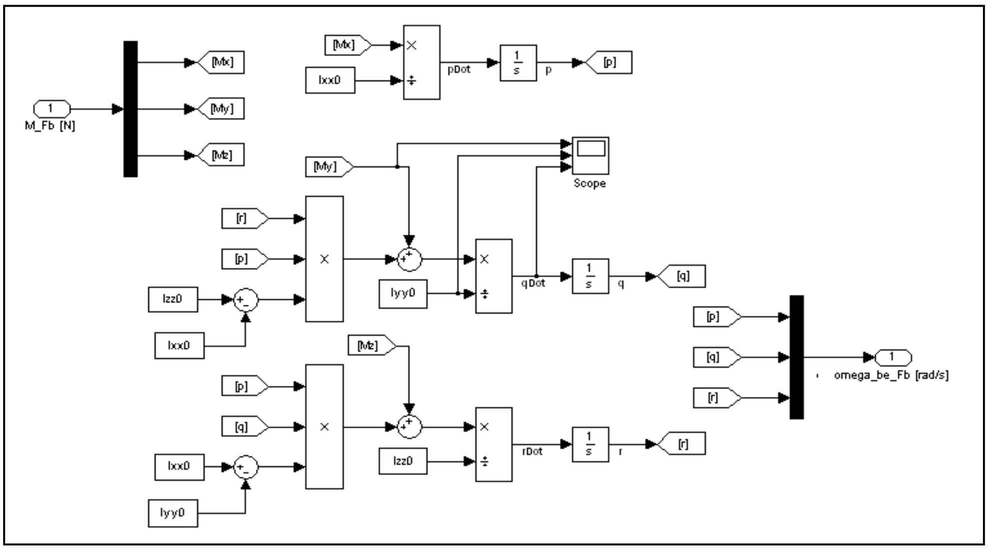

Figure 2.8 : Rotational transformation matrix.

Finally, the derivative of *Euler* angles is defined as:

$$
\begin{aligned}
\dot{\psi} &= \frac{q\sin\varphi + r\cos\varphi}{\cos\theta} \\
\dot{\theta} &= q\cos\varphi - r\sin\varphi \\
\dot{\varphi} &= p + \left(q\sin\varphi + r\cos\varphi\right)\tan\theta
\end{aligned}
\qquad \textbf{(2.28)}
$$

2.3.3 Gravitational forces

Gravitational forces always exist in the AUV. It can be assumed that gravity acts at the center of gravity (*CG*) of the vehicle. Since the centers of mass and gravity coincide in an AUV, there is no external momentum produced by gravity on the *CG*. Therefore, for the body axis system, gravity contributes only to the external force vector ***F***. Three components of the gravitational force in the body frame depend on the AUV's attitude relative to an inertia frame. The gravitational force acting upon an AUV is most obviously expressed in terms of the Earth's axes. With respect to these axes, the gravity vector ***mg***, is directed along the Z_e axis. Figure 2.9 demonstrates the alignment of the gravity vector with respect to the body-fixed axes. In Figure 0, $\boldsymbol{\theta}$ represents the pitch angle between the gravity vector and the Y_bZ_b plane; the angle is positive when the nose of the AUV goes up. $\boldsymbol{\Phi}$ represents the roll angle between Z_b axis and the projection of the gravity vector on the Y_bZ_b plane. Direct solution of the vector ***mg*** into X, Y and Z components produces:

$$\begin{aligned} g_x &= m\mathbf{g}\sin(-\theta) = -m\mathbf{g}\sin\theta \\ g_y &= m\mathbf{g}\cos(-\theta)\sin\Phi = m\mathbf{g}\cos\theta\sin\Phi \\ g_z &= m\mathbf{g}\cos(-\theta)\cos\Phi = m\mathbf{g}\cos\theta\cos\Phi \end{aligned} \qquad \textbf{(2.29)}$$

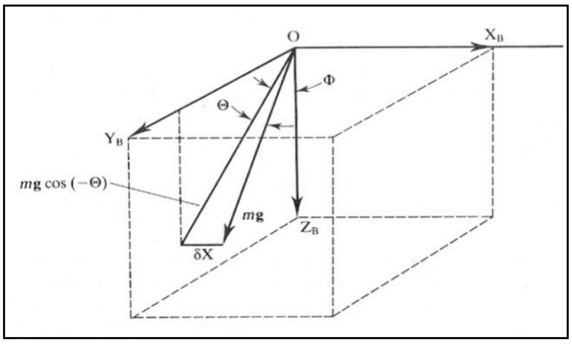

Figure 2.9 : Orientation of gravity vector with respect to the body axis [24].

In general, the *Euler* angles (Φ, θ and Ψ) are not simply the integrals of the angular velocity *p, q,* and *r* (see Equation 2.28). It is necessary to relate these and their derivatives to the angular velocities *p, q,* and *r*. This depends upon whether the gravitational vertical seen from the AUV is fixed or whether it rotates relative to inertial space [2].

The manner in which the angular orientation and velocity of the body axis system with respect to the gravity vector is expressed by depending upon the angular velocity of the body axes about the vector ***mg***.

The external forces acting on the AUV can be expressed as:

$$\begin{aligned} X &= F_x + g_x \\ Y &= F_y + g_y \\ Z &= F_z + g_z \end{aligned} \qquad \textbf{(2.30)}$$

where g_x, g_y, and g_z are the gravitational terms, and F_x, F_y, and F_z represent the hydrodynamic and thrust forces respectively. Hence, from the Equations (2.13) and (2.15), the force equations become:

$$\begin{aligned} F_x &= ma_{x_{CG}} = m(\dot{u} + qw - rv + \mathbf{g}\sin\theta) \\ F_y &= ma_{y_{CG}} = m(\dot{v} + ru - pw - \mathbf{g}\cos\theta\sin\Phi) \\ F_z &= ma_{z_{CG}} = m(\dot{w} + pv - qu - \mathbf{g}\cos\theta\cos\Phi) \end{aligned} \qquad \textbf{(2.31)}$$

In Figure 2.10, the Simulink model of gravitational force calculation is shown.

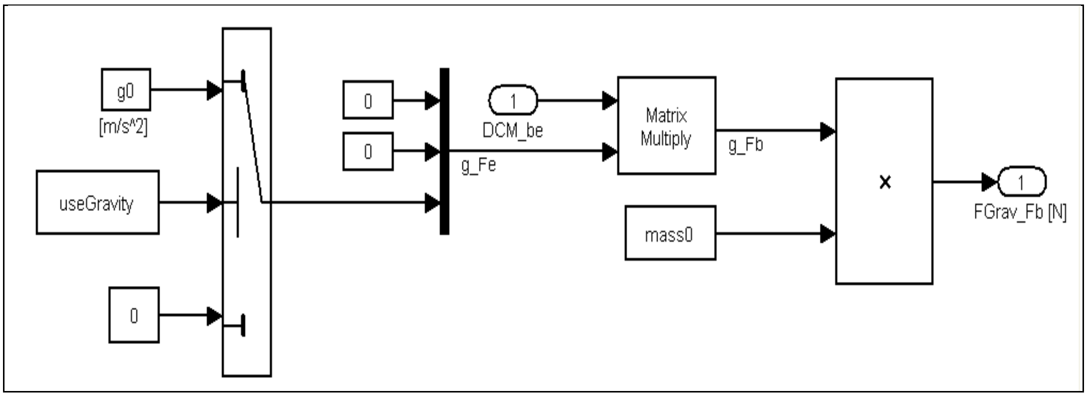

Figure 2.10 : Gravitational force calculation.

The gravitational acceleration forces and moments are represented by the weight minus buoyancy (***W*−*B***) and weight moment terms respectively [24].

2.3.4 Hydrostatic forces and moments

When an AUV is submerged in a fluid under the effect of gravity, two forces act on the vehicle: the gravitational force, which is metioned in the previous sub-section and the buoyancy, which is called “hydrostatic effect”.

The buoyancy force acting on the center of buoyancy (***CB***) is represented in the body-fixed frame (See Figure 2.11). It can be recognized that the difference between gravity and buoyancy ($W-B$) only affects the linear force acting on the vehicle. It is also clear that the restoring linear force is constant in the Earth-fixed frame [22]. On the other hand, the two vectors of the first moment of inertia ***W*** and ***B*** affect the momentum acting on the vehicle and are constant in the body-fixed frame. A solid body submerged in a fluid will have upward buoyant force acting on it equivalent to the weight of displaced fluid, enabling it to float or at least appear to become lighter. If the buoyancy exceeds the weight, then the object floats; if the weight exceeds the buoyancy, the object sinks. If the buoyancy equals the weight, the body has neutral buoyancy and may remain at its level. Discovery of the principle of buoyancy, which is a result of the hydrostatic pressure in the fluid, is attributed to Archimedes [60].

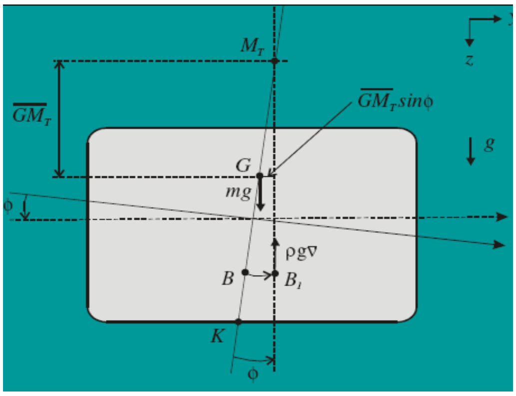

Figure 2.11 : Hydrostatic forces and moments [24].

After applying hydrostatic force coefficients to Equation 2.31, translational force equations become:

$$\left.\begin{aligned} F_x &= ma_{x_{CG}} = m(\dot{u}+qw-rv)+(W-B)\sin\theta \\ F_y &= ma_{y_{CG}} = m(\dot{v}+ru-pw)-(W-B)\cos\theta\sin\Phi \\ F_z &= ma_{z_{CG}} = m(\dot{w}+pv-qu)-(W-B)\cos\theta\cos\Phi \end{aligned}\right\} \tag{2.32}$$

Similarly, after applying the hydrostatic moment coefficients to Equation 2.26, the moment equations become:

$$
\begin{aligned}
M_x &= I_x \dot{p} + (z_g W - z_b B) cos\theta sin\phi \\
M_y &= I_y \dot{q} - \left(I_z - I_x\right) rp + (z_g W - z_b B) sin\theta \\
M_z &= I_z \dot{r} - \left(I_x - I_y\right) pq
\end{aligned} \qquad \textbf{(2.33)}
$$

In Figure 2.12, hyrostatic forces and moments are implemented in Simulink.

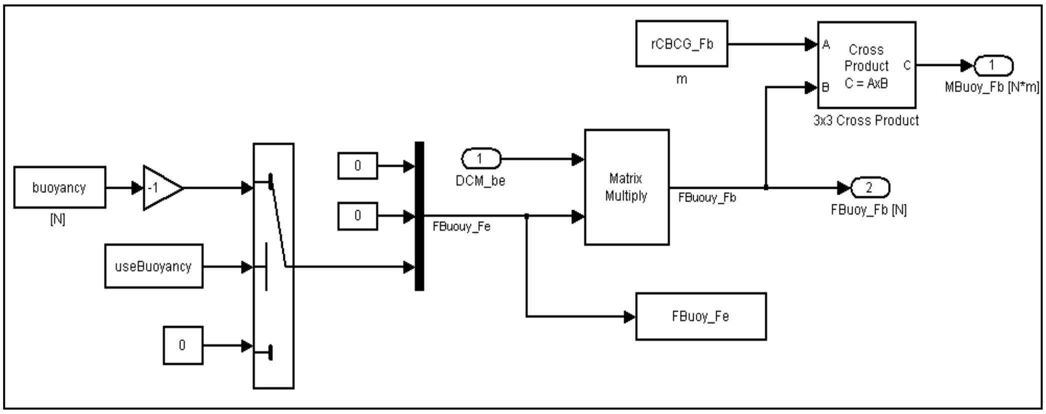

Figure 2.12 : Hydrostatic force and moment calculation.

2.3.5 Added mass and inertia

When a rigid body is moving in a fluid, the additional inertia of the fluid surrounding the body, which is accelerated by the movement of the body, has to be considered. This effect can be neglected in industrial robotics since the density of the air is much lighter than the density of a moving mechanical system. However, in underwater applications the density of the water, $\rho \approx 1000$ kg/m^3, is comparable with the density of the vehicles. In particular, at zero degrees, the density of the fresh water is 1002.68 kg/m^3; for sea water with 3.5% of salinity it is ρ = 1028.48 kg/m^3. Since the fluid surrounding the body is accelerated with the body itself, a force is then necessary to achieve this acceleration (the fluid exerts a reaction force which is equal in magnitude and opposite in direction). This reaction force is the added mass contribution [2].

The added mass is not a quantity of fluid to add to the system such that it has an increased mass. Different properties hold with respect to the six by six inertia matrix of a rigid body due to the fact that the added mass is a function of the body's surface geometry. As an example, the inertia matrix is not necessarily positive definite. The added mass has also an added *Coriolis* and *Centripetal* contribution [8].

As for the rigid body dynamics, it is desirable to separate the added mass forces and moments in terms of which belong to an added inertia matrix and a matrix of hydrodynamic *Coriolis* and *Centripetal* terms. Added (virtual) mass should be understood as pressure-induced forces and moments due to a forced harmonic motion of the body, which are proportional to the acceleration of the body [8]. Consequently, the added mass forces and acceleration will be 180˚ out of phase to the forced harmonic motion. However, this isnot true when AUV is close to the free surface.

In this study, "*Added Mass and Inertia*" effects of water is not taken into consideration.

2.3.6 Hydrodynamic forces and moments

In this section, the main hydrodynamic effects acting on an AUV moving in a fluid (seawater) will be briefly discussed. Standard EOM contain only stability derivatives for the specific AUV configuration of interest. Hence, trajectory simulation or prediction using traditional methods requires a priori knowledge of the hydrodynamic characteristics of the vehicle in the flow regimes, which may occur during the maneuver [24].

All hydrodynamic parameters are defined uniquely for a given AUV shape by formulae based on the results of theory and experiment. There are primarily three methods of determining the hydrodynamic coefficients in the design process of underwater vehicles: (1) towing tank tests, (2) numerical computations, and (3) field tests. Among these methods, the most reliable results are obtained from the field tests, where the whole designed model is tested in a real sea environment [29]. Towing tank tests are performed with a scaled model and the hydrodynamic forces and moments can accurately be determined. However, experimental testing of designs is a time consuming and costly process (construction of the models, instrumentations, test infrastructure, etc.). Numerical Computations are mainly based on semi-empirical or CFD methods. Semi-empirical or potential theory-based methods are generally utilized in the preliminary design process, where it is important to determine the hydrodynamic characteristics in a short period of time. CFD methods give accurate results and are used in the detailed design process [26].

The theory of fluid dynamics is rather complex and it is difficult to develop a reliable and robust model for most of the hydrodynamic effects. A rigorous analysis for incompressible fluids would need to resort to the *Navier-Stokes* equations, which are the basic governing equations for a viscous, heat-conducting fluid [20]. These equations describe how the velocity, pressure, temperature and density of a moving fluid are related. The hydrodynamic prediction method is coupled with a 6-DOF EOM solver to predict vehicle trajectories. The predicted motion characteristics of the AUV are also sensitive to details of the predicted hydrodynamic characteristics of the vehicle. Small perturbations in the flow field, which cause small; variations in the vehicle forces and moments, accumulate over the length of the hull, and can produce large perturbation; in the calculated trajectory.

In this thesis in order to determine hydrodynamic forces and moments, we used *SUBFLO_2*, which is an engineering physically based and commercially available software tool. *SUBFLO_2* has four major components which are hull separation vortex method, fin horseshoe vortex method, propeller/propulsion models, and 6-DOF equations of motion solver. The hydrodynamic prediction method is coupled with a 6-DOF EOM solver to predict vehicle trajectories. The predicted motion characteristics of the AUV are also sensitive to details of the predicted hydrodynamic characteristics of the vehicle. Small perturbations in the flow field, which cause small; variations in the vehicle forces and moments, accumulate over the length of the hull, and these can produce large perturbation; in the calculated trajectory [62].

In order to determine hydrodynamic coefficients with utilizing *SUBFLO_2* software tool, first we find three static hydrodynamic force coefficients of *CFx, CFy,* and *CFz,* and three static hydrodynamic moment coefficients of $CMSF_x, CMSF_y, CMSF_z$ for the predefined AUV geometry. These coefficients are calculated due to the parameters of $\delta_s, \delta_r, \alpha, \beta, V_{b/w}$,which are elevator deflection, rudder deflection, angle of attack, side slip angle, and velocity vector with respect to water, respectively. In Figure 2.13, the Simulink hydrodynamic model is shown.

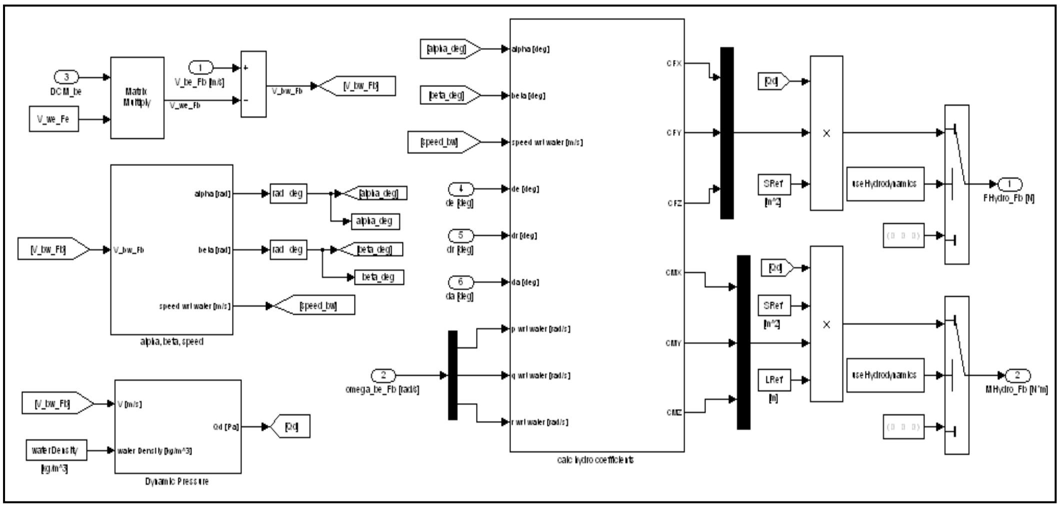

Figure 2.13 : Hydrodynamic force and moment calculation.

2.3.7 Propeller effect

The propeller produces the main thrust. Consequently, the reaction of the body to the load torque of the propeller produces a moment with respect to its rotational axis. The vehicle is a nonlinear system: all equations of motion of the system include coupled terms [29]. The main terms of this type are in the longitudinal (***X***) force and roll moment (***K***) equations because the thrust forces and moments act in the direction of the x-axis. A propeller with a rudder can produce a thrust vector within a range of directions and magnitudes in the horizontal plane for low speed maneuvering and dynamic positioning. In Figure 2.14, AUV propeller effect is shown.

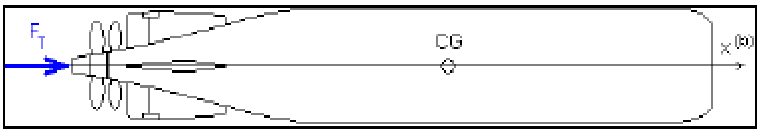

Figure 2.14 : AUV propeller effect [24].

In Figure 2.15, Simulink model of thrust calculation is shown. In this model, we used as a simple fixed-trust model due to the AUV velocity.

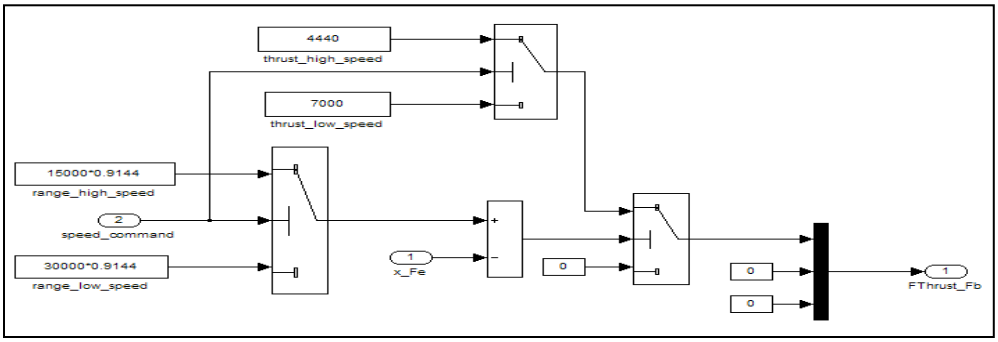

Figure 2.15 : Thrust calculation.

2.4 Mathematical Model of AUV

Detailed explanations on the theory behind the main concepts that directly influenced the design of the dynamic mathematical model of AUV are given in the previous sub-section. Now we arrive at the combined overall non-linear EOM for the AUV in 6-DOF [26] as follows:

Surge or translational motion along the x-axis:

$$\begin{aligned}X &= X_{\dot{u}}\dot{u} + m\left[-\dot{u} - z_G\dot{q} + y_G\dot{r}\right] + X_{uu}u\left|u\right| + (X_{wq} - m)wq + \\ &\left(X_{qq} + mx_g\right)q^2 + (X_{vr} + m)vr + \left(X_{rr} + mx_g\right)r^2 - mz_g pr - \\ &(W - B)\sin\theta + X_{prop}\end{aligned} \tag{2.34}$$

Sway or translational motion along the y-axis:

$$\begin{aligned}Y &= Y_{\dot{v}}\dot{v} + Y_{\dot{r}}\dot{r} + m\left[-\dot{v} + z_g\dot{p} - x_g\dot{r}\right] + Y_{uv}uv + \left(Y_{wp} + m\right)wp + \\ &(Y_{ur} - m)ur - \left(mz_g\right)qr + \left(Y_{pq} - mx_g\right)pq + Y_{vv}v\left|v\right| + Y_{rr}r\left|r\right| + \\ &(W - B)\cos\theta\sin\phi + Y_{uu\delta_r}u^2\delta_r\end{aligned} \tag{2.35}$$

Heave or translational motion along the z-axis:

$$\begin{aligned}Z &= Z_{\dot{w}}\dot{w} + Z_{\dot{q}}\dot{q} + m\left[-\dot{w} + x_g\dot{q} - y_g\dot{p}\right] + \left(Z_{uq} + m\right)uq + \left(Z_{vp} - m\right)vp + \\ &\left(mz_g\right)p^2 + Z_{uw}uw + \left(mz_g\right)q^2 + \left(Z_{rp} - mx_g\right)rp + Z_{ww}w\left|w\right| + Z_{qq}q\left|q\right| + \\ &(W - B)\cos\theta\cos\phi + Z_{uu\delta_e}u^2\delta_e\end{aligned} \tag{2.36}$$

Roll or rotation about the x-axis:

$$\begin{aligned}\mathrm{K} &= \mathrm{m}z_g\dot{\mathrm{u}} - my_g\dot{r} - \left(I_{xx} - K_{\dot{p}}\right)\dot{p} + \left(my_g\right)\dot{w} - \left(I_{zz} - I_{yy}\right)qr - \\ &\left(mz_g\right)wp + \left(mz_g\right)ur - \left(z_gW - z_bB\right)\cos\theta\sin\psi - \\ &\left(y_gW - y_bB\right)\cos\theta\cos\psi + K_{pp}p\left|p\right| + K_{prop}\end{aligned} \tag{2.37}$$

Pitch or rotation about the y-axis:

$$\begin{aligned}M &= -mz_g\dot{u} + \left(mx_g + M_{\dot{w}}\right)\dot{w} - \left(I_{yy} - M_{\dot{q}}\right)\dot{q} + \\ &\left(M_{rp} + I_{zz} - I_{xx}\right)rp + \left(mz_g\right)vr - \left(mz_g\right)wq + \left(Muq - mx_g\right)uq + \\ &M_{uw}uw + \left(M_{vp} + mx_g\right)vp + M_{qq}q\left|q\right| + M_{ww}w\left|w\right| - \\ &\left(z_gW - z_bB\right)\sin\theta - \left(x_gW - x_bB\right)\cos\theta\cos\psi + M_{uu\delta_e}u^2\delta_e\end{aligned} \tag{2.38}$$

Yaw or rotation about the z-axis:

$$\begin{aligned}N &= my_g\dot{u} + \left(N_{\dot{v}} - mx_g\right)\dot{v} + \left(N_{\dot{r}} - I_{zz}\right)\dot{r} + \left(Npq + I_{xx} - I_{yy}\right)pq + \\ &\left(N_{wp} - mx_g\right)wp + \left(N_{ur} - mx_g\right)ur + N_{uv}uv + N_{rr}r\left|r\right| + N_{vv}v\left|v\right| + \\ &\left(x_gW - x_bB\right)\cos\theta\sin\psi + \left(y_gW - y_bB\right)\sin\theta + N_{uu\delta_r}u^2\delta_r\end{aligned} \tag{2.39}$$

where; ***X, Y, Z, K, M,*** and ***N*** represent the resultant forces and moments with respect to the body-fixed coordinates.

Finally, these equations can be summarized in matrix form

$$\begin{bmatrix} \dot{u} \\ \dot{v} \\ \dot{w} \\ \dot{p} \\ \dot{q} \\ \dot{r} \end{bmatrix} = \begin{bmatrix} (m - X_{\dot{u}}) & 0 & 0 & 0 & mz_g & -my_g \\ 0 & (m - Y_{\dot{v}}) & 0 & -mz_g & 0 & (mx_g - Y_{\dot{r}}) \\ 0 & 0 & (m - Z_{\dot{w}}) & my_g & -(mx_g + Z_{\dot{q}}) & 0 \\ 0 & -mz_g & my_g & (I_{xx} - K_{\dot{p}}) & 0 & 0 \\ mz_g & 0 & -(mx_g + M_{\dot{w}}) & 0 & (I_{yy} - M_{\dot{q}}) & 0 \\ -my_g & (mx_g - N_{\dot{v}}) & 0 & 0 & 0 & (I_{zz} - N_{\dot{r}}) \end{bmatrix}^{-1} \begin{bmatrix} \sum X \\ \sum Y \\ \sum Z \\ \sum K \\ \sum M \\ \sum N \end{bmatrix} \quad \textbf{(2.40)}$$

Table 2.2 : AUV physical parameters [45].

Parameter	Value	SCI unit	Definition
ρ	1010	g/m^3	Fluid density
g	9.81	m/s^2	Gravitational acceleration
x_n	0.6	m	Distance from nose to aerodynamic force center
x_t	-0.73	m	Distance from the aerodynamic force center of the hull to Aerodynamic force center of the horizontal tail
d	0.191	m	Hull cylindrical radius
l	1.33	m	Overall hull length
S_w	0.7981	m^2	Submerged Area (πdl)
A_p	0.2540	m^2	Body base area (dl)
A_f	0.0287	m^2	Body cross area ($\pi d^2/4$)
c_{ds}	0.004	-	Surface drag coefficient
c_{dF}	0.3	-	Drag coefficient (A_f)
c_{da}	0.0166	-	Total drag coefficient (for S_w)
l_{cp}	0.2645	m	Distance to center of pressure
t_{fin}	1010	g/m^3	Fluid density
h_{fin}	0.0960	m	Rudder hight
A_r, A_s	0.0071	m^2	Vertical/horizantal rudder surface area
c_{df}	1.558	-	Rudder drag coefficient
c_r, c_s	2.3685	-	Vertical/horizantal rudder bouyancy
l_{fin}	0.8190	m	Rudder moment length
W	300	N	AUV weight
B	306	N	Bouyant force
x_b	0	m	Bouyancy center about the x-axis
y_b	0	m	Bouyancy center about the y-axis
z_b	0	m	Bouyancy center about the z-axis
x_q	0	m	Gravity center about the x-axis
y_q	-0.008	m	Gravity center about the y-axis
z_g	0.0196	m	Gravity center about the z-axis
I_{xx}	0.177	kg m^2	Moment of inertia about the x-axis
I_{yy}	3.45	kg m^2	Moment of inertia about the y-axis
I_{zz}	3.45	kg m^2	Moment of inertia about the z-axis
R	5.87E-2	m	Diameter of propeller
u_0	1.5	m/s	Design velocity

Table 2.3 : AUV hydrodynamic force coefficients [45].

Parameter	Value	SCI unit	Definition
$X_{u\|u\|}$	-6.68	kg/m	Axial drag
$X_{\dot{u}}$	-0.513	kg	Added mass
$Y_{v\|v\|}$	-196.26	kg/m	Cross flow drag
$Y_{r\|r\|}$	8.30	kg m/rad^2	Cross flow drag
Y_{uv}	-38.39	kg/m	Body and rudder bouyancy
$Y_{\dot{v}}$	-42.13	kg	Added mass
$Y_{\dot{r}}$	-5.16	kg m/rad	Added mass
Y_{ur}	13.41	kg/rad	Added mass + Rudder bouyancy
$Y_{uu\delta_r}$	16.99	kg/m/rad	Bouyant force of rudder
$Z_{w\|w\|}$	-196.26	kg/m	Cross flow drag
$Z_{q\|q\|}$	-8.30	kg m/rad^2	Cross flow drag
Z_{uw}	-38.39	kg/m	Body and rudder bouyancy
$Z_{\dot{w}}$	-42.13	kg	Added mass
$Z_{\dot{q}}$	5.16	kg m/rad	Added mass
Z_{uq}	-13.41	kg/rad	Added mass + Rudder bouyancy
$Z_{uu\delta_s}$	-16.99	kg/m/rad	Rudder bouyancy

Table 2.4 : AUV hydrodynamic moment coefficients [45].

Parametre	Değer	Birim	Tanım
$K_{p\|p\|}$	-5.03	kg m^2/rad^2	Roll drag
$K_{\dot{p}}$	-0.095	kg m^2/rad^2	Added mass moment
$M_{w\|w\|}$	7.95	kg	Cross flow drag
$M_{q\|q\|}$	-24.13	kg m^2/rad^2	Cross flow drag
M_{uw}	21.89	kg	Added mass + Rudder bouyancy + Munk Momenti
$M_{\dot{w}}$	5.16	kg m	Added Mass Inetia
$M_{\dot{q}}$	-7.57	kg m^2/rad	Added Mass Inetia
M_{uq}	-16.56	kg m/rad	Added mass + Rudder bouyancy
$M_{uu\delta_s}$	-13.92	kg/rad	Rudder Bouyancy Moment
$N_{v\|v\|}$	-7.95	kg	Cross flow drag
$N_{r\|r\|}$	-24.13	kg m^2/rad	Cross flow drag
N_{uv}	-21.89	kg	Added mass + Rudder bouyancy + Munk Momenti
$N_{\dot{v}}$	-5.16	kg m	Added Mass Inertia
$N_{\dot{r}}$	-7.57	kg m^2/rad	Added Mass Inertia
$N_{uu\delta_r}$	-13.92	kg rad	Rudder Bouyancy Moment

2.5 Numerical Integration of The AUV EOM

The nonlinear differential equations defining the AUV accelerations and the kinematic equations give us the vehicle accelerations in two different reference frames. Given the complex and non-linear nature of these equations, we will use numerical integration to solve for the vehicle speed, position, and attitude in time frame [42]. Consider that at each time step, we can express nonlinear differential equation as follows:

$$\dot{x}_n = f\left(x_n, u_n\right) \tag{2.41}$$

where x is the AUV state vector:

$$x = [u \ v \ w \ p \ q \ r \ x \ y \ z \ \phi \ \theta \ \psi]^T \tag{2.42}$$

and u_n , is the input vector:

$$u_n = \left[\delta_s \ \delta_r \ \mathrm{X}_{prop} \ K_{prop}\right]^T \tag{2.43}$$

There are two common numerical iteration methods to solve the non-linear differential equation: one is *Euler*'s method and the other is Runge-Kutta method.

2.5.1 Euler's method first order

We will first consider *Euler*'s method, a simple numerical approximation that consists of applying the iterative formula:

$$x_{n+1} = x_n + f\left(x_n, u_n\right).\Delta t \tag{2.44}$$

where, Δt is the modeling time step.

Although the least computationally intensive method, *Euler*'s method is unacceptable as it can lead to divergent solutions for large time steps [42].

2.5.2 Runge-Kutta method

In this subsection, we will introduce one of the most powerful predictor-corrector algorithms —one which is so accurate, that most computer packages designed to find numerical solutions for differential equations will use it by default—the *Runge-Kutta* fourth order method. The *Runge-Kutta* method further improves the accuracy of the approximation by averaging the slope at four points [42]. We used this method to solve the nonlinear dynamic model of the AUV. In this method, numerical approximations that consist of applying the iterative formula:

$$\begin{aligned}
k_1 &= x_n + f\left(x_n, u_n\right) \\
k_2 &= f\left(x + \frac{\Delta t}{2} k_1, u_{n+\frac{1}{2}}\right) \\
k_3 &= f\left(x + \frac{\Delta t}{2} k_2, u_{n+\frac{1}{2}}\right) \\
k_4 &= f\left(x + \Delta t k_3, u_{n+1}\right)
\end{aligned} \tag{2.45}$$

where the interpolated input vector is:

$$u_{n+\frac{1}{2}} = \frac{1}{2}\left(u_n + u_{n+1}\right) \tag{2.46}$$

The combination of these two Equations (2.45 – 2.46) yields to:

$$x_{n+1} = x_n + \frac{\Delta t}{6}\left(k_1 + 2k_2 + 2k_3 + k_4\right) \tag{2.47}$$

which is simply the ***x***-value of the current point plus a weighted average of four different x-jump estimates for the interval, with the estimates based on the slope at the midpoint being weighted twice as heavily as those using the slope at the end-points [42]. For estimations of rigid-body dynamic models, the second order *Runge-Kutta* algorithm is usually adequate and hence recommended during the initial iterations of the iterative estimation algorithms, switching over the forth-order *Runge-Kutta* only during the final iteration [31].

2.6 AUV Control

Sliding-mode control (SMC) is one of the robust and nonlinear control methods. In control theory, *SMC* is a nonlinear control method that alters the dynamics of a nonlinear system by application of a discontinuous control signal that forces the system to slide along a cross-section of the system's normal behavior. The statefeedback control law is not a continuous function of time. Instead, it can switch from one continuous structure to another based on the current position in the state space. Hence, SMC is a variable structure control method [62]. Consider the problem of doing set point control for a system of the form

$$x^{(n)} = f(x) + b(x)u \qquad \textbf{(2.48)}$$

Where $x, u \in \Re$. Further, we seek a solution that is robust to uncertainties in *f(x)* and *b(x).*

Note that the system can be re-written in vector form. It is then equivalent to

$$\begin{pmatrix} \dot{x}_1 \\ \vdots \\ \dot{x}_{n-1} \\ \dot{x}_n \end{pmatrix} = \begin{pmatrix} x_2 \\ \vdots \\ x_n \\ f(x) + b(x)u \end{pmatrix}, \text{ with } x = \begin{pmatrix} \dot{x}_1 \\ \vdots \\ \dot{x}_{n-1} \\ \dot{x}_n \end{pmatrix} \qquad \textbf{(2.49)}$$

The system is a diagonal nonlinear system.

Define x_d (setpoint) and $\tilde{x}$ (the error signal) the difference between *x* and x_d.

We take a 2-step approach to designing the controller:

1. Define the *sliding mode*. This is a surface that is invariant of the controlled dynamics, where the controlled dynamics are exponentially stable, and where the system tracks the desired set-point
2. Define the control that drives the state to the sliding mode in finite time

Define the sliding mode $S(t)$ as follows:

$$S(t) = \{x | s(x,t) = 0\} \qquad \textbf{(2.50)}$$

where $s(x,t)$ is defined by

$$\mathrm{s}(x,t) = \left(\frac{\mathrm{d}}{\mathrm{dt}} + \lambda\right)^{\mathrm{n}-1} \tilde{x}(t), \lambda > 0 \qquad \textbf{(2.51)}$$

Note that on the surface $S(t)$, the error dynamics are governed by the equation

$$\left(\frac{\mathrm{d}}{\mathrm{dt}} + \lambda\right)^{\mathrm{n}-1} \tilde{x}(t) > 0 \qquad \textbf{(2.52)}$$

On this surface, the error will converge to zero exponentially. This implies that if there exists a control input u such that $x(t)$ is in *S(t)* it follows that $x(T)$ is in $S(T)$ for all *T,t* and the error will converge exponentially to *zero* for this control input. Namely, the objective of SMC is to force both error and derivative of error to the equilibrium point. Then the selected sliding surface $s(t)$, tends to zero in a finite time and the system states should remain on the surface.

In this thesis, the parameters of the controller are tuned because of avoiding complicated calculations which may cause large chattering.

The control input of course is

$$\mathrm{u} = \psi - \Delta\psi - \lambda\left(r - \Delta\dot{\psi}\right) \tag{2.53}$$

The SMC law for course control of AUV is

$$\frac{-5\pi}{18}|u|sign(u) \tag{2.54}$$

The control strategy used for physically based model of AUV is depicted in Figure 2.16, which is the Simulink model of sliding mode control of yaw (ψ).

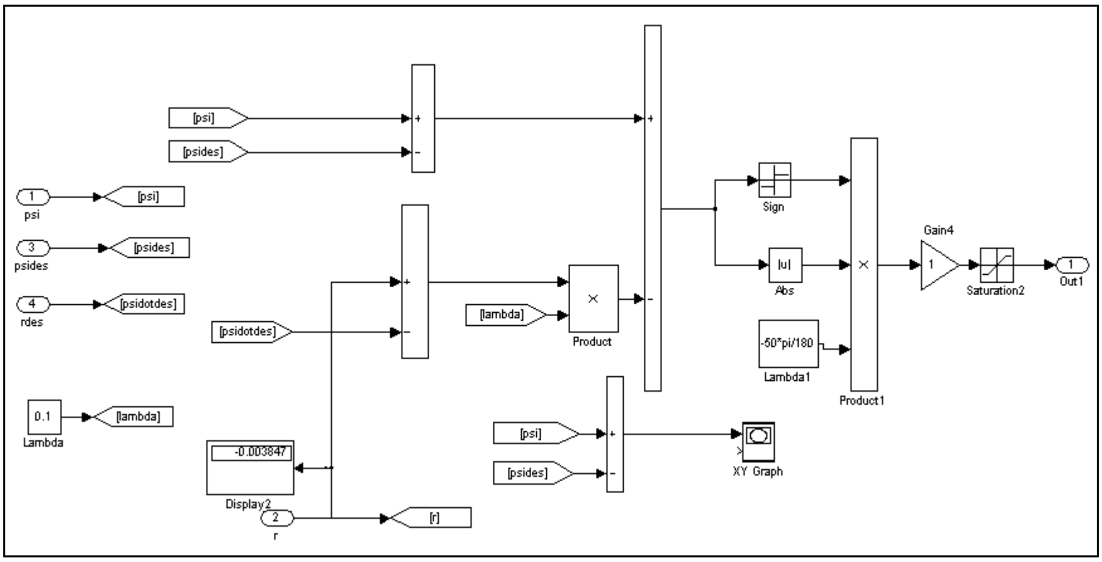

Figure 2.16 : Simulink model of sliding mode control

2.7 Dynamic Simulink Model of AUV

The data achieved from the modeling and identification process of the AUV was implemented into a vehicle which was used in a MATLAB Simulink environment. This makes it possible to simulate the behaviour of the AUV or programs without the need of a real sea environment.

The detailed AUV Simulink models are depicted in Figure 2.17. In this model, hydrodynamic, hydrostatic, gravitational, and kinematic EOM of AUV and sliding mode control are implemented in the MATLAB version 7.5 Simulink environment.

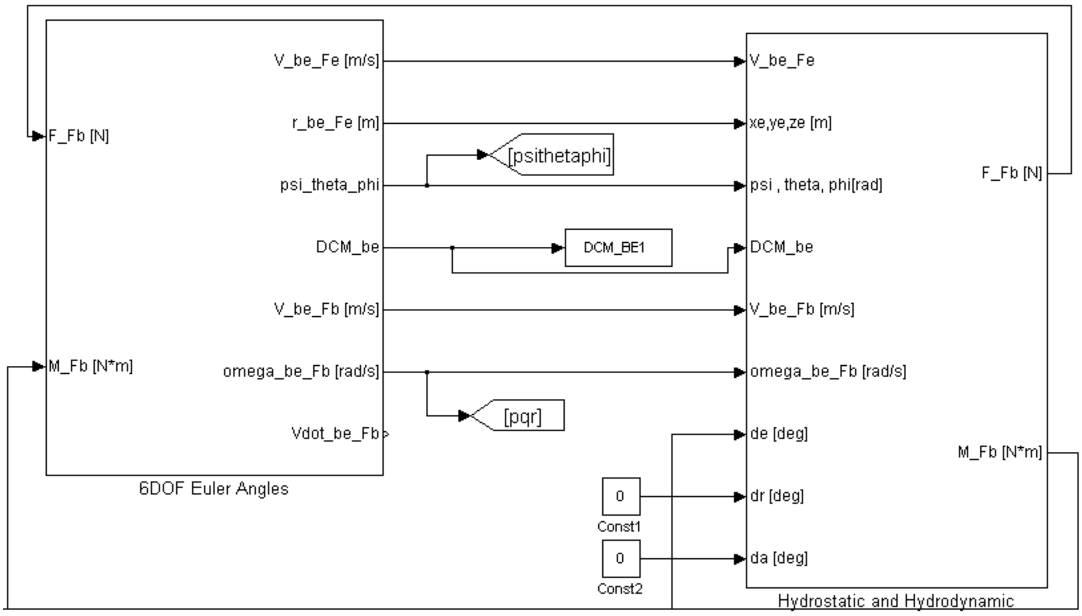

Figure 2.17 : Full AUV Simulink model and sliding mode control.

2.8 Simulation Results

The simulation of the dynamic model is developed by using the MATLAB version 7.5 Simulink environment. Numerical simulations are made to show the dynamic model of the AUV.

In Figure 2.20 and 2.21, the AUV dynamic model simulation results are shown. For this simulation, the AUV has a maneuver speed of 8 m/s and rudder angle applies to 10 deg. From the start, elevator angle applies to 1 deg, and the simulation time is 50 sec.

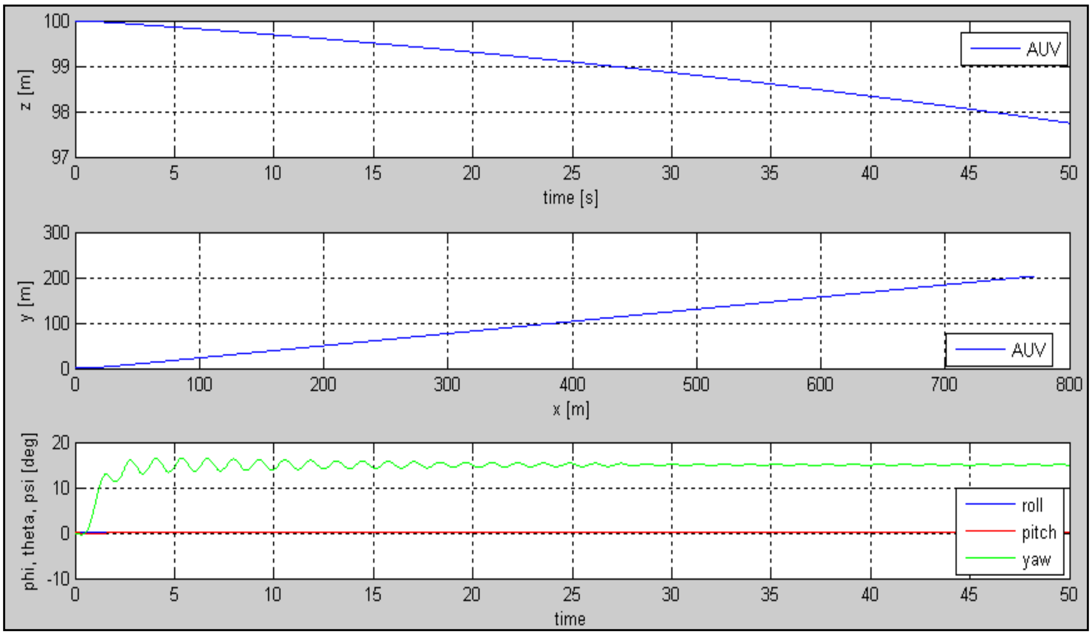

Figure 2.18 : Simulation results of *x*, *y*, *z*, roll, pitch and yaw angles (50 sec.).

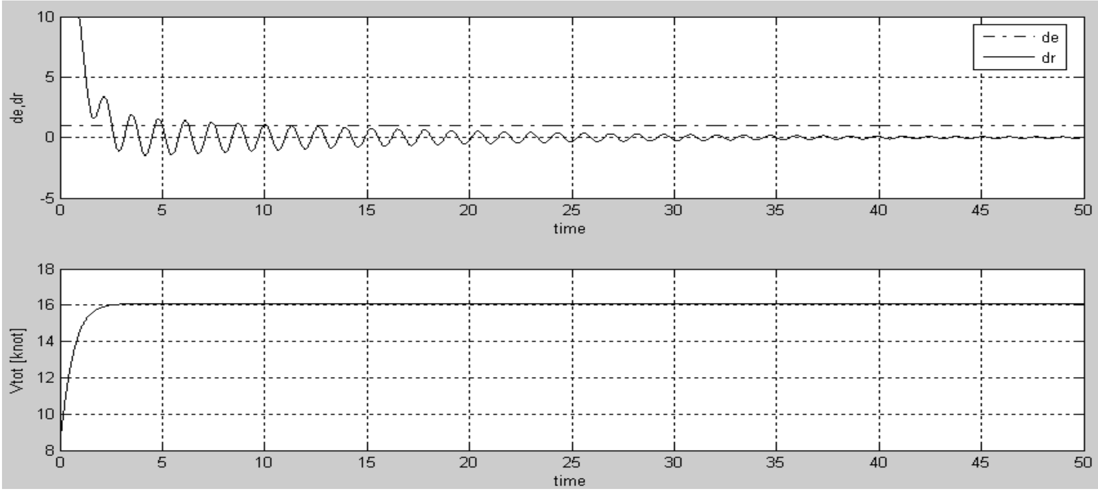

Figure 2.19 : Simulation results of V_tot, δr and δe (50 sec.).

.

3. DEVELOPMENT OF INS MODEL

3.1 Purpose

The aim of this chapter is to explain how to develop an INS, which is the main navigational component applied to nonlineer dynamic model of AUV. The key element of the AUV navigational system is INS, which is accomplished by integrating the output of a set of sensors (including gyros and accelerometers) to compute position, velocity, and attitude.

Typically, INS is a self-contained system with high short-term stability and is not influenced by interference. INS is a stand-alone navigational system using motion sensors to continuously keep track of position, orientation and velocity of a vehicle [48]. An INS contains an Inertial Measurement Unit (IMU), including an accelerometer and a gyroscope for all three axes, measuring the linear acceleration and angular velocity of a vehicle with a 6-DOF. By processing signals from these sensors, it is possible to track the position and orientation of a device. The INS system is usually mounted in a gimbaled or strap-down, using updating algorithms based on *Euler* angles, kinematics and integration to keep track of position and orientation. Without requiring any external references, an INS determines vehicle's position, orientation, or velocity once it has been initialized. The major drawback of inertial navigational is that initialization and sensor errors cause the computed quantities to drift [51]. Therefore, INS does not indicate position perfectly because of errors in components (the gyroscopes and accelerometers) and therefore produces errors in the model of the gravity field that the INS implements.

Today, INS is commonly used in a wide range of vehicles such as: airplanes, ships, cars, submarines, UAVs, UUVs, and guided missles and bombs. Recent technological advances in the construction of Micro-Electro-Mechanical System

(MEMS) devices have made it possible to manufacture small, low cost, and light weight INSs [48].

3.2 Inertial Measurement Unit

The INS is based on measurements of vehicle specific forces and rotation rates obtained from on-board instrumentation consisting of triads of gyros and accelerometers that create an IMU. These inertial sensors have for decades served as essential navigational tools especially in the aerospace industry. In Figure 3.1, an example of MEMS IMU sensor is shown. Recent advancements in MEMS technology enabled production of low-cost inertial sensors. Therefore, the application area of these sensors quickly expanded particularly in the automotive, robotics, AUV, and UAV industries.

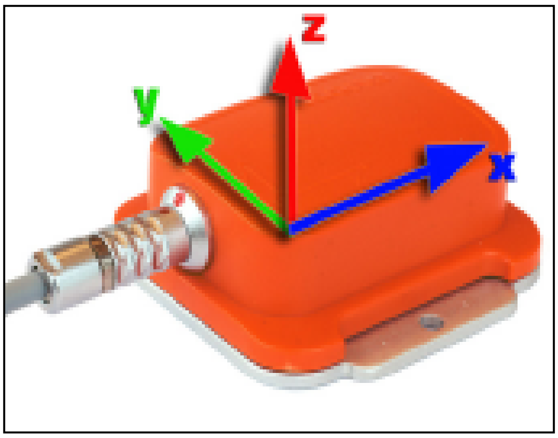

Figure 3.1 : Xsens MEMS IMU system [53].

Inertial sensors are non-jammable, non-radiating, and self-consistent, so they cannot be disturbed by any external factors and do not affect anything else around themselves. However, even in the highest quality MEMS inertial sensors which are used in AUVs, there are still errors corrupting useful data. Whether the inertial sensor error is caused by internal mechanical imperfections, electronics errors, or other sources, the effect is to cause errors in the indicated outputs of these devices. For the gyros, the major errors are in measuring angular rates. For the accelerometers, the major errors are in measuring acceleration [45]. For both instruments, the largest errors are usually a bias instability (measured in deg/hr for gyro bias drift or micro g (μg) for the accelerometer bias), and scale-factor stability (which is usually measured in parts per million (*ppm*) of the sensed inertial quantity) [52]. The smaller the inertial sensor errors we have, the better the quality of the instruments, the improved accuracy of the resulting navigation solution, and the higher the cost of the system.

3.2.1 Rate gyros

Rate gyros are sensors that measure angular velocities in contrast to attitude angles measured by free gyros, which are typically mounted in gimbaled platforms. Rate gyros sense the vehicle's angular rate relative to the inertial space [53]. These rate components are the craft angular rate relative to the Earth ω_{nb}, a angular rate as it moves about the spherical Earth ω_{en} and the angular rate of the Earth itself ω_{ie}. The vector sum of these angular rates ω_{ib} is given by:

$$\omega_{ib}^b = \omega_{ie}^b + \omega_{en}^b + \omega_{nb}^b \qquad \textbf{(3.1)}$$

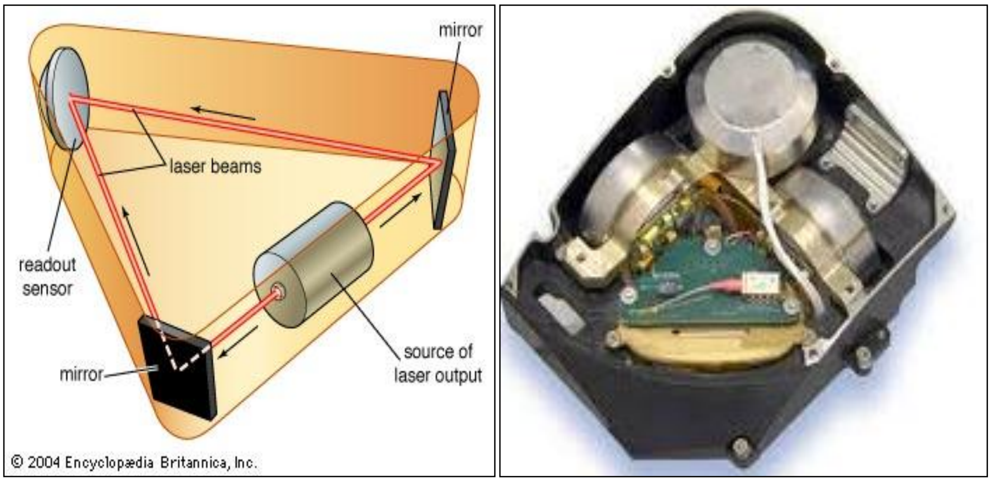

(a) (b)

Figure 3.2 : a) Ring laser gyro. **b)** Fibre optic gyro [56].

There are three types of gyro technology used in today's IMU systems:

- Ring Laser Gyro (RLG).
- Fibre Optic Gyro (FOG).
- MEMS.

The RLG has recently seen increased usage in strap-down navigational system mechanizations. Most current RLG sensors are single DOF sensors requiring three mechanizations for an INS implementation. A single DOF RLG is shown schematically in Figure 3.2 : (a). This figure illustrates a triangular version on the RLG. The gyro includes a laser as a source, a closed-path cavity, mirrors at each intermediate corner in the path, and an interferometer / photodetector. The operation of the gyro is based on optical and electronic phenomena rather than the mechanical phenomena.

On the other hand, the FOG is a maturing gyro technology. FOGs in comparison to RLGs require no mechanical dither for their operation and thus eliminate a troublesome noise source. They do not require high voltage for the laser plasma, hence reduce power consumption; and, with the exception of a laser diode for the light source are composed of passive optical components and thus yield extremely high reliability compared to any other available technology [55]. A typical FOG is shown in Figure 3.2 : (b).

As a “rule-of-thumb,” an INS equipped with gyros whose bias stability is 0.01 deg/hr will see its navigational error grow at a rate of 1 nmi/hr of operation [48]. Solid-state inertial sensors, such as MEMS devices, have potentially significant cost, size, and weight advantages. The MEMS and Interferometric FOG (IFOG) technologies are expected to replace many of the current systems using RLGs and mechanical instruments. However, one particular area where the RLG is expected to retain its superiority over the IFOG is in applications requiring extremely high scale-factor stability [48]. The change to all-MEMS technology hinges primarily on MEMS gyro development. The performance of MEMS sensors is continually improving, and they are currently being developed for many applications. This low cost device can only be attained by leveraging off the consumer industry, which will provide the infrastructure for supplying the MEMS sensors in extremely large quantities. The use of these techniques will result in low-cost, high-reliability, small-size, and light-weight inertial sensors into the systems which they will be integrated.

3.2.2 Accelerometers

Accelerometers in comparison to gyros have more mature technology. An accelerometer is a device that converts acceleration into an electrical signal. Both dynamic and static acceleration can be measured using an accelerometer where dynamic acceleration is the acceleration due to any force except for the gravitational force applied on a rigid body and the static acceleration (or gravitational acceleration) is due to the gravitational force. The output of an accelerometer can be analog or digital. In the analog case, the output voltage or the duty cycle of a square wave is directly proportional to the acceleration. On the one hand, the output of a digital accelerometer can be directly accessed using protocols such as serial interfaces [3]. The principle of accelerometer is illustrated simply in Figure 3.3.

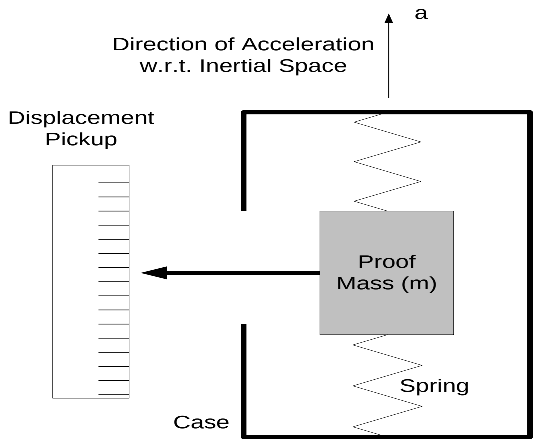

Figure 3.3 : Principle of accelerometer [52].

The accelerometer is a specific force sensor that senses both AUV inertial acceleration a_i, and the gravitational field vector g_m which is the force of mass attraction to the Earth. Therefore the accelerometer sensed AUV specific force a**,** is given by

$$a = a_i - g_m \tag{3.2}$$

3.3 INS Framework and Design

The INS employs a dead-reckoning algorithm that computes attitude, velocity and position based on the inertial sensors. The idea behind the INS is simply to integrate accelerometer signal to determine velocity, and position in a desired coordinate system and to integrate gyro signals to determine attitude information [53]. However, The INS has poor accuracy in the long term, which arises from the unbounded growth in the position and velocity errors due to the integration of inertial measurements containing various forms of errors.

INS typically has the properties of

- initialization is needed.
- high position and velocity accuracy over the short term.
- accuracy decreasing with time.
- affected by gravity.
- high measurement output rate.
- not affected by electromagnetic interference.
- autonomous.

The position and velocity of the vehicle is predictable for all times. It is when changes in motion occur that the concept of forces comes into play. Two types of forces determine the motion of a vehicle: gravity and inertia. Gravitational mass has been described as being like a charge the object feels in proportion to its gravitational mass, whereas inertial mass describes the resistance of a vehicle to changing the state of motion. There are a number of inertial forces. The most commonly encountered are thrust, lift, and drag [10].

The major drawbacks of inertial navigational are initialization and sensor errors, which cause the computed quantities to drift. INS donot indicate position perfectly because of errors in components (the gyroscopes and accelerometers) and errors in the model of the gravity field that the INS implements. Those errors cause the error in indicated position to grow with time [45]. For vehicles with short mission times, such errors might be acceptable. For longer missions, it is usually necessary to provide periodic updates to the navigational system such that the errors caused by the inertial system are reset as close to zero as possible [10].

For an INS, the navigational equation of a vehicle based on the Earth-center-Earth fixed reference coordinates can be obtained with the differential equations from the instrument coordinates, considering the frame rotation and acceleration, coordinate transformation, and sensor error dynamics. In the navigational frame mechanism, the ground speed is expressed in the navigational coordinates to give *Vx*, *Vy*, and *Vz* velocities. The rate of change of velocities with respect to navigational axes can be expressed in terms of its rate of change in inertial axes. The rate of change in x, y and z can be expressed in terms of the Earth radius and the speed of the vehicle in the navigational coordinate [36].

The diagram in Figure 3.4 briefly depicts the computational flow of the inertial navigation equations that we used in this study. The main input data to this diagram are the three gyros ($\omega^b{}_{ib}$) and accelerometer (a^b) measurements in 6-DOF of the body frame. The Earth spin rate ($\omega^e{}_{ie}$) is assumed as a constant input to the system. The gravity vector (g^n) is aslo shown as an input, which would be constant if it does not vary significantly. Otherwise it will be computed as a function of height (h) and the Earth's latitude (Φ). Finally, the data flow in this diagram merely shows the variable interdependence but not necessarily the actual computation in the navigational computer.

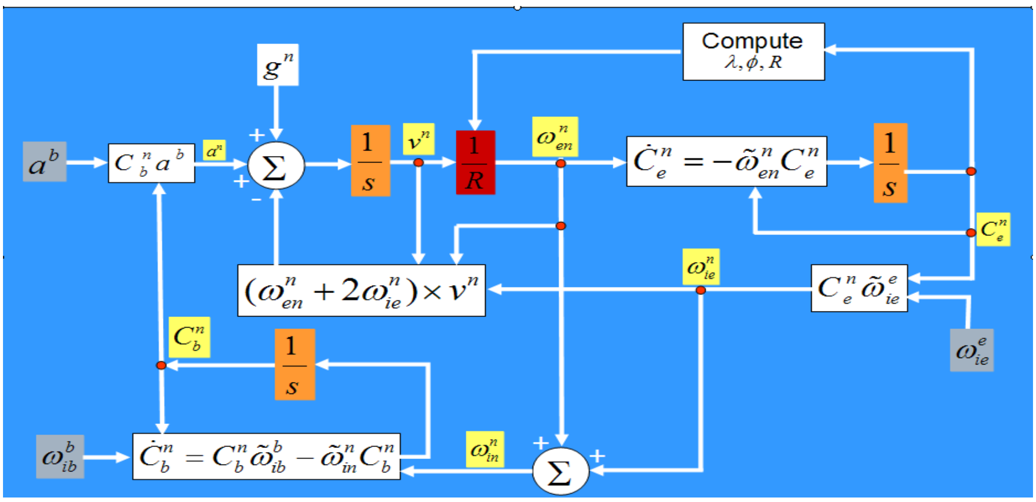

Figure 3.4 : INS framework [3].

As depicted in Figure 3.4 : above, the essential functions of an INS may be defined as follows [3]:

- Determination of the angular motion of a vehicle using gyroscopes, from which its attitude is relative to a reference frame may be derived.
- Measure specific forces using accelerometers.
- Resolve the specific force measurements into the reference frame using the knowledge of attitude derived from the information provided by the gyroscopes.
- Evaluate the force resulting from the gravitational field – the gravitational attraction of the Earth in the case of systems operating in the vicinity of the Earth.
- Integrate the resolved specific force measurements to obtain estimates of the velocity and position of the vehicle.

The INS framework in Figure 3.4 :5 below is implemented in MATLAB version 7.5 Simulink environment. This INS module is used as a main navigational tool applied to AUV dynamic model.

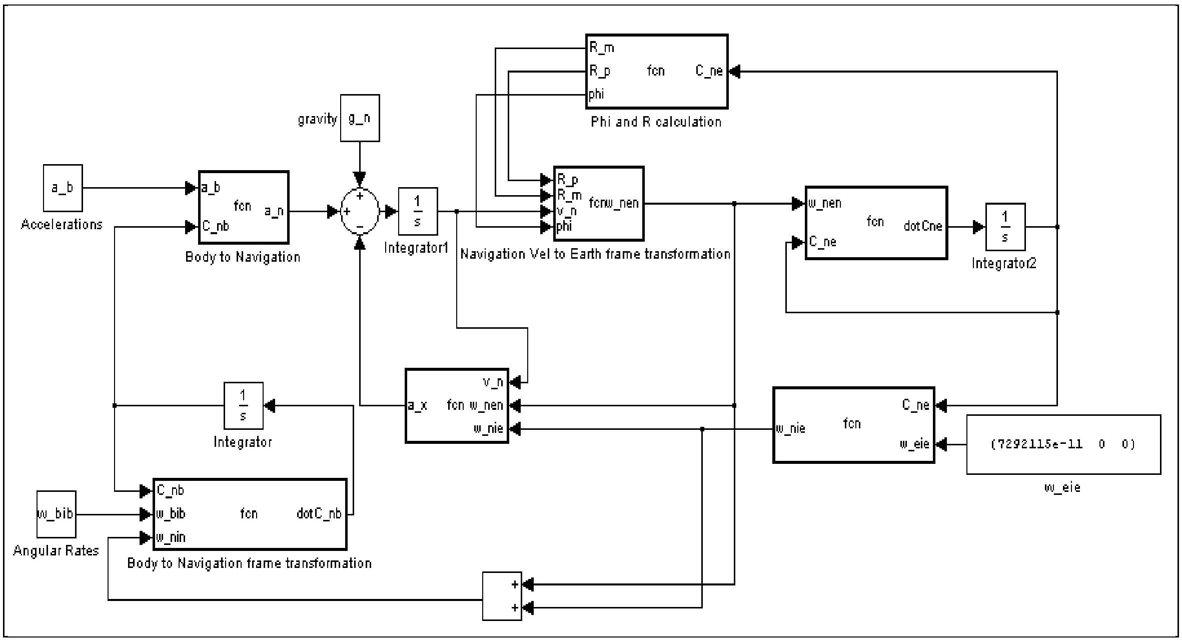

Figure 3.5 : INS Simulink model.

4. DEVELOPMENT OF THE INTEGRATED AUV NAVIGATIONAL SYSTEM

4.1 Objectives

The goal of this chapter is to explain how to develop an Integrated AUV Navigational System. AUVs require a precise navigation system for localization, positioning, path tracking, guidance, and control. In the following paragraphs, we will try to explain how to achieve a more accurate and reliable navigational system for AUVs by combining multi-sensor data based on the Kalman filtering technique.

For decades, GPS and INS are the standard navigational systems, which are widely used in surveying or service and maintenance applications that requires the most accurate navigational information [6]. However, underwater navigation requires different kinds of sensors than commonly used airborne or land vehicle navigational applications due to the limited usage of GPS signals in the water [39].

Primarily, the challenge in INS is maintaining the accuracy of an AUV's position over the course of a long mission time. An initially accurate position can quickly become uncertain through maneuvers and variations in the AUV's motion. As mentioned earlier, the key problem of INS is that it exhibits position errors that grow unbounded with time, which are caused by the accumulation of gyro and accelerometer errors over time, as well as oscillatory velocity errors [3]. During the long duty cycle, these inaccuracies become significant. Strong sea currents and other underwater phenomena affect the motion of the AUV. This therefore cannot be precisely modeled because data will be skewed by greater inaccuracies.

Any AUV navigational system that requires accurate navigation over long duty cycle must use an external sensor reference. Mainly for this reason, in long-term AUV navigational applications, the INS is often used in conjunction with various navigational aids: such as acoustic devices, compass, pressure depth sensor, DVL, terrain-based techniques, and surface GPS [7]. Additionally, the improvements in computer technology and increased data processing rates brought the ability to improve the navigational systems of both air and underwater vehicles in precision, robustness, correctness, and reliability.

4.2 Integrated AUV Navigational System Framework

We developed an Integrated AUV navigational system solution, which is illustrated in Figure 4.1. In the left hand side of this framework, the IMU inputs with its gyros and accelerometers exist. The navigational equations read these three gyros and three accelerometers with a 100 Hz or more data rate. Based on these measurements; the navigational equations resident in the INS calculate the change in position, velocity and attitude. Due to noise and errors in the readings, errors in the calculation increase with time if it is not corrected for. To the right, we see the KF. It estimates the attitude, velocity, position, and sensor errors. It also calculates the accuracy of each estimate. The input to the KF is the difference between the values calculated by the navigational equations and the external aiding devices` measurements such as the compass, DVL, and pressure sensor.

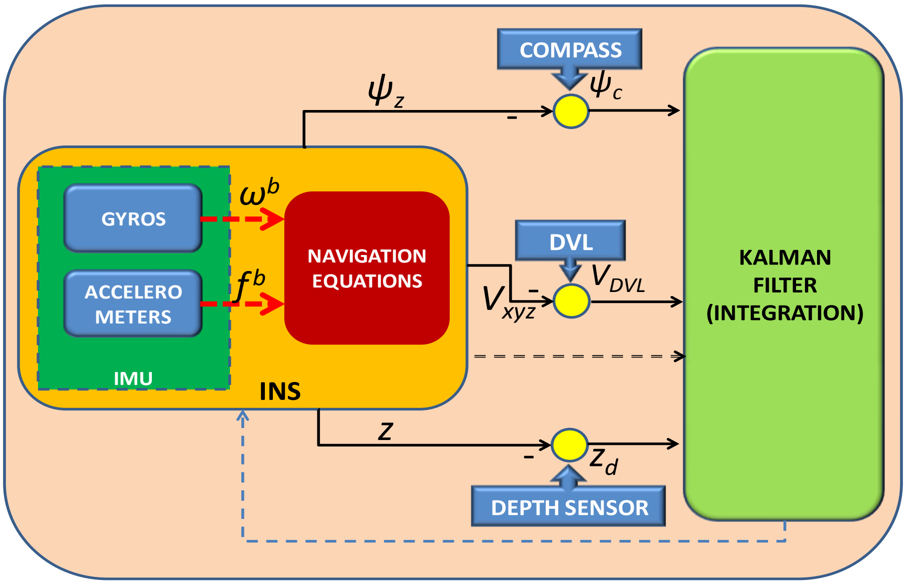

Figure 4.1 : Integrated AUV navigational system solution.

4.3 Navigational Aiding Devices

The navigational system of UVs plays a crucial role together with the sensor architecture in the degree of system autonomy that can be achieved. A typical navigational sensor outfit for an AUV may consist of standard components such as a compass, pressure depth sensor, and some class of INS [45]. In the following subsections, we briefly explain the aiding devices of DVL, compass, and pressure depth sensor that we used in this study.

4.3.1 Doppler velocity logger

One of the most important devices that has been developed to aid the INS is the Doppler Velocity Log (DVL). The DVL is a sonar used to measure both speed and height above the sea bottom, and relies on the Doppler effect. The DVL measures ground velocity in the vehicle frame and since the heading is known from the INS; the incremental change of position in the geographic frame can be calculated. In practice the longer-term position error will eventually grow to an unacceptable level and this is a general drawback of pure dead reckoning techniques. It should be noted however, that sea currents do not influence DVL/INS integrated navigation since the DVL can measure the true ground speed [45]. This is the main advantage of DVL.

Figure 4.2 : Doppler velocity log [12].

Since the DVL works properly the distance to the bottom must be limited, which varies from a maximum of 30 m to 200 m of depth, depending on the frequency of sound emmited by the DVL. However, the DVL can only generate accurate velocity measurements as long as the distance to the seafloor is within a certain boundary depth.

4.3.2 Pressure depth sensor

Depth sensor, which measures the water pressure from sea surface, gives the vehicle’s depth. At depths beyond a few hundred meters, the equation of the state of seawater must be invoked to produce an accurate depth estimate based on the ambient pressure. With a high-quality sensor, these estimates are reliable and accurate, giving a small error of order 0.01%.

A pressure sensor is determined by calculating the static pressure head (also called elevation head) [21]:

$$h = \mathrm{p}/\rho \mathrm{g} \tag{4.1}$$

where

h = depth below the still water surface
p = pressure
ρ = density
g = gravitational acceleration

4.3.3 Compass

A compass measures the heading or direction of the vehicle it sits on. Tpically, there are two types of compass: gyrocompass and magnetic. A gyrocompass can provide an estimate of geodetic north accurate to a fraction of a degree. Magnetic compasses can provide estimates of magnetic north with an accuracy of less than 1° if carefully calibrated to compensate for magnetic disturbances from the vehicle itself. Tables or models can be used to convert from magnetic north to geodetic north.

4.4 Error Models of INS and Its Aiding Devices

In the following subsections, we explain the error models used for the INS and its aiding devices in this study.

4.4.1 INS error model

Error analysis of INS not only affects the accuracy of various types of data which is provided by the INS, but also the basis of theory and practice of various sections. The error source of INS sensors are commonly measurement errors, acceleration-dependent biases, scale factor errors, nonlinearity, axis misalignment, and gyro sensitivity to the force applied. The errors of inertial sensors and gyros of an INS can generally be modeled as a combination of random bias and random noise [37].

The INS error model simulates IMU measurement data. The simulation is based on parameterisation of the general IMU errors. The error model includes noise, bias, scaling, (cross) coupling and quantisation of both the gyro and the accelerometer.

The perturbation method is used to derive the error equation of the INS algorithm. The perturbation method analyzes the navigational system by defining the error as the difference between the estimated and true values. For a nonlinear system, this method can be applied when the error is small. In this study, the error model of INS is derived consisting of nine parameters, which includes three potion error (*x*, *y* and *z*), three linear velocities (V_x ,V_y, and V_z) and ψ_x, ψ_y, and ψ_z are the attitude errors of the vehicle with respect to the navigation coordinates along the *x*, *y*, and *z* direction, respectively. Assuming the errors exist in the position, velocity, and attitude error, the perturbation method induces the corresponding differential equations:

$$\Delta\dot{x}_{\mathrm{INS}} = \Delta V_x + \left(\frac{\mathrm{V_x}}{\mathrm{R}}\tan\varphi\right)\Delta \mathrm{y} + \frac{\mathrm{V_x}}{\mathrm{R}}\Delta x \tag{4.2}$$

$$\Delta\dot{y}_{\mathrm{INS}} = \Delta V_y - \left(\frac{\mathrm{V_x}}{\mathrm{R}}\tan\varphi\right)\Delta \mathrm{x} + \frac{\mathrm{V_x}}{\mathrm{R}}\Delta x \tag{4.3}$$

$$\Delta\dot{z}_{\mathrm{INS}} = \Delta V_z - \left(\frac{\mathrm{V_y}}{\mathrm{R}}\tan\varphi\right)\Delta \mathrm{x} + \frac{\mathrm{V_x}}{\mathrm{R}}\Delta x \tag{4.4}$$

$$\Delta\dot{V}_{x_{\mathrm{INS}}} = -\frac{\mathrm{g}}{R}\Delta x + \left(2\omega_{ie}\sin\varphi + \frac{\mathrm{V_x}}{\mathrm{R}}\tan\varphi\right)\Delta V_{\mathrm{y}} + \left(2\omega_{ie}\cos\varphi + \frac{\mathrm{V_x}}{\mathrm{R}}\right)\Delta V_z + \mathrm{a}_z\psi_{\mathrm{y}} - \mathrm{a}_y\psi_z + \nabla_x \tag{4.5}$$

$$\Delta\dot{V}_{y_{\mathrm{INS}}} = -\frac{\mathrm{g}}{R}\Delta y - \left(2\omega_{ie}\sin\varphi + \frac{\mathrm{V_x}}{\mathrm{R}}\tan\varphi\right)\Delta V_{\mathrm{x}} + \frac{\mathrm{V}_y}{\mathrm{R}}\Delta V_z + \mathrm{a}_x\psi_z - \mathrm{a}_z\psi_x + \nabla_y \tag{4.6}$$

$$\Delta\dot{V}_{z_{\mathrm{INS}}} = 2\frac{\mathrm{g}}{R}\Delta z - \frac{\mathrm{V}_y}{\mathrm{R}}\Delta V_y - \left(2\omega_{ie}\cos\varphi + \frac{\mathrm{V_x}}{\mathrm{R}}\right)\Delta V_{\mathrm{x}} + \mathrm{a}_y\psi_x - \mathrm{a}_x\psi_y + \nabla_z \tag{4.7}$$

$$\dot{\psi}_{x_{\mathrm{INS}}} = \left(\omega_{ie}\sin\varphi + \frac{\mathrm{V_x}}{\mathrm{R}}\tan\varphi\right)\psi_{\mathrm{y}} + \left(\omega_{ie}\cos\varphi + \frac{\mathrm{V}_x}{\mathrm{R}}\right)\psi_z + \varepsilon_{\mathrm{x}} \tag{4.8}$$

$$\dot{\psi}_{y_{\mathrm{INS}}} = -\left(\omega_{ie}\sin\varphi + \frac{\mathrm{V_x}}{\mathrm{R}}\tan\varphi\right)\psi_x + \frac{\mathrm{V}_y}{\mathrm{R}}\psi_z + \varepsilon_y \tag{4.9}$$

$$\dot{\psi}_{z_{\mathrm{INS}}} = -\frac{\mathrm{V}_y}{\mathrm{R}}\psi_y - \left(\omega_{ie}\cos\varphi + \frac{\mathrm{V}_x}{\mathrm{R}}\right)\psi_x + \varepsilon_z \tag{4.10}$$

The output errors of gyros $\varepsilon_x, \varepsilon_{\mathrm{y}}, \varepsilon_z$ and those of accelerometers $\nabla_x, \nabla_y, \nabla_z$ of IMU can be expressed as the first-order Markov process variables and white noise vector

$$\dot{\varepsilon}_x = -\beta_{\text{gyro}}\varepsilon_x + w_{gx} \tag{4.11}$$

$$\dot{\varepsilon}_y = -\beta_{\text{gyro}}\varepsilon_y + w_{gy} \tag{4.12}$$

$$\dot{\varepsilon}_z = -\beta_{\text{gyro}}\varepsilon_z + w_{gz} \tag{4.13}$$

$$\dot{\nabla}_x = -\beta_{\text{acc}}\nabla_x + w_{ax} \tag{4.14}$$

$$\dot{\nabla}_y = -\beta_{\text{acc}}\nabla_y + w_{ay} \tag{4.15}$$

$$\dot{\nabla}_z = -\beta_{\text{acc}}\nabla_z + w_{az} \tag{4.16}$$

$$w_g(t) \sim N(0, Q_g), \quad w_a(t) \sim N(0, Q_a) \tag{4.17}$$

The bias errors of the accelerometers $\nabla_x, \nabla_y, \nabla_z$ and gyros $\varepsilon_x, \varepsilon_y, \varepsilon_z$ are assumed to be random constant drift, which are irregular values decided when the sensors are turned on. Furthermore, the random measurement errors of gyros w_{gx}, w_{gy}, w_{gz} and accelerometers w_{ax}, w_{ay}, w_{az}, are assumed to be white noise [66]. Finally, β_{acc} and β_{gyro} are correlative time constants of accelerometers and gyros respectively.

4.4.2 Error models of aiding devices

Auxiliary navigational sensors can improve the navigational performance and accuracy by correcting the state variables in the navigational equation. The auxiliary navigational sensors that is the pressure depth sensor, DVL, and the magnetic compass are good complementary sensors for the INS. In this study, we modeled the errors of the auxilary devices as the summation of random constants, white noises, and the first order Markov process similar to the accelerometers and the gyros [36]. We assumed that the random constants of the biases are unknown but the variances of the initial values are known.

According to the principle of DVL, it measures the velocity and log angle relative to the seabed. The measuring error consists of the velocity offset error, log misalignment angle error expressed by first-order Markov process, and the scale coefficient error, which is a random constant drift [66]. After the appropriate coordinate transformation, DVL velocities are expressed in *x*, *y* and *z* on the Earth's fixed coordinate system. The measuring DVL velocity errors are expressed:

$$\dot{\nabla}_{Vx_{dvl}} = -\beta_{x_{dvl}} \nabla_{Vx} + w_{x_{dvl}} \qquad \textbf{(4.18)}$$

$$\dot{\nabla}_{Vy_{dvl}} = -\beta_{y_{dvl}} \nabla_{Vy} + w_{y_{dvl}} \qquad \textbf{(4.19)}$$

$$\dot{\nabla}_{Vz_{dvl}} = -\beta_{z_{dvl}} \nabla_{Vz} + w_{z_{dvl}} \qquad \textbf{(4.20)}$$

$$w_{DVL}(t) \sim N(0, Q_{DVL}) \qquad \textbf{(4.21)}$$

where

$\beta_{x_{dvl}}, \beta_{y_{dvl}}, \beta_{z_{dvl}}$ ---correlative time constants of velocities,

$w_{x_{dvl}}, w_{y_{dvl}}, w_{z_{dvl}}$ ---stimulating Gaussian white noises.

Similarly, the error model of pressure the depth sensor and magnetic compass used in this study are expressed as the summation of random bias and white noises. The pressure measurement is modelled as the correct water depth with superimposed white noise. Correspondingly, the heading measurement is modelled as the correct direction of the vehicle with superimposed Gaussian white noise.

$$\Delta_{z_d} = Bias_{z_d} + \mathrm{w}_{z_d} \qquad \textbf{(4.22)}$$

$$\Delta_{\psi_{com}} = Bias_{\psi_{com}} + w_{\psi_{com}} \qquad \textbf{(4.23)}$$

Where, $\omega_{z_d}, \omega_{\psi_{com}}$ --- Gaussian white noises.

4.5 Kalman Filter Techniques

4.5.1 Objectives

The goal of this section is to explain the Kalman Filter (KF) algorithm and how to develop a KF for Integrated AUV Navigational System that consists of an error-state KF that estimates the drift parameters in the inertial sensors, using the external information as the measurement vector [21].

KF was first improved by Rudolf Emil Kalman in 1960 to estimate the linear dynamic of a system. The least mean-square estimation approach of random parameters is the foundation of KF [33]. The optimality criterion of KF comes from the criterion of minimizing the state variable error standard deviation [42].

Today, KF techniques are widely used in many real world applications, i.e., navigation, sensor fusion, state estimation, tracking land, air and underwater vehicles, computer vision applications, economics, weather forecasting, earthquake prediction, deformation monitoring in geodesy, and dynamic and kinematics monitoring of objects.

A distinctive feature of a KF is that its mathematical formulation is described in terms of state-space concepts. Another novel feature of a KF is that its solution is computed recursively. In particular, each updated estimate of the state is computed from the previous estimate and the new input data, so only the previous estimate requires storage [1]. In addition to eliminating the need for storing the entire past observed data, a KF is computationally more efficient than computing the estimate directiy from the entire past observed data at each step of the filtering process.

4.5.2 Optimal linear kalman filter

The linear KF is a set of mathematical equations that provides an efficient recursive computational solution of the least-squares estimation. The KF is very powerful in several aspects and supports estimations of past, present, and even future states. Additionally, the KF is an algorithm for the computation of best estimates of system variables arising from sensor-based data and a dynamic system model. The algorithm is a recursive algorithm that is well suited to the use of digital computers. Essentially, the data from measurements together with a measurement model are used in a system model to provide the least squares fit estimate of system states based on those measurements [58].

KF is widely used in the processing of navigational problems. This filter is used for:

- Minimizing the measurement errors and obtaining more accurate measurement values.
- Mixing various information sources.
- Obtaining non-measurable state variables of a vehicle.

- Diagnosing of noises in a vehicle.

Let us consider the discrete linear dynamical system. The state equation statesthe dynamics of the system, and the observation equation states the measurement mechanism. These equations are written below for the linear system:

State equation of KF:

$$x(k+1) = \phi(k+1,k)x(k) + G(k+1,k)w(k) \tag{4.24}$$

Where $x(k)$ is the n dimensional system state vector. $\phi(k+1,k)$ is its *nxn* dimensional transfer matrix, $w(k)$ is the r dimensional zero-mean Gaussian noise vector (process noise), with the correlation matrix $E[w(k)wT(j)]Q(k)\delta(kj)$, in which E is stochastic mean operator and $\delta(kj)$ is the Kroenecker delta symbol.

$$\delta(kj) = \begin{cases} 1, & k = j \\ 0, & k \neq j \end{cases} \tag{4.25}$$

Finally, $G(k+1,k)$ is the *nxr* dimensional transfer matrix of system noise.

Observation or measurement equation of KF:

$$z(k) = H(k)x(k) + v(k) \tag{4.26}$$

Where $z(k)$ is s dimensional observation vector, $H(k)$ is *sxn* dimensional observation matrix, $v(k)$ is s dimensional noise vector of the measurements with zero-mean Gaussian noise, and the correlation matrix is $E[w(k)vT(j)] = 0,\ Vk,\ j$.

However, there is no correlation between process noise $w(k)$ and measurement noise $v(k)$. When desired to estimate the state vector due to the $z(k)$ observation vector sequences, the linear filter method based on the KF approach should be used.

The optimal evaluation algorithm of the linear discrete system state vector is expressed with the following equations:

$\hat{x}(k/k)$ is the state estimation:

$$\hat{x}(k/k) = \phi(k,k-1)\hat{x}(k-1/k-1) + K(k)[z(k) - H(k)\phi(k,k-1)\hat{x}(k-1/k-1)]$$
$$\hat{x}(k/k) = \hat{x}(k/k-1) + K(k)\tilde{z}(k/k-1) \quad \textbf{(4.27)}$$

K(k) is the KF gain:

$$K(k) = P(k/k)H^T(k)R^{-1}(k)$$
$$K(k) = P(k/k-1)H^T(k)[H(k)P(k/k-1)H^T(k) + R(k)]^{-1} \quad \textbf{(4.28)}$$

Correlation matrix $P(k/k)$ of KF estimate error is:

$$P(k/k) = P(k/k-1) - P(k/k-1)H^T(k)[H(k)P(k/k-1)H^T + R(k)]^{-1}H(k)P(k/k-1) \quad \textbf{(4.29)}$$

Correlation matrix of extrapolation error:

$$P(k/k-1) = \phi(k,k-1)P(k-1/k-1)\phi^T(k,k-1)Q(k-1)G^T(k,k-1) \quad \textbf{(4.30)}$$

Initial conditions: $\hat{x}(0/0) = \overline{x(0)}$
$P(0/0) = P(0)$

The optimal filter algorithm stated in equations (4.27)-(4.30) is called the KF; the following equivalent equations are also valid for $K(k)$ and $P(k/k)$;

$$K(k) = P(k/k)H^T(k)R^{-1}(k)$$
$$P(k/k) = [I - K(k)H(k)]P(k/k-1)$$
$$P(k/k) = [P^{-1}(k/k-1) + H^T(k)R^{-1}(k)H(k)P(k/k-1)]^{-1} \quad \textbf{(4.31)}$$
$$P(k/k) = P^{-1}(k/k-1)[I + H^T(k)R^{-1}(k)H(k)P(k/k-1)]^{-1}$$

where *I* is the unity matrix.

$$\Delta(k) = z(k) - H(k)\hat{x}(k/k-1) \quad \textbf{(4.32)}$$

Expression (4.32) is called an innovation process $\Delta(k)$, and after rearranging Equation (4.27), we obtain;

$$\hat{x}(k/k) = \hat{x}(k/k-1) + K(k)\Delta(k) \quad \textbf{(4.33)}$$

x(0) and *P(0)* are initial conditions that is known. In this algorithm, *P(k/k)* is the error covariance and *Q(k)* is the process noise covariance. The gain matrix *K(k)* is determined from the Riccati equation and the measurement noise covariance *R(k)* is determined by satisfying the Lyapunov function of error. In practice, the process noise covariance *Q(k)* and measurement noise covariance *R(k)* matrices might change with each time step or measurement, therefore for this study we assume they are constant [58].

Based on the formula (4.33), the estimation is the sum of the $\hat{x}(k/k-1)$ extrapolation value and the $K(k)\tilde{z}(k/k-1)$ correction difference. The extrapolation value is obtained by the multiplication of the value of previous steps by the system transfer matrix. Then, the extrapolated value is give an innovation. Namely, The KF works on the principle of innovating the estimated value.

The process of the evolution of the KF estimate in time is demonstrated in Figure 4.3 :. Typical KF cycles involve the following processes:

- Estimation of the value one step further(finding of the extrapolation value) $\hat{x}(k/k-1)$.
- Multiplication of $\hat{x}(k/k-1)$ by $H(k)$ from the left, which is the estimation of measurement.
- Finding the difference between the measurement and the extrapolation value (the innovation process) $\tilde{z}(k/k-1) = z(k) - H(k)\hat{x}(k/k-1)$.
- Multiplication of $\tilde{z}(k/k-1)$ from left by *K(k)* and summation with $\hat{x}(k/k-1)$, thus obtaining $\hat{x}(k/k)$.
- Storage of the $\hat{x}(k/k)$ estimation for the next cycle and repeating the process.

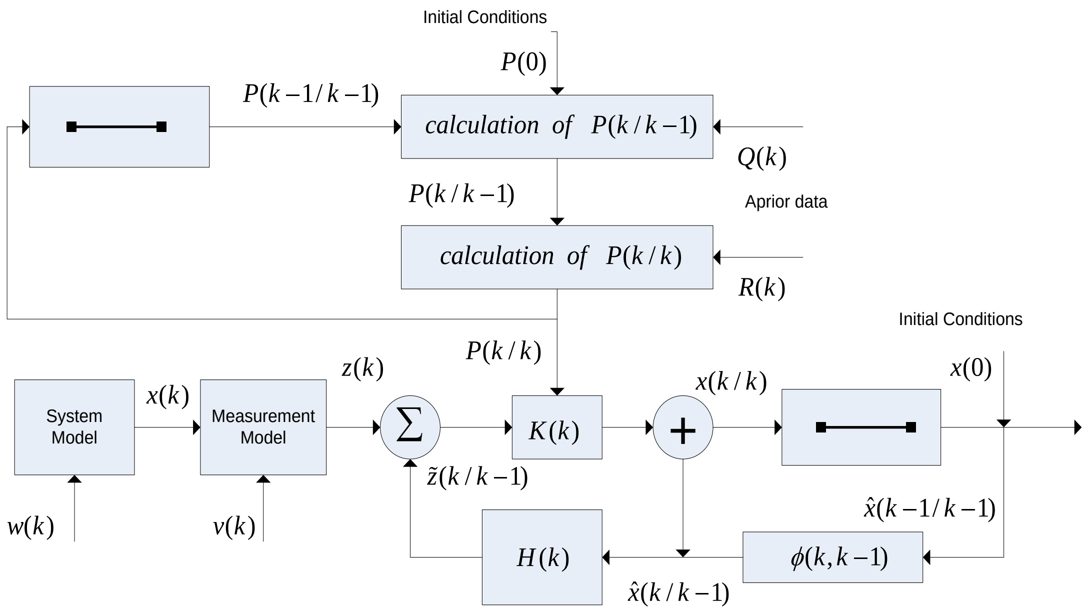

Figure 4.3 : Structural KF schematics [16].

Based on this structure, key features of the KF are as follows:

- The KF estimate is more linear compared to the measurement value.
- For the reason of this filter being linear, the correlation matrix *P(k/k)* of the estimate error is not coupled with the measurement *z(k)*, and can be calculated beforehand.
- When the mathematical model of the dynamical system is clearly stated, the filter algorithm can easily be performed by the help of a computer.
- The filtering algorithms can easily be deployed for multidimensional states.

4.6 Integration Method Used for AUV Navigational System

One of the main purposes of this study is to integrate INS and auxiliary navigational devices on the base of an Optimal KF. Instead of system state variable estimates, the system's navigational error estimates will be obtained by the KF.

The integrated AUV navigational system framework is shown in Figure 4.1 above. The high frequency of sampling feature of the INS is used in the integrated system. The other sensors have a longer sampling period than the INS. However, time synchronization is made between INS and auxiliary sensors during the Kalman filtering process.

4.7 KF based Integrated Navigational System Applied to AUV Dynamics

The integration algorithm utilizes the KF, which provides optimal performance for linear systems. INS error model Equations (4.2)–(4.10) for the variations of position, velocity, attitude, and angular velocities, and the inertial sensor output errors in Equations (4.11)–(4.16) constitute the navigational system error model. Additionally, Equations (4.18)–(4.20) and (4.22)–(4.23) are also used as the auxiliary sensor measurement for the KF. The system error model of the AUV navigation can be written as follows:

$$x(k+1) = Ax(k) + w(k) \tag{4.38}$$

where, $w(t) \sim N\left(0, Q(t)\right)$ zero mean Gaussian system noise vector.

We used three different approaches for integration of navigation systems because of the limited number of observations, which are five, in contrary to higher number of error state vector.

4.7.1 AUV integrated navigation system with INS calibration

In this approach, we assume that DVL, compass, Depth sensor, gyros and accelometers are calibrated properly and and the errors of these sensors are minimized to the reasonable level in the laboratory environment. The system error state vector with required parameters [n=9] is as follows:

$$x = \left[X,\ Y,\ Z,\ V_x,\ V_y,\ V_z,\ \psi_x,\ \psi_y,\ \psi_z\right]^T \tag{4.39}$$

Where $[X,\ Y,\ Z]$ are the position errors of INS, $\left[V_x,\ V_y,\ V_z\right]$ are the velocity errors of INS, and $\left[\psi_x, \psi_y, \psi_z\right]$ are attitude errors for each variables in the Cartesian coordinates. The error model of the INS can be expressed in a discrete matrix form as follows:

.

$$
\begin{bmatrix} X(k+1) \\ Y(k+1) \\ Z(k+1) \\ V_x(k+1) \\ V_y(k+1) \\ V_z(k+1) \\ \psi_x(k+1) \\ \psi_y(k+1) \\ \psi_z(k+1) \end{bmatrix}
=
\begin{bmatrix}
1+\frac{V_x}{R} & \frac{V_x \tan\phi}{R} & 0 & 1 & 0 & 0 & 0 & 0 & 0 \\
\frac{-V_x \tan\phi + V_x}{R} & 1 & 0 & 0 & 1 & 0 & 0 & 0 & 0 \\
\frac{-V_y \tan\phi + V_x}{R} & 0 & 1 & 0 & 0 & 1 & 0 & 0 & 0 \\
\frac{-g}{R} & 0 & 0 & 1 & 2\omega_{ie}\sin\phi + \frac{V_x \tan\phi}{R} & 2\omega_{ie}\cos\phi + \frac{V_x}{R} & 0 & a_z & -a_y \\
0 & \frac{-g}{R} & 0 & -2\omega_{ie}\sin\phi - \frac{V_x \tan\phi}{R} & 1 & \frac{V_y}{R} & -a_z & 0 & a_x \\
0 & 0 & \frac{2g}{R} & -2\omega_{ie}\cos\phi - \frac{V_x}{R} & \frac{-V_y}{R} & 1 & a_y & -a_x & 0 \\
0 & 0 & 0 & 0 & 0 & 0 & 1 & -(\omega_{ie}\sin\phi + \frac{V_x \tan\phi}{R}) & \omega_{ie}\cos\phi + V_x / R \\
0 & 0 & 0 & 0 & 0 & 0 & -(\omega_{ie}\sin\phi + \frac{V_x}{R}) & 1 & \frac{V_y}{R} \\
0 & 0 & 0 & 0 & 0 & 0 & -(\omega_{ie}\sin\phi + \frac{V_x}{R}) & \frac{-V_y}{R} & 1
\end{bmatrix}
x
\begin{bmatrix} X(k) \\ Y(k) \\ Z(k) \\ V_x(k) \\ V_y(k) \\ V_z(k) \\ \psi_x(k) \\ \psi_y(k) \\ \psi_z(k) \end{bmatrix}
\quad \textbf{(4.40)}
$$

Using the INS error model and auxiliary aiding devices measurement differences as measurements observation vector in the KF, the observation vector can be expressed as:

$$\begin{aligned} z_1(k) &= V_{Z_{INS}} + v_{V_{INSz}} - v_{V_D} \\ z_2(k) &= V_{V_{INSx}} + v_{V_{INSx}} - v_{V_{DVLx}} \\ z_3(k) &= V_{V_{INSy}} + v_{V_{INSy}} - v_{V_{DVLy}} \\ z_4(k) &= V_{V_{INSz}} + v_{V_{INSz}} - v_{V_{DVLz}} \\ z_5(k) &= V_{\psi_{INS}} + v_{\psi_{INS}} - v_{\psi_{Comp}} \end{aligned} \quad (4.41)$$

In Equation (4.41), $\boldsymbol{V_{z_{INS}}}$, $\boldsymbol{V_{V_{INSx}}}$, $\boldsymbol{V_{V_{INSy}}}$, $\boldsymbol{V_{V_{INSz}}}$, $\boldsymbol{V_{\psi_{INS}}}$ are the z position, x, y and z velocities and yaw measurement errors of the INS respectively and $\boldsymbol{v_{z_{INS}}}$, $\boldsymbol{v_{V_{INSx}}}$, $\boldsymbol{v_{V_{INSy}}}$, $\boldsymbol{v_{V_{INSz}}}$, $\boldsymbol{v_{\psi_{INS}}}$ and $\boldsymbol{v_{z_D}}$, $\boldsymbol{v_{V_{DVLx}}}$, $\boldsymbol{v_{V_{DVLy}}}$, $\boldsymbol{v_{V_{DVLz}}}$, $\boldsymbol{v_{\psi_{Comp}}}$ are the zero-mean Gaussian noises of INS, the depth sensor, DVL and compass respectively. However, this information includes the random noises of both systems.

The measurements in Equation (4.41) is rewritten in matrix form:

$$z(k) = \begin{bmatrix} z_1(k) \\ z_2(k) \\ z_3(k) \\ z_4(k) \\ z_5(k) \end{bmatrix} = \begin{bmatrix} Z_{INS} - Z_d \\ V_{INS_X} - V_{DVL_X} \\ V_{INS_Y} - V_{DVL_Y} \\ V_{INS_Z} - V_{DVL_Z} \\ \psi_{INS_Z} - \psi_{comp} \end{bmatrix} = \underbrace{\begin{bmatrix} 0 & 0 & 1 & 0 & 0 & 0 & 0 & 0 & 0 \\ 0 & 0 & 0 & 1 & 0 & 0 & 0 & 0 & 0 \\ 0 & 0 & 0 & 0 & 1 & 0 & 0 & 0 & 0 \\ 0 & 0 & 0 & 0 & 0 & 1 & 0 & 0 & 0 \\ 0 & 0 & 0 & 0 & 0 & 0 & 0 & 0 & 1 \end{bmatrix}}_{H(k)} x(k) + \begin{bmatrix} v_Z - v_{Z_d} \\ v_{Vx} - v_{V_{DVL_X}} \\ v_{Vy} - v_{V_{DVL_y}} \\ v_{Vz} - v_{V_{DVLz}} \\ v_{\psi_z} - v_{\psi_{comp}} \end{bmatrix} \quad (4.42)$$

To obtain true INS error values that will be used in the simulation, the system error model is used:

$$X(k+1) = \phi(k+1, k) X(k) + w(k) \quad (4.43)$$

Solving (4.43) according to the initial values, the true error values are obtained. Here ϕ is the transfer matrix of the system error model which describes the evolution of the system error at Equation (4.42).

Since the system noise involves position, speed, and attitude errors, the noise transfer matrix becomes a unity matrix and the noise correlation matrix *Q(k)* is defined as

$$Q(k)=\begin{bmatrix} 0.001 & 0 & 0 & 0 & 0 & 0 & 0 & 0 & 0 \\ 0 & 0.001 & 0 & 0 & 0 & 0 & 0 & 0 & 0 \\ 0 & 0 & 0.001 & 0 & 0 & 0 & 0 & 0 & 0 \\ 0 & 0 & 0 & 0.001 & 0 & 0 & 0 & 0 & 0 \\ 0 & 0 & 0 & 0 & 0.001 & 0 & 0 & 0 & 0 \\ 0 & 0 & 0 & 0 & 0 & 0.001 & 0 & 0 & 0 \\ 0 & 0 & 0 & 0 & 0 & 0 & 0.001 & 0 & 0 \\ 0 & 0 & 0 & 0 & 0 & 0 & 0 & 0.001 & 0 \\ 0 & 0 & 0 & 0 & 0 & 0 & 0 & 0 & 0.001 \end{bmatrix} \quad \textbf{(4.44)}$$

The initial correlation matrix *P(0/0)* of KF are defined as:

$$P(0/0)=\begin{bmatrix} 100 & 0 & 0 & 0 & 0 & 0 & 0 & 0 & 0 \\ 0 & 100 & 0 & 0 & 0 & 0 & 0 & 0 & 0 \\ 0 & 0 & 100 & 0 & 0 & 0 & 0 & 0 & 0 \\ 0 & 0 & 0 & 50 & 0 & 0 & 0 & 0 & 0 \\ 0 & 0 & 0 & 0 & 50 & 0 & 0 & 0 & 0 \\ 0 & 0 & 0 & 0 & 0 & 50 & 0 & 0 & 0 \\ 0 & 0 & 0 & 0 & 0 & 0 & 50 & 0 & 0 \\ 0 & 0 & 0 & 0 & 0 & 0 & 0 & 50 & 0 \\ 0 & 0 & 0 & 0 & 0 & 0 & 0 & 0 & 50 \end{bmatrix} \quad \textbf{(4.45)}$$

The diagonal correlation matrix *R(k)* are obtained by summing the standard deviations of the INS ***z***-position, and depth, INS and DVL velocities and INS yaw and compass heading error, respectively.

$$R(k)=\begin{bmatrix} \sigma^2_{V_{Z_{INS}}}+\sigma^2_{V_{Zd}} & 0 & 0 & 0 & 0 \\ 0 & \sigma^2_{V_{V_{INSx}}}+\sigma^2_{V_{V_{DVLx}}} & 0 & 0 & 0 \\ 0 & 0 & \sigma^2_{V_{V_{INSy}}}+\sigma^2_{V_{V_{DVLy}}} & 0 & 0 \\ 0 & 0 & 0 & \sigma^2_{V_{V_{INSy}}}+\sigma^2_{V_{V_{DVLy}}} & 0 \\ 0 & 0 & 0 & 0 & \sigma^2_{V_{\psi INSz}}+\sigma^2_{V_{\psi Comp}} \end{bmatrix} \quad \textbf{(4.46)}$$

4.7.2 AUV integrated navigation system with INS, gyro, and accelometer calibration

In this approach, we assume that DVL, compass, and Depth sensor are calibrated properly and and the errors of these sensors are minimized to the reasonable level in the laboratory environment.

The system error state vector with required parameters [n=15] is as follows:

$$x=\left[X,\ Y,\ Z,\ V_x,\ V_y,\ V_z,\ \psi_x,\ \psi_y,\ \psi_z,\varepsilon_x,\varepsilon_y,\varepsilon_z,\nabla_x,\nabla_y,\nabla_z\right]^T \quad \textbf{(4.47)}$$

Where $[X,\ Y,\ Z]$ are the position errors of INS, $\left[V_x,\ V_y,\ V_z\right]$ are the velocity errors of INS, $\left[\psi_x,\psi_y,\psi_z\right]$ are attitude errors and $\left[\varepsilon_x,\varepsilon_y,\varepsilon_z,\nabla_x,\nabla_y,\nabla_z\right]$ are the drifts of gyros and accelometers for each variables in the Cartesian coordinates. Using the INS error model and auxiliary aiding devices measurement differences as measurements observation vector in the KF, the observation vector can be expressed as:

$$
\begin{aligned}
z_1(k) &= V_{Z_{INS}} + v_{V_{INSz}} - v_{V_D} \\
z_2(k) &= V_{V_{INSx}} + v_{V_{INSx}} - v_{V_{DVLx}} \\
z_3(k) &= V_{V_{INSy}} + v_{V_{INSy}} - v_{V_{DVLy}} \\
z_4(k) &= V_{V_{INSz}} + v_{V_{INSz}} - v_{V_{DVLz}} \\
z_5(k) &= V_{\psi_{INS}} + v_{\psi_{INS}} - v_{\psi_{Comp}}
\end{aligned}
\tag{4.48}
$$

In Equation (4.48), $\boldsymbol{V_{z_{INS}}}$, $\boldsymbol{V_{V_{INSx}}}$, $\boldsymbol{V_{V_{INSy}}}$, $\boldsymbol{V_{V_{INSz}}}$, $\boldsymbol{V_{\psi_{INS}}}$ are the z position, x, y and z velocities and yaw measurement errors of the INS respectively and $\boldsymbol{v_{z_{INS}}}$, $\boldsymbol{v_{V_{INSx}}}$, $\boldsymbol{v_{V_{INSy}}}$, $\boldsymbol{v_{V_{INSz}}}$, $\boldsymbol{v_{\psi_{INS}}}$ and $\boldsymbol{v_{z_D}}$, $\boldsymbol{v_{V_{DVLx}}}$, $\boldsymbol{v_{V_{DVLy}}}$, $\boldsymbol{v_{V_{DVLz}}}$, $\boldsymbol{v_{\psi_{Comp}}}$ are the zero-mean Gaussian noises of INS, the depth sensor, DVL and compass respectively. However, this information includes the random noises of both systems.

The measurements in Equation (4.48) is rewritten in matrix form:

$$
z(k) = \begin{bmatrix} z_1(k) \\ z_2(k) \\ z_3(k) \\ z_4(k) \\ z_5(k) \end{bmatrix}
= \begin{bmatrix} Z_{INS} - Z_d \\ V_{INS_X} - V_{DVL_X} \\ V_{INS_Y} - V_{DVL_Y} \\ V_{INS_Z} - V_{DVL_Z} \\ \psi_{INS_Z} - \psi_{comp} \end{bmatrix}
= \underbrace{\begin{bmatrix}
0&0&1&0&0&0&0&0&0&0&0&0&0&0&0 \\
0&0&0&1&0&0&0&0&0&0&0&0&0&0&0 \\
0&0&0&0&1&0&0&0&0&0&0&0&0&0&0 \\
0&0&0&0&0&1&0&0&0&0&0&0&0&0&0 \\
0&0&0&0&0&0&0&0&1&0&0&0&0&0&0
\end{bmatrix}}_{H(k)} x(k) + \begin{bmatrix} v_Z - v_{Z_d} \\ v_{Vx} - v_{V_{DVLX}} \\ v_{Vy} - v_{V_{DVLy}} \\ v_{Vz} - v_{V_{DVLz}} \\ v_{\psi_z} - v_{\psi_{comp}} \end{bmatrix}
\tag{4.49}
$$

To obtain true INS error values that will be used in the simulation, the system error model is used:

$$
X(k+1) = \phi(k+1,k)X(k) + w(k) \tag{4.50}
$$

Solving (4.50) according to the initial values, the true error values are obtained. Here ϕ is the transfer matrix of the system error model which describes the evolution of the system error at (4.49).

The error model of the INS can be expressed in a discrete matrix form as follows:

$$
\begin{bmatrix} X(k+1) \\ Y(k+1) \\ Z(k+1) \\ V_x(k+1) \\ V_y(k+1) \\ V_z(k+1) \\ \psi_x(k+1) \\ \psi_y(k+1) \\ \psi_z(k+1) \\ \nabla a_x(k+1) \\ \nabla a_y(k+1) \\ \nabla a_z(k+1) \\ \varepsilon_{gx}(k+1) \\ \varepsilon_{gy}(k+1) \\ \varepsilon_{gz}(k+1) \end{bmatrix}
=
\underbrace{\begin{bmatrix}
1+\frac{V_x}{R} & \frac{V_x\tan\phi}{R} & 0 & 1 & 0 & 0 & 0 & 0 & 0 & 0 & 0 & 0 & 0 & 0 & 0 \\
\frac{-V_x\tan\phi+V_x}{R} & 1 & 0 & 0 & 1 & 0 & 0 & 0 & 0 & 0 & 0 & 0 & 0 & 0 & 0 \\
\frac{-V_y\tan\phi+V_x}{R} & 0 & 1 & 0 & 0 & 1 & 0 & 0 & 0 & 0 & 0 & 0 & 0 & 0 & 0 \\
\frac{-g}{R} & 0 & 0 & 1 & 2\omega_{ie}\sin\phi+\frac{V_x\tan\phi}{R} & 2\omega_{ie}\cos\phi+\frac{V_x}{R} & 0 & a_z & -a_y & 1 & 0 & 0 & 0 & 0 & 0 \\
0 & \frac{-g}{R} & 0 & -2\omega_{ie}\sin\phi-\frac{V_x\tan\phi}{R} & 1 & \frac{V_y}{R} & -a_z & 0 & a_x & 0 & 1 & 0 & 0 & 0 & 0 \\
0 & 0 & \frac{2g}{R} & -2\omega_{ie}\cos\phi-\frac{V_x}{R} & \frac{-V_y}{R} & 1 & a_y & -a_x & 0 & 0 & 0 & 1 & 0 & 0 & 0 \\
0 & 0 & 0 & 0 & 0 & 0 & 1 & (\omega_{ie}\sin\phi+V_x\tan\phi/R) & \omega_{ie}\cos\phi+V_x/R & 0 & 0 & 0 & 1 & 0 & 0 \\
0 & 0 & 0 & 0 & 0 & 0 & -(\omega_{ie}\sin\phi+\frac{V_x\tan\phi}{R}) & 1 & \frac{V_y}{R} & 0 & 0 & 0 & 0 & 1 & 0 \\
0 & 0 & 0 & 0 & 0 & 0 & -(\omega_{ie}\sin\phi+\frac{V_x}{R}) & \frac{-V_y}{R} & 1 & 0 & 0 & 0 & 0 & 0 & 1 \\
0 & 0 & 0 & 0 & 0 & 0 & 0 & 0 & 0 & 1-\beta_{acc} & 0 & 0 & 0 & 0 & 0 \\
0 & 0 & 0 & 0 & 0 & 0 & 0 & 0 & 0 & 0 & 1-\beta_{acc} & 0 & 0 & 0 & 0 \\
0 & 0 & 0 & 0 & 0 & 0 & 0 & 0 & 0 & 0 & 0 & 1-\beta_{acc} & 0 & 0 & 0 \\
0 & 0 & 0 & 0 & 0 & 0 & 0 & 0 & 0 & 0 & 0 & 0 & 1-\beta_{gyro} & 0 & 0 \\
0 & 0 & 0 & 0 & 0 & 0 & 0 & 0 & 0 & 0 & 0 & 0 & 0 & 1-\beta_{gyro} & 0 \\
0 & 0 & 0 & 0 & 0 & 0 & 0 & 0 & 0 & 0 & 0 & 0 & 0 & 0 & 1-\beta_{gyro}
\end{bmatrix}}_{\phi}
x
\begin{bmatrix} X(k) \\ Y(k) \\ Z(k) \\ V_x(k) \\ V_y(k) \\ V_z(k) \\ \psi_x(k) \\ \psi_y(k) \\ \psi_z(k) \\ \nabla a_x(k) \\ \nabla a_y(k) \\ \nabla a_z(k) \\ \varepsilon_{gx}(k) \\ \varepsilon_{gy}(k) \\ \varepsilon_{gz}(k) \end{bmatrix}
+
\underbrace{\begin{bmatrix} 0 \\ 0 \\ 0 \\ 0 \\ 0 \\ 0 \\ 0 \\ 0 \\ 0 \\ w_{ax}(k) \\ w_{ay}(k) \\ w_{az}(k) \\ w_{gx}(k) \\ w_{gy}(k) \\ w_{gz}(k) \end{bmatrix}}_{w(k)}
\qquad \textbf{(4.51)}
$$

Since the system noise involves position, speed, and attitude errors, the noise transfer matrix becomes a unity matrix and the noise correlation matrix *Q(k)* is defined as

$$Q(k)=\begin{bmatrix}
0.001&0&0&0&0&0&0&0&0&0&0&0&0&0&0\\
0&0.001&0&0&0&0&0&0&0&0&0&0&0&0&0\\
0&0&0.001&0&0&0&0&0&0&0&0&0&0&0&0\\
0&0&0&0.001&0&0&0&0&0&0&0&0&0&0&0\\
0&0&0&0&0.001&0&0&0&0&0&0&0&0&0&0\\
0&0&0&0&0&0.001&0&0&0&0&0&0&0&0&0\\
0&0&0&0&0&0&0.001&0&0&0&0&0&0&0&0\\
0&0&0&0&0&0&0&0.001&0&0&0&0&0&0&0\\
0&0&0&0&0&0&0&0&0.001&0&0&0&0&0&0\\
0&0&0&0&0&0&0&0&0&0.001&0&0&0&0&0\\
0&0&0&0&0&0&0&0&0&0&0.001&0&0&0&0\\
0&0&0&0&0&0&0&0&0&0&0&0.001&0&0&0\\
0&0&0&0&0&0&0&0&0&0&0&0&0.001&0&0\\
0&0&0&0&0&0&0&0&0&0&0&0&0&0.001&0\\
0&0&0&0&0&0&0&0&0&0&0&0&0&0&0.001
\end{bmatrix} \qquad \textbf{(4.52)}$$

The initial correlation matrix *P(0/0)* of KF are defined as:

$$P(0/0)=\begin{bmatrix}
100&0&0&0&0&0&0&0&0&0&0&0&0&0&0\\
0&100&0&0&0&0&0&0&0&0&0&0&0&0&0\\
0&0&100&0&0&0&0&0&0&0&0&0&0&0&0\\
0&0&0&100&0&0&0&0&0&0&0&0&0&0&0\\
0&0&0&0&100&0&0&0&0&0&0&0&0&0&0\\
0&0&0&0&0&100&0&0&0&0&0&0&0&0&0\\
0&0&0&0&0&0&100&0&0&0&0&0&0&0&0\\
0&0&0&0&0&0&0&100&0&0&0&0&0&0&0\\
0&0&0&0&0&0&0&0&100&0&0&0&0&0&0\\
0&0&0&0&0&0&0&0&0&100&0&0&0&0&0\\
0&0&0&0&0&0&0&0&0&0&100&0&0&0&0\\
0&0&0&0&0&0&0&0&0&0&0&100&0&0&0\\
0&0&0&0&0&0&0&0&0&0&0&0&100&0&0\\
0&0&0&0&0&0&0&0&0&0&0&0&0&100&0\\
0&0&0&0&0&0&0&0&0&0&0&0&0&0&100
\end{bmatrix} \qquad \textbf{(4.53)}$$

The diagonal correlation matrix *R(k)* are obtained by summing the standard deviations of the INS ***z***-position, and depth, INS and DVL velocities and INS yaw and compass heading error, respectively.

$$R(k)=\begin{bmatrix}
\sigma^2_{V_{Z_{INS}}}+\sigma^2_{V_{Zd}}&0&0&0&0\\
0&\sigma^2_{V_{V_{INSx}}}+\sigma^2_{V_{V_{DVLx}}}&0&0&0\\
0&0&\sigma^2_{V_{V_{INSy}}}+\sigma^2_{V_{V_{DVLy}}}&0&0\\
0&0&0&\sigma^2_{V_{V_{INSy}}}+\sigma^2_{V_{V_{DVLy}}}&0\\
0&0&0&0&\sigma^2_{V_{\psi_{INSz}}}+\sigma^2_{V_{\psi_{Comp}}}
\end{bmatrix} \qquad \textbf{(4.54)}$$

4.7.3 AUV integrated navigation system with INS, DVL, compass, and depth sensor calibaration

In this approach, we assume that gyro and accelometer sensors are calibrated properly and and the errors of these sensors are minimized to the reasonable level in the laboratory environment.

The system error state vector with required parameters [n=14] is as follows:

$$x=\left[X,\ Y,\ Z,\ V_x,\ V_y,\ V_z,\ \psi_x,\ \psi_y,\ \psi_z, V_{DVLx}, V_{DVLy}, V_{DVLz}, Z_{Depth}, \psi_{Comp_z}\right]^T \tag{4.55}$$

Where $[X,\ Y,\ Z]$ are the position errors of INS, $\left[V_x,\ V_y,\ V_z\right]$ are the velocity errors of INS, $\left[\psi_x, \psi_y, \psi_z\right]$ are attitude errors and $\left[\varepsilon_x, \varepsilon_y, \varepsilon_z, \nabla_x, \nabla_y, \nabla_z\right]$ are the drifts of gyros and accelometers for each variables in the Cartesian coordinates.

Using the INS error model and auxiliary aiding devices measurement differences as measurements observation vector in the KF, the observation vector can be expressed as:

$$\begin{aligned}
z_1(k) &= V_{Z_{INS}} + v_{V_{INSz}} - v_{V_D} \\
z_2(k) &= V_{V_{INSx}} + v_{V_{INSx}} - v_{V_{DVLx}} \\
z_3(k) &= V_{V_{INSy}} + v_{V_{INSy}} - v_{V_{DVLy}} \\
z_4(k) &= V_{V_{INSz}} + v_{V_{INSz}} - v_{V_{DVLz}} \\
z_5(k) &= V_{\psi_{INS}} + v_{\psi_{INS}} - v_{\psi_{Comp}}
\end{aligned} \tag{4.56}$$

In Equation (4.56), $\boldsymbol{V_{z_{INS}}}$, $\boldsymbol{V_{V_{INSx}}}$, $\boldsymbol{V_{V_{INSy}}}$, $\boldsymbol{V_{V_{INSz}}}$, $\boldsymbol{V_{\psi_{INS}}}$ are the z position, x, y and z velocities and yaw measurement errors of the INS respectively and $\boldsymbol{v_{z_{INS}}}$, $\boldsymbol{v_{V_{INSx}}}$, $\boldsymbol{v_{V_{INSy}}}$, $\boldsymbol{v_{V_{INSz}}}$, $\boldsymbol{v_{\psi_{INS}}}$ and $\boldsymbol{v_{z_D}}$, $\boldsymbol{v_{V_{DVLx}}}$, $\boldsymbol{v_{V_{DVLy}}}$, $\boldsymbol{v_{V_{DVLz}}}$, $\boldsymbol{v_{\psi_{Comp}}}$ are the zero-mean Gaussian noises of INS, the depth sensor, DVL and compass respectively. However, this information includes the random noises of both systems.

The measurements in Equation (4.56) is rewritten in matrix form:

$$z(k)=\begin{bmatrix} z_1(k) \\ z_2(k) \\ z_3(k) \\ z_4(k) \\ z_5(k) \end{bmatrix} = \begin{bmatrix} Z_{INS} - Z_d \\ V_{INS_X} - V_{DVL_X} \\ V_{INS_Y} - V_{DVL_Y} \\ V_{INS_Z} - V_{DVL_Z} \\ \psi_{INS_Z} - \psi_{comp} \end{bmatrix} = \underbrace{\begin{bmatrix} 0 & 0 & 1 & 0 & 0 & 0 & 0 & 0 & 0 & 0 & 0 & 0 & -1 & 0 \\ 0 & 0 & 0 & 1 & 0 & 0 & 0 & 0 & 0 & -1 & 0 & 0 & 0 & 0 \\ 0 & 0 & 0 & 0 & 1 & 0 & 0 & 0 & 0 & 0 & 0 & -1 & 0 & 0 \\ 0 & 0 & 0 & 0 & 0 & 1 & 0 & 0 & 0 & 0 & 0 & 0 & -1 & 0 \\ 0 & 0 & 0 & 0 & 0 & 0 & 0 & 0 & 1 & 0 & 0 & 0 & 0 & -1 \end{bmatrix}}_{H(k)} x(k) + \begin{bmatrix} v_Z - v_{Z_d} \\ v_{Vx} - v_{V_{DVL_X}} \\ v_{Vy} - v_{V_{DVL_y}} \\ v_{Vz} - v_{V_{DVLz}} \\ v_{\psi_z} - v_{\psi_{comp}} \end{bmatrix} \tag{4.57}$$

To obtain true INS error values that will be used in the simulation, the system error model is used:

$$X(k+1) = \phi(k+1,k)X(k) + w\left(k\right) \qquad \textbf{(4.58)}$$

Solving (4.58) according to the initial values, the true error values are obtained. Here ϕ is the transfer matrix of the system error model which describes the evolution of the system error at (4.57).

Since the system noise involves position, speed, and attitude errors, the noise transfer matrix becomes a unity matrix and the noise correlation matrix *Q(k)* is defined as

$$Q(k) = \begin{bmatrix}
0.001 & 0 & 0 & 0 & 0 & 0 & 0 & 0 & 0 & 0 & 0 & 0 & 0 & 0 \\
0 & 0.001 & 0 & 0 & 0 & 0 & 0 & 0 & 0 & 0 & 0 & 0 & 0 & 0 \\
0 & 0 & 0.001 & 0 & 0 & 0 & 0 & 0 & 0 & 0 & 0 & 0 & 0 & 0 \\
0 & 0 & 0 & 0.001 & 0 & 0 & 0 & 0 & 0 & 0 & 0 & 0 & 0 & 0 \\
0 & 0 & 0 & 0 & 0.001 & 0 & 0 & 0 & 0 & 0 & 0 & 0 & 0 & 0 \\
0 & 0 & 0 & 0 & 0 & 0.001 & 0 & 0 & 0 & 0 & 0 & 0 & 0 & 0 \\
0 & 0 & 0 & 0 & 0 & 0 & 0.001 & 0 & 0 & 0 & 0 & 0 & 0 & 0 \\
1\; 0 & 0 & 0 & 0 & 0 & 0 & 0 & 0.001 & 0 & 0 & 0 & 0 & 0 & 0 \\
0 & 0 & 0 & 0 & 0 & 0 & 0 & 0 & 0.001 & 0 & 0 & 0 & 0 & 0 \\
0 & 0 & 0 & 0 & 0 & 0 & 0 & 0 & 0 & 0.001 & 0 & 0 & 0 & 0 \\
0 & 0 & 0 & 0 & 0 & 0 & 0 & 0 & 0 & 0 & 0.001 & 0 & 0 & 0 \\
0 & 0 & 0 & 0 & 0 & 0 & 0 & 0 & 0 & 0 & 0 & 0.001 & 0 & 0 \\
0 & 0 & 0 & 0 & 0 & 0 & 0 & 0 & 0 & 0 & 0 & 0 & 0.001 & 0 \\
0 & 0 & 0 & 0 & 0 & 0 & 0 & 0 & 0 & 0 & 0 & 0 & 0 & 0.001
\end{bmatrix} \qquad \textbf{(4.59)}$$

The initial correlation matrix *P(0/0)* of KF are defined as:

$$P(0/0) = \begin{bmatrix}
100 & 0 & 0 & 0 & 0 & 0 & 0 & 0 & 0 & 0 & 0 & 0 & 0 & 0 \\
0 & 100 & 0 & 0 & 0 & 0 & 0 & 0 & 0 & 0 & 0 & 0 & 0 & 0 \\
0 & 0 & 100 & 0 & 0 & 0 & 0 & 0 & 0 & 0 & 0 & 0 & 0 & 0 \\
0 & 0 & 0 & 100 & 0 & 0 & 0 & 0 & 0 & 0 & 0 & 0 & 0 & 0 \\
0 & 0 & 0 & 0 & 100 & 0 & 0 & 0 & 0 & 0 & 0 & 0 & 0 & 0 \\
0 & 0 & 0 & 0 & 0 & 100 & 0 & 0 & 0 & 0 & 0 & 0 & 0 & 0 \\
0 & 0 & 0 & 0 & 0 & 0 & 100 & 0 & 0 & 0 & 0 & 0 & 0 & 0 \\
0 & 0 & 0 & 0 & 0 & 0 & 0 & 100 & 0 & 0 & 0 & 0 & 0 & 0 \\
0 & 0 & 0 & 0 & 0 & 0 & 0 & 0 & 100 & 0 & 0 & 0 & 0 & 0 \\
0 & 0 & 0 & 0 & 0 & 0 & 0 & 0 & 0 & 100 & 0 & 0 & 0 & 0 \\
0 & 0 & 0 & 0 & 0 & 0 & 0 & 0 & 0 & 0 & 100 & 0 & 0 & 0 \\
0 & 0 & 0 & 0 & 0 & 0 & 0 & 0 & 0 & 0 & 0 & 100 & 0 & 0 \\
0 & 0 & 0 & 0 & 0 & 0 & 0 & 0 & 0 & 0 & 0 & 0 & 100 & 0 \\
0 & 0 & 0 & 0 & 0 & 0 & 0 & 0 & 0 & 0 & 0 & 0 & 0 & 100
\end{bmatrix} \qquad \textbf{(4.60)}$$

The diagonal correlation matrix *R(k)* are obtained by summing the standard deviations of the INS ***z***-position, and depth, INS and DVL velocities and INS yaw and compass heading error, respectively.

$$R(k) = \begin{bmatrix}
\sigma^2_{V_{Z_{INS}}} + \sigma^2_{V_{Zd}} & 0 & 0 & 0 & 0 \\
0 & \sigma^2_{V_{V_{INSx}}} + \sigma^2_{V_{V_{DVLx}}} & 0 & 0 & 0 \\
0 & 0 & \sigma^2_{V_{V_{INSy}}} + \sigma^2_{V_{V_{DVLy}}} & 0 & 0 \\
0 & 0 & 0 & \sigma^2_{V_{V_{INSy}}} + \sigma^2_{V_{V_{DVLy}}} & 0 \\
0 & 0 & 0 & 0 & \sigma^2_{V_{\psi INSz}} + \sigma^2_{V_{\psi Comp}}
\end{bmatrix} \qquad \textbf{(4.61)}$$

The error model of the INS, DVL, compass and depth sensors can be expressed in a discrete matrix form as follows:

$$
\begin{bmatrix} X(k+1) \\ Y(k+1) \\ Z(k+1) \\ V_x(k+1) \\ V_y(k+1) \\ V_z(k+1) \\ \psi_x(k+1) \\ \psi_y(k+1) \\ \psi_z(k+1) \\ V_{DVLx}(k+1) \\ V_{DVLy}(k+1) \\ V_{DVLz}(k+1) \\ Z_{Dept}(k+1) \\ \psi_{Comp}(k+1) \end{bmatrix}
=
\underbrace{\begin{bmatrix}
1+\frac{V_x}{R} & \frac{V_x \tan\phi}{R} & 0 & 1 & 0 & 0 & 0 & 0 & 0 & 0 & 0 & 0 & 0 & 0 \\
\frac{-V_x \tan\phi + V_x}{R} & 1 & 0 & 0 & 1 & 0 & 0 & 0 & 0 & 0 & 0 & 0 & 0 & 0 \\
\frac{-V_y \tan\phi + V_x}{R} & 0 & 1 & 0 & 0 & 1 & 0 & 0 & 0 & 0 & 0 & 0 & 0 & 0 \\
\frac{-g}{R} & 0 & 0 & 1 & 2\omega_{ie}\sin\phi + \frac{V_x \tan\phi}{R} & 2\omega_{ie}\cos\phi + \frac{V_x}{R} & 0 & a_z & -a_y & 1 & 0 & 0 & 0 & 0 \\
0 & \frac{-g}{R} & 0 & -2\omega_{ie}\sin\phi - \frac{V_x \tan\phi}{R} & 1 & \frac{V_y}{R} & -a_z & 0 & a_x & 0 & 1 & 0 & 0 & 0 \\
0 & 0 & \frac{2g}{R} & -2\omega_{ie}\cos\phi - \frac{V_x}{R} & \frac{-V_y}{R} & 1 & a_y & -a_x & 0 & 0 & 0 & 1 & 0 & 0 \\
0 & 0 & 0 & 0 & 0 & 0 & 1 & (\omega_{ie}\sin\phi + V_x \tan\phi / R) & \omega_{ie}\cos\phi + V_x / R & 0 & 0 & 0 & 1 & 0 \\
0 & 0 & 0 & 0 & 0 & 0 & -(\omega_{ie}\sin\phi + \frac{V_x \tan\phi}{R}) & 1 & \frac{V_y}{R} & 0 & 0 & 0 & 0 & 1 \\
0 & 0 & 0 & 0 & 0 & 0 & -(\omega_{ie}\sin\phi + \frac{V_x}{R}) & \frac{-V_y}{R} & 1 & 0 & 0 & 0 & 0 & 0 \\
0 & 0 & 0 & 0 & 0 & 0 & 0 & 0 & 0 & 1-\beta_{DVLx} & 0 & 0 & 0 & 0 \\
0 & 0 & 0 & 0 & 0 & 0 & 0 & 0 & 0 & 0 & 1-\beta_{DVLy} & 0 & 0 & 0 \\
0 & 0 & 0 & 0 & 0 & 0 & 0 & 0 & 0 & 0 & 0 & 1-\beta_{DVLz} & 0 & 0 \\
0 & 0 & 0 & 0 & 0 & 0 & 0 & 0 & 0 & 0 & 0 & 0 & 1 & 0 \\
0 & 0 & 0 & 0 & 0 & 0 & 0 & 0 & 0 & 0 & 0 & 0 & 0 & 1
\end{bmatrix}}_{\phi}
x
\begin{bmatrix} X(k) \\ Y(k) \\ Z(k) \\ V_x(k) \\ V_y(k) \\ V_z(k) \\ \psi_x(k) \\ \psi_y(k) \\ \psi_z(k) \\ V_{DVLx}(k) \\ V_{DVLy}(k) \\ V_{DVLz}(k) \\ Z_{Dept}(k) \\ \psi_{Comp}(k) \end{bmatrix}
+
\underbrace{\begin{bmatrix} 0 \\ 0 \\ 0 \\ 0 \\ 0 \\ 0 \\ 0 \\ 0 \\ 0 \\ w_{DVLx}(k) \\ w_{DVLy}(k) \\ w_{DVLz}(k) \\ w_{Dept}(k) \\ w_{Comp}(k) \end{bmatrix}}_{w(k)}
\qquad \textbf{(4.62)}
$$

5. PARAMETER IDENTIFICATION WITH LEAST SQUARES ESTIMATION

5.1 Objectives

This section focuses on the parameter identification of hydrodynamic coefficients of AUVs based on the *Least Square Estimation* (LSE) algorithm for a nonlinear mathematical modeling of AUVs. Hydrodynamic coefficients strongly affect the dynamic performance of an AUV. Therefore, it is important to have the true values of these coefficients in order to accurately simulate the AUV's dynamic performance. The estimated coefficients can be used as inputs not only for a mathematical model to analyze the maneuvering performance but also for a controller model to design AUVs under development. However, parameter identification of AUV dynamics is complicated because of its nonlinear identification models and the combination of noisy and biased sensor measurements.

5.2 AUV System Identification

System identification is the determination on the basis of an observation of input and output, of a system within a specified class of systems to which the system under test is equivalent [31]. When the system identification is applied to AUVs, the equations governing the AUV dynamic motion are postulated and an experiment is designed to obtain measurements of input and output variables [35].

The hydrodynamic forces and moments acting on AUV cannot be measured directly. However, hydrodynamic modeling followed by parameter estimation allows determination of specific hydrodynamic characteristics (such as lift, drag, and side force coefficients, and rolling, pitching, and yawing moment coefficients in terms of stability and control derivatives) from the related measurements such as accelerations, angular rates, etc. [31].

The selected EOM for system identification are sway and yaw

$$Y = Y_{\dot{v}}\dot{v} + Y_{\dot{r}}\dot{r} + m\left[-\dot{v} + z_g\dot{p} - x_g\dot{r}\right] + Y_{uv}uv + \left(Y_{wp} + m\right)wp + \left(Y_{ur} - m\right)ur - \left(mz_g\right)qr + \left(Y_{pq} - mx_g\right)pq + Y_{vv}v|v| + Y_{rr}r|r| + \left(W - B\right)\cos\theta\sin\phi + Y_{uu\delta_r}u^2\delta_r \quad \textbf{(5.1)}$$

$$N = my_g\dot{u} + \left(N_{\dot{v}} - mx_g\right)\dot{v} + \left(N_{\dot{r}} - I_{zz}\right)\dot{r} + \left(Npq + I_{xx} - I_{yy}\right)pq + \left(N_{wp} - mx_g\right)wp + \left(N_{ur} - mx_g\right)ur + N_{uv}uv + N_{rr}r|r| + N_{vv}v|v| + \left(x_gW - x_bB\right)\cos\theta\sin\psi + \left(y_gW - y_bB\right)\sin\theta + N_{uu\delta_r}u^2\delta_r \quad \textbf{(5.2)}$$

The dynamic Equations (5.1) and (5.2) are augmented with output equations that specify the connection of AUV states and controls to measured outputs, along with measurement equations describing the measurement process [35].

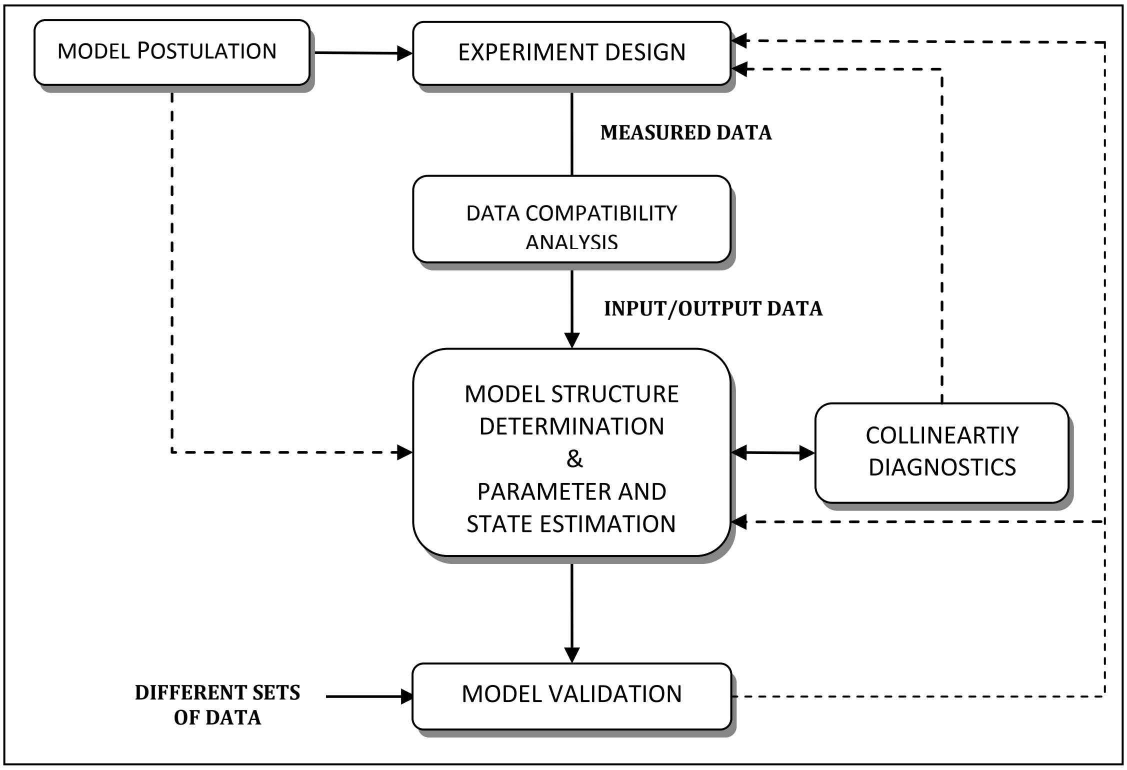

Figure 5.1 : AUV system identification method [35].

In Figure 5.1, *Model Postulation* is based on a priori knowledge about the AUV kinematics and hydrodynamics. The *Experiment Design* includes selection of an instrumentation system, and specification of an AUV configuration and maneuvers for system identification. *Data Compatibility Analysis*, in practice, measured AUV response data that can contain systematic errors, even after careful instrumentation and experimental procedures. To verify data accuracy, data comapatibility analysis can be applied to measured AUV responses. *Model Structure Determination* in AUV system identification means selecting a specific form for modeling from a class of models, based on measured data. *Parameter and State Estimation* constitute a principal part of the AUV system identification procedure. Parameter estimation for linear dynamic systems based on maximum likelihood and the least squares principles can also be formulated in the frequency domain. *Collinearity diagnostics* is in almost all practical applications of linear regression and the model terms are correlated to some extent. Diagnostic information can aid in deciding what corrective actions are necessary. *Model Validation* is the last step in the identification process. The identified model must demonstrate that its parameters have physically reasonable values and acceptible accuracy, and that the model has a good prediction capability on comparable maneuvers [35].

5.3 Parameter Estimation for AUV

The parameters can be estimated from calculating the first principles of dynamics of AUVs, from statistical LSE of experimental data, or a combination of the two. The identification of the parameters of the item being tracked can be approached in many different ways. The parameters can be determined once, from a model of the expected input signal. It also could be done adaptively utilizing a recursive method to identify the parameters of the incoming signal.

The modern era of system identification is marked by the implementation of the maximum-likelihood method [31]. Therefore, we used the *Least Square model* for the uncertainities in the parameters and measurements in this study. Based on this model, $\boldsymbol{\theta}$ is a vector of unknown constant parameters and $\boldsymbol{v}$ is a random vector of measurement noise. There are two different models that are Bayesian and Fisher [35]. The LSE algorithm always gives the best linear fit when the noise is white and Gaussian. Moreover, it is easier to tune the identification process in the latter part with a priori knowledge of the system [40]. A recursive LSE was chosen in this study for the parameter estimation since it is easy to apply the system dynamic and allows for the consideration of modeling and measurement errors.

The parameter estimation process consists of finding values of unknown model parameter $\boldsymbol{\theta}$ in an assumed model structure, based on noisy measurements $\boldsymbol{z}$. An estimator is a function of the random variable $\boldsymbol{z}$ that produces an estimate $\hat{\boldsymbol{\theta}}$ of the unknown parameters $\boldsymbol{\theta}$. Since the estimator computes $\hat{\boldsymbol{\theta}}$ based on noisy measurements $\boldsymbol{z}$, $\hat{\boldsymbol{\theta}}$ is a random variable [35].

In order to estimate the hydrodynamic coefficients of AUVs, the LSE is designed using the observer model. The state variable yields to

$$\boldsymbol{\theta} = \left[Y_{vv}\ Y_{rr}\ Y_{uv}\ Y_{ur}\ Y_{wp}\ N_{vv}\ N_{rr}\ N_{uv}\ N_{ur}\ N_{wp}\ \right] \tag{5.3}$$

The output variables are chosen as two types according to these measurements.

A model is called linear in the parameters if the output $\boldsymbol{y}$ is given by:

$$y = X\theta \tag{5.4}$$

where, the matrix X is assumed to be known. Then the measurement equation can be expressed as:

$$z = X\theta + \nu \tag{5.5}$$

where;

$\boldsymbol{z} = [z(1)\ z(2) \ldots z(N)]^T = N \times 1$ is the length measurement vector,

$\boldsymbol{\theta} = [\theta_0\ \ \theta_1\ \ldots\ \theta_n]^T = n_p \times 1$ is the vector of unknown parameters ($n_p = n + 1$),

$\boldsymbol{X} = [1\ \xi_1\ \ldots\ \xi_n] = N \times n_p$ is the matrix of vectors of ones and regressors,

$\boldsymbol{\nu} = [\nu(1)\ \nu(2) \ldots \nu(N)]^T = N \times 1$ is the vector of measurement errors.

In general, there are n_0 measured outputs, and a vector of measurements is taken at each sample i, where $i = 1,2,3,\ldots\ldots, N$ is the number of sampled data points. A single measured output is assumed, so $n_0 = 1$, and $\boldsymbol{z}$ is a vector composed of N scalar measurements [35].

Neglecting interactions from other parts of the system, the sway and yaw measurement subsystems can be modeled as

$$Z_{Ymeas} = Y - mwp + \left(mz_g\right)qr + \left(mx_g\right)pq - Y_{uu\delta_r}u^2\delta_r \tag{5.6}$$

This measurement equation is rewritten as

$$Z_{Ymeas} = Y_{uv}uv - \left(Y_{wp} - m\right)wp + \left(Y_{ur} - m\right)ur + Y_{vv}v\left|v\right| + Y_{rr}r\left|r\right| \tag{5.7}$$

$$Z_{Nmeas} = N - \left(N_{pq} + I_{xx} - I_{yy}\right)pq + \left(y_g W\right)\sin\theta + N_{uu\delta_r}u^2\delta_r \tag{5.8}$$

This measurement equation is rewritten as

$$Z_{Nmeas} = N_{wp}wp - N_{ur}ur + N_{uv}uv + N_{vv}v\left|v\right| + N_{rr}r\left|r\right| \tag{5.9}$$

The difference between measurement vector $\boldsymbol{z}$ and estimation result $\boldsymbol{y}$ gives us $\boldsymbol{v}$.

$$v = z - y = z - X\theta = z - X(X^T X)^{-1} X^T z \tag{5.10}$$

For the *least squares model*, there are no probability statements regarding $\boldsymbol{\theta}$ or $\boldsymbol{v}$**,** but $\boldsymbol{v}$ is assumed to be zero mean and uncorrelated, with a constant variance:

$$E(\boldsymbol{v}) = 0 \qquad E(\boldsymbol{v}\boldsymbol{v}^T) = \sigma^2\boldsymbol{I} \tag{5.11}$$

Then the maximum likelihood estimate is:

$$\widehat{\boldsymbol{\theta}} = \begin{matrix} max \\ \theta \end{matrix}\ \mathbb{L}(z;\theta) \tag{5.12}$$

which minimizes the cost function

$$J(\theta) = \frac{1}{2}(z - X\theta)^T (z - X\theta) \tag{5.13}$$

In specifying the form of the *least-squares model*, no uncertainity models for $\boldsymbol{\theta}$ and $\boldsymbol{v}$ are used. An estimate for the *least-squares model* can be obtained by the reasoning that, given $\boldsymbol{z}$, the "best" estimate of $\boldsymbol{\theta}$ comes from minimizing the weighted sum of squared differences between the measured outputs and the model outputs [35]. The parameter estimate $\widehat{\boldsymbol{\theta}}$ that minimizes the cost fuction $J(\boldsymbol{\theta})$ must satisfy

$$\frac{\partial J}{\partial \Theta} = -X^T z + X^T X \hat{\Theta} = 0 \qquad \text{or;} \qquad X^T X \hat{\Theta} = X^T z \tag{5.14}$$

The $\boldsymbol{n_p}$ = n+1 equations represented in Equation (5.13) are called the normal equations. The solution of these equations for the unknown parameter vector $\boldsymbol{\theta}$ gives the formula for the least square estimator,

$$\hat{\theta} = (X^T X)^{-1} X^T z \tag{5.15}$$

The $n_p \times n_p$ matrix $X^T X$ matrix is always symmetric. If the regressor vectors that make up the columns of X are linearly independent, then $X^T X$ is positive definite and the eigen values of $X^T X$ are positive real numbers, and the associated eigenvectors are mutually orthogonal so the $X^T X$ exists (Klein & Morelli, 2006).

Finally, the covariance matrix of the parameter estimate $\widehat{\boldsymbol{\theta}}$, also known as the covariance marix of the estimation error $\widehat{\boldsymbol{\theta}} - \boldsymbol{\theta}$, is simplified to

$$\mathrm{Cov}(\widehat{\boldsymbol{\theta}}) \equiv E\left[(\widehat{\boldsymbol{\theta}} - \boldsymbol{\theta})(\widehat{\boldsymbol{\theta}} - \boldsymbol{\theta})^T\right] = \sigma^2 (X^T X)^{-1} \tag{5.16}$$

5.4 Model Verification

Development of the theory of identification and application of contemporary computer technology has made it possible to assure necessary conditions for the realisation of methods for constructing adequate mathematical models of dynamical systems with measurements obtained during the operation of real systems. It is impossible to construct an identification algorithm with a zero error probability. As a result, the identification is a multistage process whose last stage is the verification of the accuracy of of the real model [11].

The process of selecting important features and associated mathematical approximations needed to represent the reality of interest in the mathematical model is termed modeling. Assessing the correctness of the modeling is termed confirmation. The verification activity focuses on the identification and removal of errors in the software implementation of the mathematical model [3].

Typically, model verification is generally done to ensure that:

- The model is programmed correctly.
- The algorithms have been implemented properly.
- The model does not contain errors, oversights, or bugs.

Verification ensures that the specification is complete and that mistakes have not been made in implementing the model. Verifications do not ensure the model will:

- Solve an important problem.
- Meet a specified set of model requirements.
- Correctly reflect the workings of a real world process.

We used *Hotelling's T-Square* statistics for verification of model proposed.

5.4.1 Hotelling's T-square distribution

In this study, *Hotelling's T-squared* distribution is used for model verification because it arises as the distribution of a set of statistics which are natural generalizations of the statistics. In particular, the distribution arises in multivariate hypothesis testing in undertaking tests of the differences between the (multivariate) means of different populations, where tests for univariate problems would make use of a *t-test* [61].

We assume that the given two hypotheses below are true:

$\boldsymbol{H_0}$: Model verified.

$\boldsymbol{H_1}$: Model not verified.

If the notation $\boldsymbol{T^2_{p,m}}$ is used to denote a random variable having a *Hotelling's T-squared* distribution with parameters $\boldsymbol{p}$ and $\boldsymbol{m}$, then if a random variable $\boldsymbol{X}$ has *Hotelling's T-squared* distribution:

$\boldsymbol{X \sim T^2_{p,m}}$ then

Hotelling's T-squared statistic is defined as follows [28]. Let $\boldsymbol{\mathcal{N}_p(\mu, \Sigma)}$ denote a $\boldsymbol{p}$-variate normal distribution with location $\boldsymbol{\mu}$ and covariance $\boldsymbol{\Sigma}$. Let

$$\mathbf{x_1}, \mathbf{x_2}, \ldots \ldots \mathbf{x}_{\boldsymbol{n}} \sim \boldsymbol{\mathcal{N}_p(\mu, \Sigma)} \qquad \textbf{(5.17)}$$

be $\boldsymbol{n}$ independent random variables, which may be represented by ***px1*** as column vectors of real numbers. Defined as:

$$\bar{\mathbf{x}} = \frac{\mathbf{x_1} + \mathbf{x_2} \ldots \ldots \mathbf{x}_{\boldsymbol{n}}}{\boldsymbol{n}} \equiv \frac{\mathbf{1}}{\boldsymbol{n}} \sum_{\boldsymbol{i=1}}^{\boldsymbol{n}} \boldsymbol{x_i} \qquad \textbf{(5.18)}$$

to be the sample mean. It can be shown that:

$$\boldsymbol{n}(\bar{\mathbf{x}} - \boldsymbol{\mu})^{\boldsymbol{T}} \boldsymbol{\Sigma}^{-\mathbf{1}} (\bar{\mathbf{x}} - \boldsymbol{\mu}) \sim \boldsymbol{X^2_p} \qquad \textbf{(5.19)}$$

where $\boldsymbol{X^2_p}$ is the *chi-squared distribution* with $\boldsymbol{p}$ degrees of freedom. To show this use the fact that and then derive the characteristic function of the random variable [61]. However, $\boldsymbol{\Sigma}$ is often unknown and we wish to do hypothesis testing on the location $\boldsymbol{\mu}$. Defined as:

$$\boldsymbol{W} = \frac{\mathbf{1}}{\boldsymbol{n} - \mathbf{1}} \sum_{\boldsymbol{i=1}}^{\boldsymbol{n}} (\boldsymbol{x_i} - \bar{\mathbf{x}})(\boldsymbol{x_i} - \bar{\mathbf{x}})' \qquad \textbf{(5.20)}$$

to be the sample covariance. Here we denote the transposition by an apostrophe. It can be shown that $\boldsymbol{W}$ is a positive-definite and follows a $\boldsymbol{p}$- variate *Wishart distribution* with $\boldsymbol{n - 1}$ degrees of freedom [61]. *Hotelling's T-squared* statistic is then defined to be:

$$\boldsymbol{t^2} = \boldsymbol{n}(\bar{\mathbf{x}} - \boldsymbol{\mu})'\mathbf{W}^{-\mathbf{1}}(\bar{\mathbf{x}} - \boldsymbol{\mu}) \tag{5.21}$$

because it can be shown that:

$$\boldsymbol{t^2} \sim \boldsymbol{T^2_{p,n-1}}$$

Better results can be obtained from the transformation of the Hotelling $\boldsymbol{T^2}$ statistic as with the $\boldsymbol{F}$ distribution. A transformation of $\boldsymbol{t^2}$ yields an exact $\boldsymbol{F}$ distribution such that:

$$\frac{(\boldsymbol{n} - \boldsymbol{p})}{\boldsymbol{p}(\boldsymbol{n} - \mathbf{1})}\boldsymbol{t^2} \sim \boldsymbol{F^2_{p,n-p}} \tag{5.22}$$

When $\boldsymbol{H_1}$ hypothesis is true and the statistical value $\boldsymbol{t^2}$ will be larger than the $\boldsymbol{T^2_{p,n-1}}$, the distribution ***n-1*** safety tolerance value is:

$$\begin{aligned} &\boldsymbol{H_0}: \mathrm{t}^2 \leq \mathrm{T}^2_{\mathrm{p,n-1}} \qquad \forall k \\ &\boldsymbol{H_1}: \mathrm{t}^2 > \mathrm{T}^2_{\mathrm{p,n-1}} \qquad \exists k \end{aligned} \tag{5.23}$$

.

6. SIMULATION

The simulations included physically based models of AUV systems and the sensor units. This study derived a measurement model for the integrated navigational system including a range model to implement an optimal KF. The navigational system predicts the errors of the state variables based on the IMU sensors with the KF, while the bias and scale errors of the state equation are updated indirectly whenever external measurements are available. Numerical simulations were conducted using the 6-DOF equations of motion of an AUV in a specific mode. The performance of the INS is first examined for the AUV excluding bottom-fixed DVL, compass, and pressure depth sensor. Then, we examined the performance of INS including these auxiliary devices and simulation results illustrated the effectiveness of the integrated navigational system compared with the conventional dead reckoning navigation.

In this study, all simulations were done in the MATLAB version 7.5 environment. Simulation methods are introduced here to demonstrate the validity of the proposed method.

6.1 Simulation Parameters

The EOM that would be used in the AUV dynamic model are:

$$\dot{x} = Ax + w \tag{6.1}$$

where; $\boldsymbol{x}$ is the vector matrix that contains the state variables, $\dot{\boldsymbol{x}}$ is the output vector, $\boldsymbol{u}$ is the control or input vector, $\boldsymbol{A}$ is the state matrix, $\boldsymbol{w}$ is the noise wector of the dynamic system.

The state vector of physically based AUV model is:

$$x = [u, \mathrm{v}, \mathrm{w}, \mathrm{p}, \mathrm{q}, \mathrm{r}, X,\ Y,\ Z,\ \phi,\ \theta,\ \psi]^T$$
$$u_i = [\delta_r,\ \delta_e,\ u_0] \qquad \textbf{(6.2)}$$

where the order of the state vector is 12.

The variables in the state vector (6.2) are:

u: AUV speed in direction *X*(m/sec)

v: AUV speed in direction *Z*(m/sec)

w: AUV speed in direction *Z*(m/sec)

ϕ : roll angle (degree)

θ : pitch angle (degree)

ψ : yaw angle (degree)

p: roll angular speed(degree/sec)

q: pitch angular speed(degree/sec)

r: yaw angular speed(degree/sec)

Standard deviations and bias errors of sensors are defined in Table6.1.

Table 6.1 : Standard deviations and bias errors of sensors.

	Bias error	**Random noise (std. dev.)**
Accelerometer	5 mg	500.0 µg
Gyro	0.5 °/h	0.31 °/s
Magnetic Compass	1.0°	1.0 °
Depth Sensor	0.5m	0.5 m
DVL	0.01 m/s	0.1 m/s

Correlation times of gyros and accelometers are defined as:

$$\beta_{gyros} = 1/1300\ [s^{-1}], \quad \beta_{accel} = 1/1500\ [s^{-1}]$$

Correlation times of DVL ***x, y, z*** velocities are defined as:

$$\beta_{V_{DVLx}} = 1/700\ [s^{-1}],\ \beta_{V_{DVLy}} = 1/900\ [s^{-1}],\ \beta_{V_{DVLz}} = 1/850\ [s^{-1}]$$

Sampling time interval is taken at *T*=0.002 [sec] in the simulation.

6.2 Simulation Results of AUV Model and Navigation System Errors

The combined performance of navigation was evaluated in the simulation with a nonlinear model of the vehicle using the MATLAB version 7.5 environment. The simulation included physically based models of AUV systems. Trajectory simulation results of the AUV are shown in Figure 6.1 – 6.3.

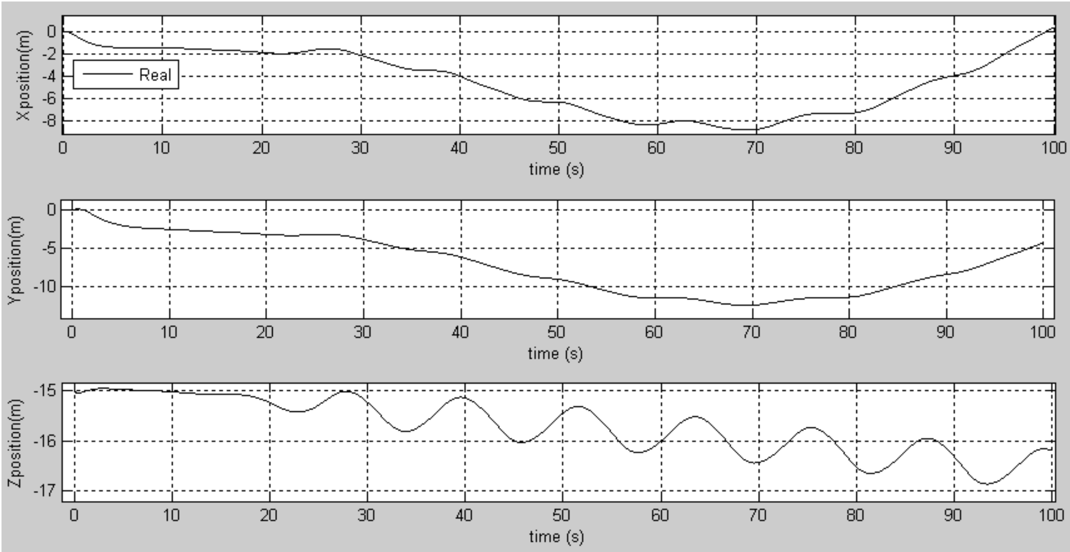

Figure 6.1 : Position simulation results of physically based AUV model (100 sec).

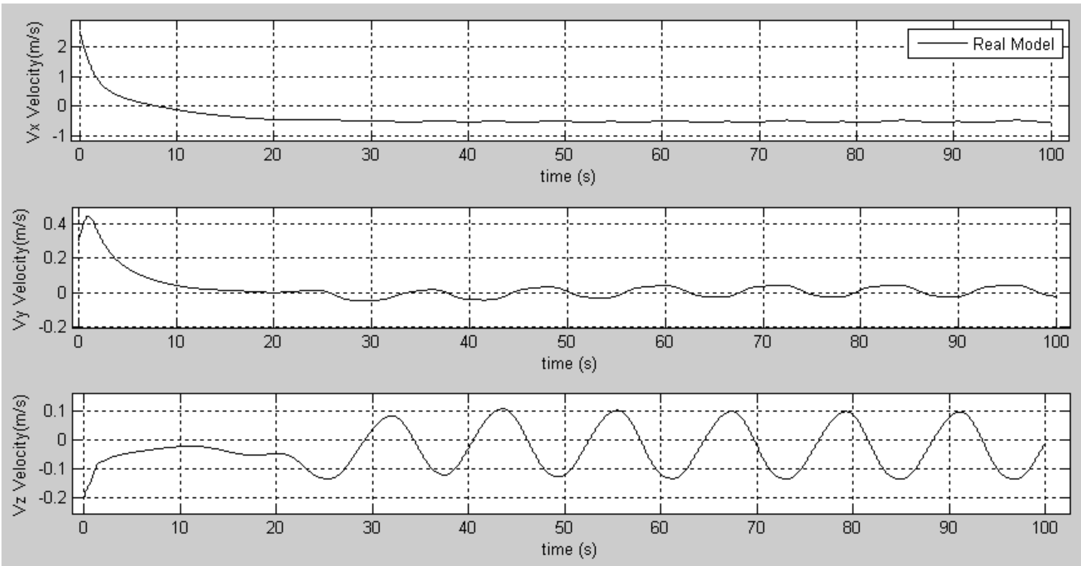

Figure 6.2 : Velocity simulation results of physically based AUV model (100 sec).

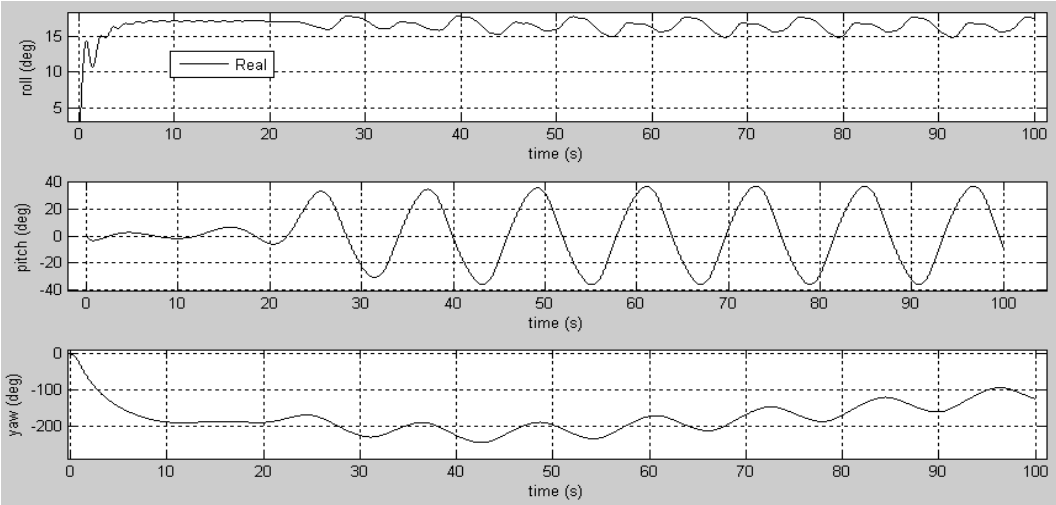

Figure 6.3 : Attitude simulation results of physically based AUV model (100 sec).

Similarly, in Figure 6.4-6.7, the error model simulation results of INS, accelometers, gyros, DVL, compass, and pressure depth sensor are shown respectively.

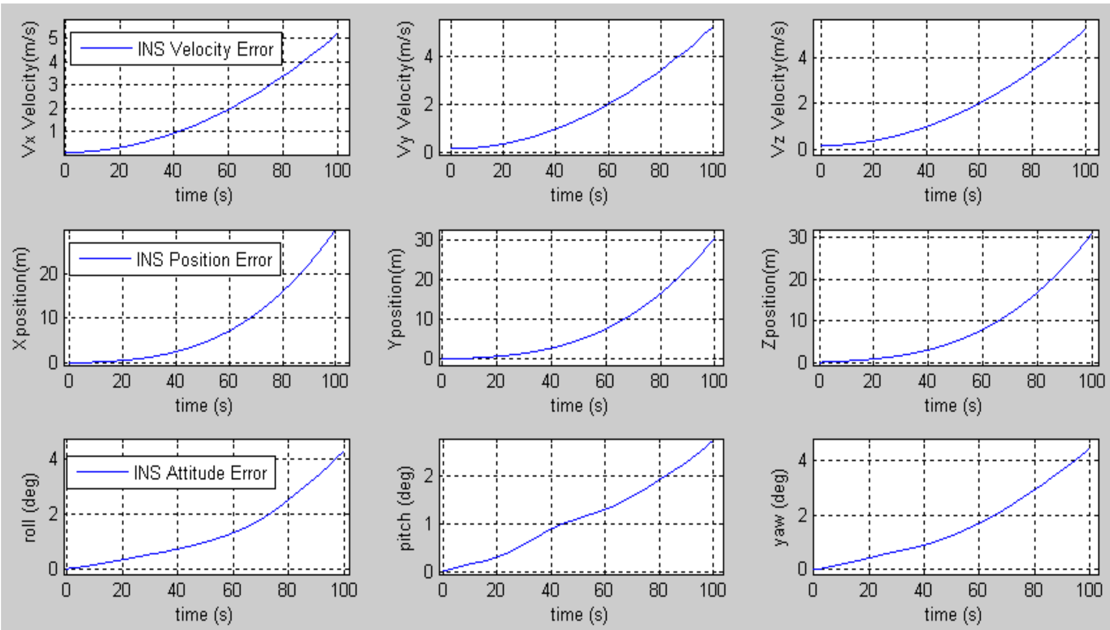

Figure 6.4 : Simulation results of INS error model.

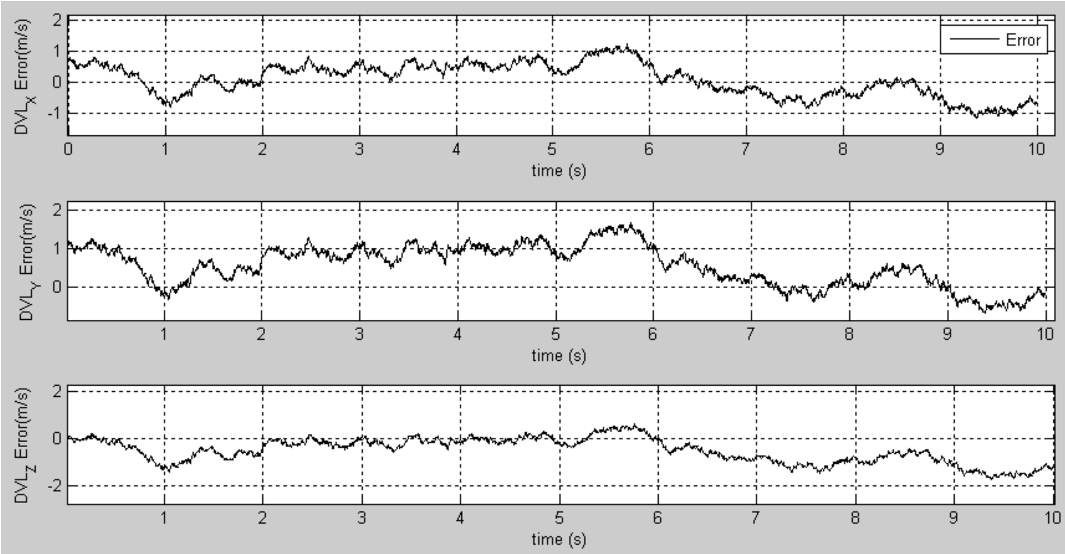

Figure 6.5 : Simulation results of DVL error model.

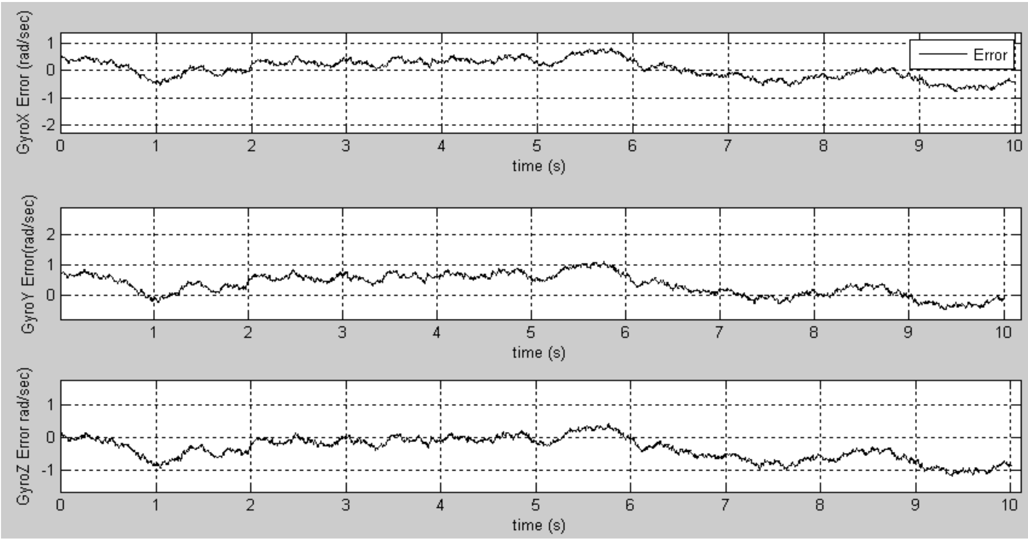

Figure 6.6 : Simulation results of gyro error models.

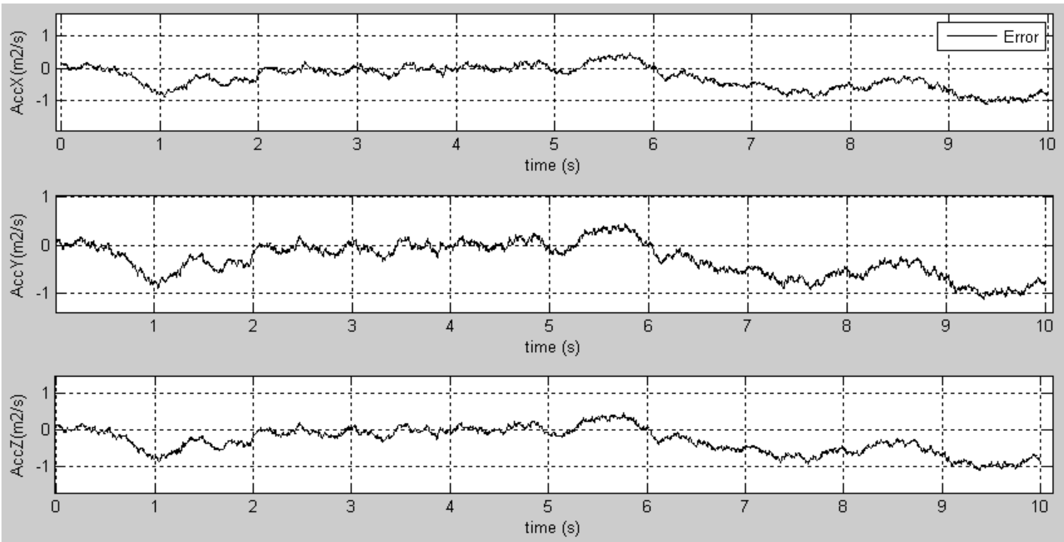

Figure 6.7 : Simulation results of accelometer error models.

6.3 Simulation Results of Integrated Navigation Systems

6.3.1 Simulation results of INS calibration

Simulation results of physically based AUV model combined with integrated navigation solution and diagonal elements of covariance matrix are shown in Figure 6.8 – 6.13. For this, the trajectory of an AUV was generated and models of the strapdown INS sensor errors were developed. The trajectory is characterized by minimum changes of movement parameters without a control.

In the graphs, the blue line represents the real physically based AUV model, and the red line corresponds to integrated navigation solution of position, velocity and attitude angles, respectively. As seen from the graphs below, red and blue lines overlapped most of the time because the integrated navigation system gives the best results.

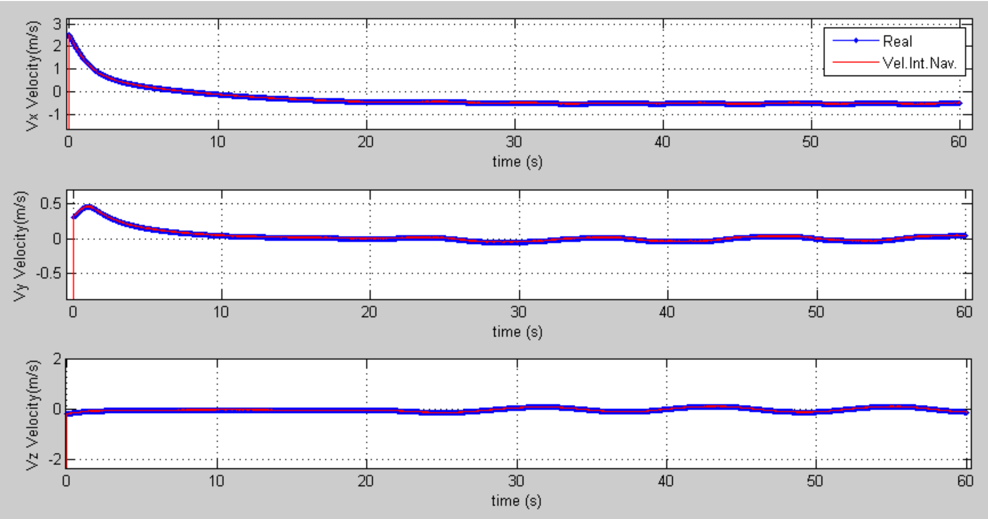

Figure 6.8 : Simulation results of AUV model & INS velocity estimation.

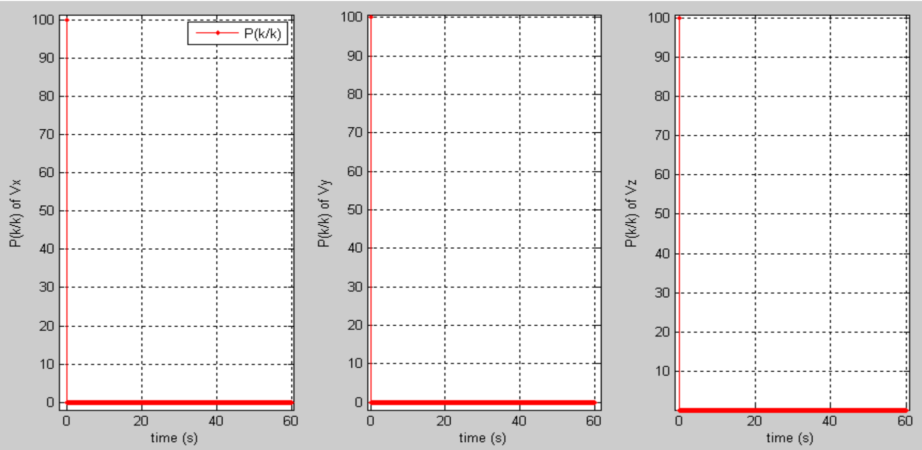

Figure 6.9 : Diagonal elements of covariance matrix for velocities.

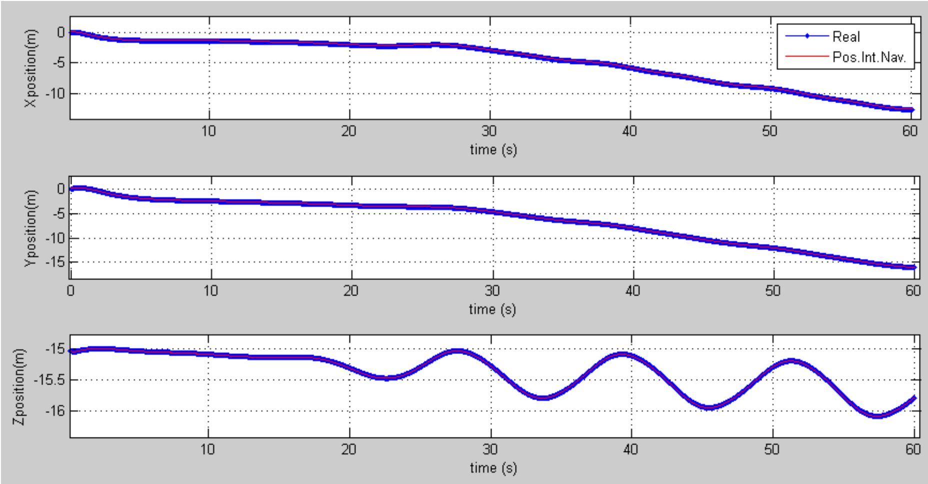

Figure 6.10 : Simulation results of AUV model & INS position estimation.

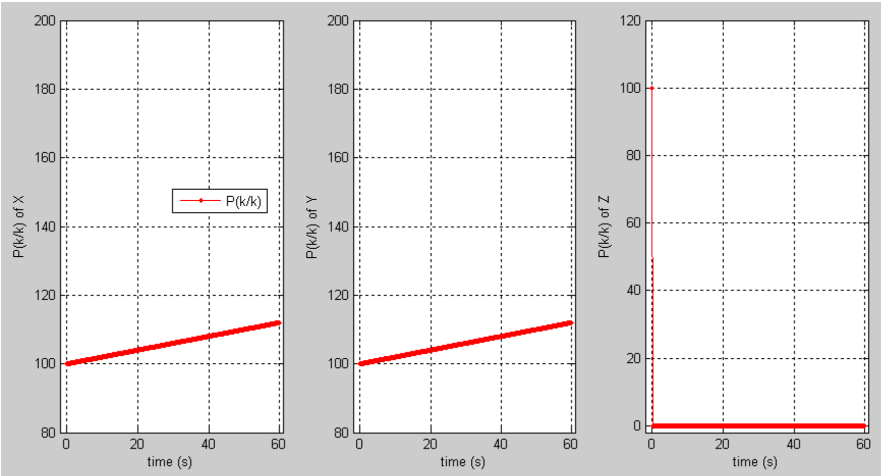

Figure 6.11 : Diagonal elements of covariance matrix for positions.

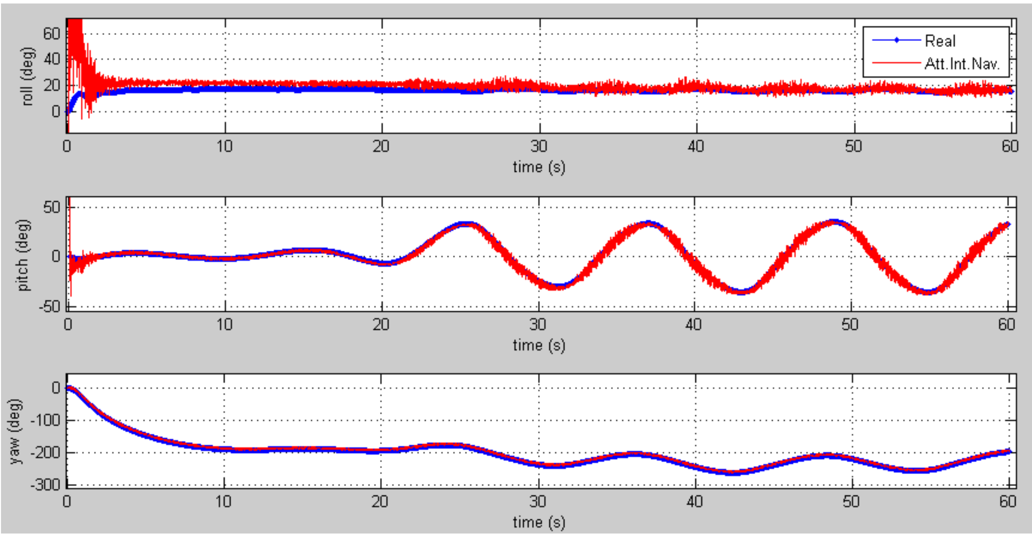

Figure 6.12 : Simulation results of AUV model & INS attitude estimation.

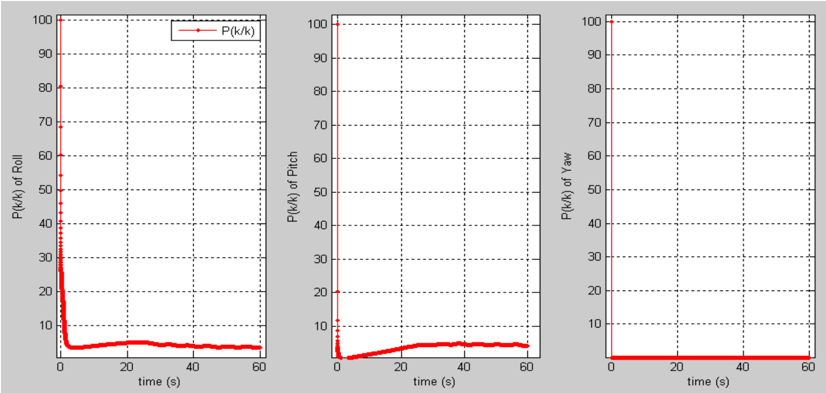

Figure 6.13 : Diagonal elements of covariance matrix for attitude anlges.

6.3.2 Simulation results of INS, gyro, and accelometer calibration

Simulation results of the physically based AUV model combined with integrated navigation solution and diagonal elements of covariance matrix are shown in Figure 6.14 – 6.19. For this, the trajectory of an AUV was generated and models of the strapdown INS sensor errors were developed. Errors of the IMU were modeled in the navigation grade systems where accelerometer errors are biased at 0.02 m/s^2 and noise at 2 mm/s^2/Hz$^{-1/2}$, and the rate gyro errors are modeled with a bias of 5 deg/h and noise at 0.1deg/h /Hz$^{-1/2}$. The trajectory is characterized by minimum changes of movement parameters without a control.

In the graphs, the blue line represents the real physically based AUV model, and the red line corresponds to integrated navigation solution of position, velocity and attitude angles, respectively. As seen from the graphs below, red and blue lines overlapped most of the time because the integrated navigation system gives the best results.

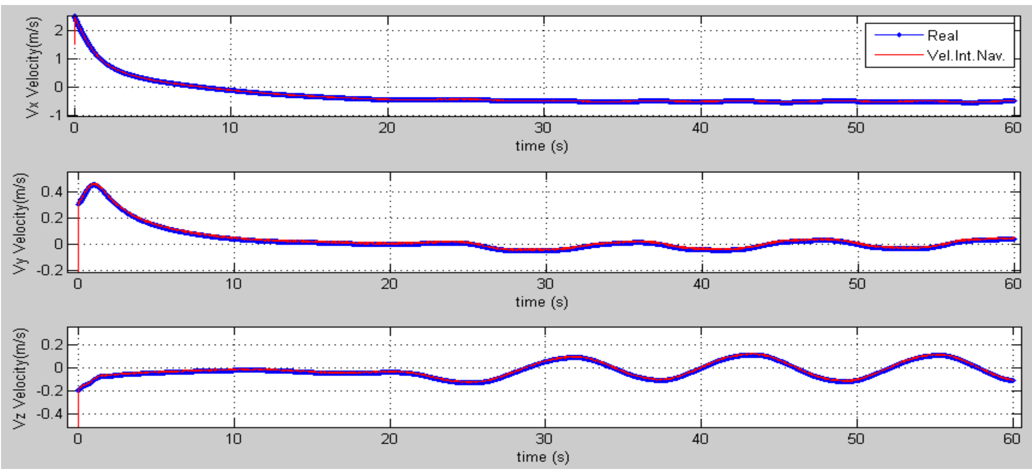

Figure 6.14 : Simulation results of AUV model & INS velocity estimation.

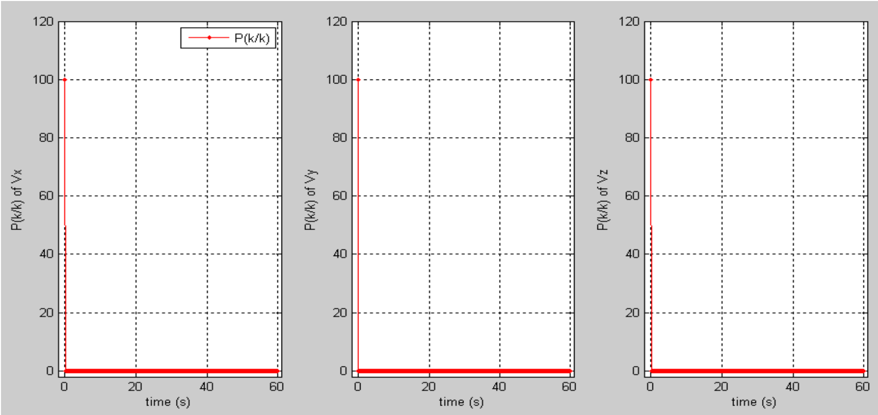

Figure 6.15 : Diagonal elements of covariance matrix for velocities.

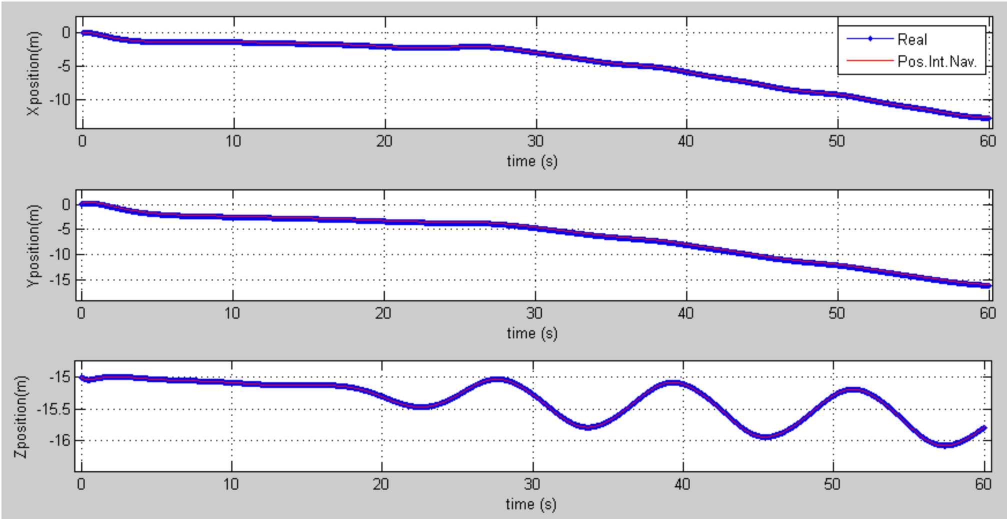

Figure 6.16 : Simulation results of AUV model & INS position estimation.

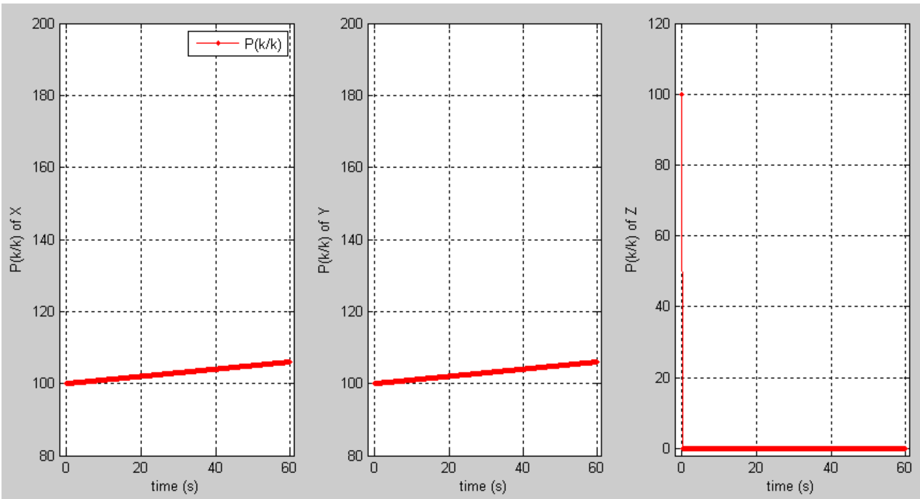

Figure 6.17 : Diagonal elements of covariance matrix for positions.

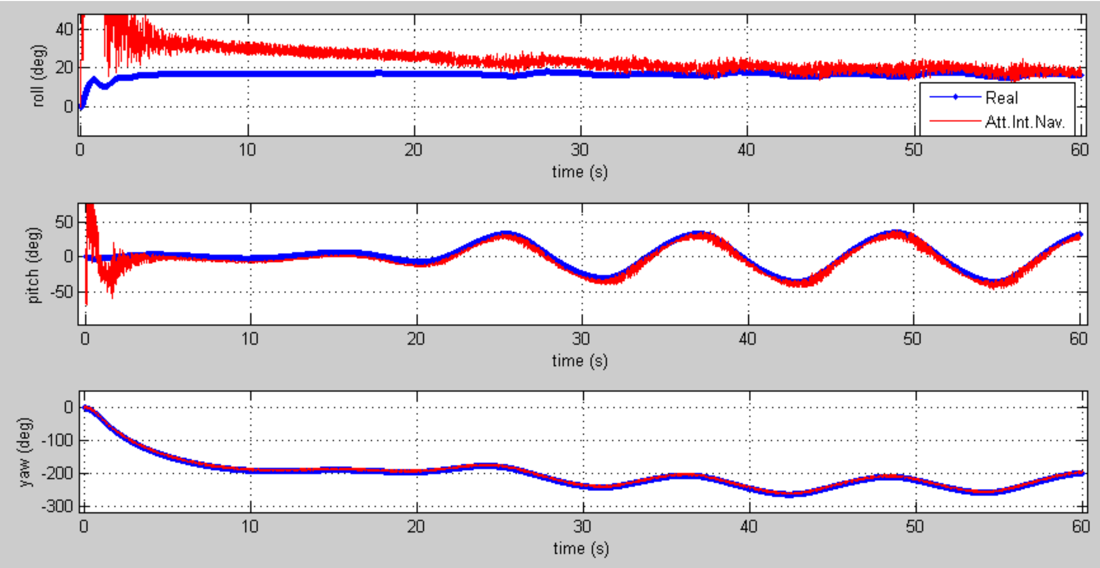

Figure 6.18 : Simulation results of AUV model & INS attitude estimation.

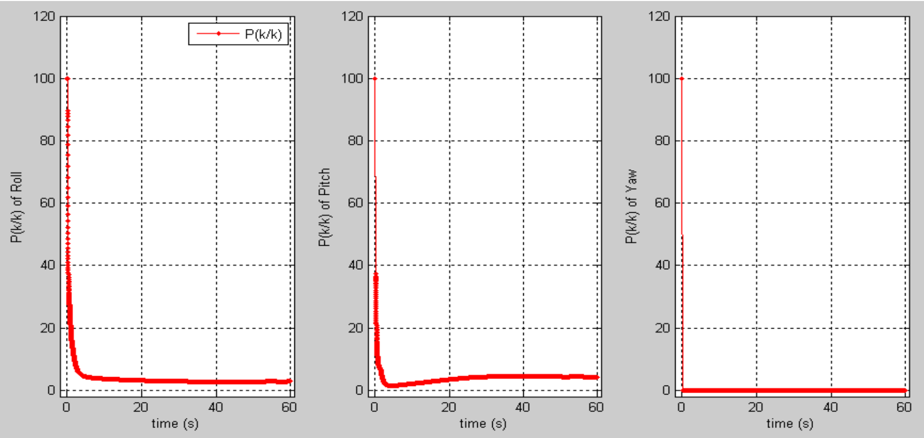

Figure 6.19 : Diagonal elements of covariance matrix for attitude anlges.

6.3.3 Simulation results of INS, DVL, compass, and depth sensor calibration

Simulation results of the physically based AUV model combined with integrated navigation solution with INS, DVL, compass and depth sensor calibration, and diagonal elements of covariance matrix are shown in Figure 6.20 – 6.25. The trajectory is characterized by minimum changes of movement parameters without a control.

In the graphs, the blue line represents the real physically based AUV model, and the red line corresponds to integrated navigation solution of position, velocity and attitude angles, respectively. As seen from the graphs below, red and blue lines overlapped most of the time because the integrated navigation system gives the best results.

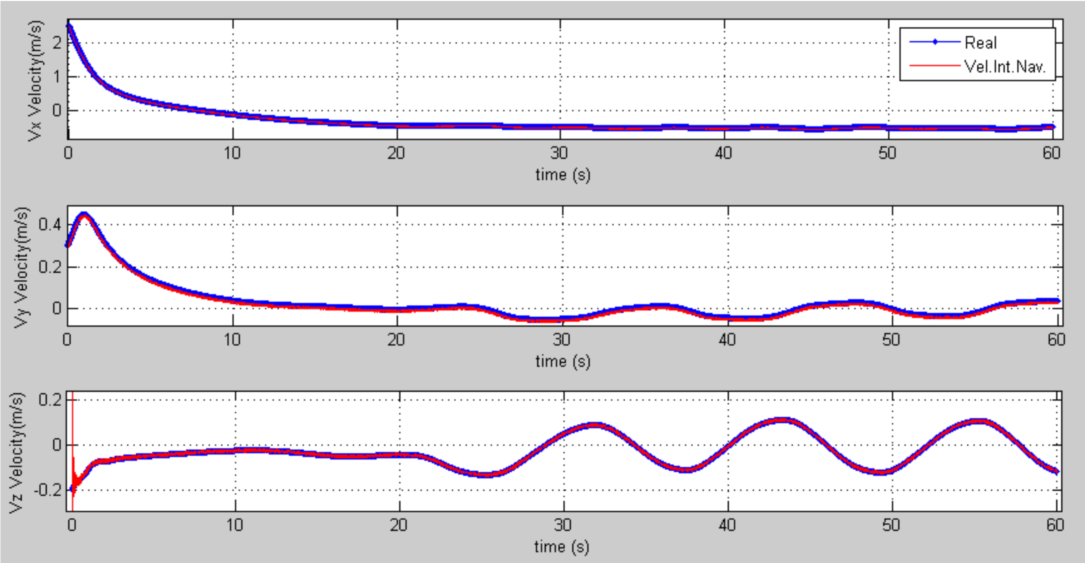

Figure 6.20 : Simulation results of AUV model & INS velocity estimation.

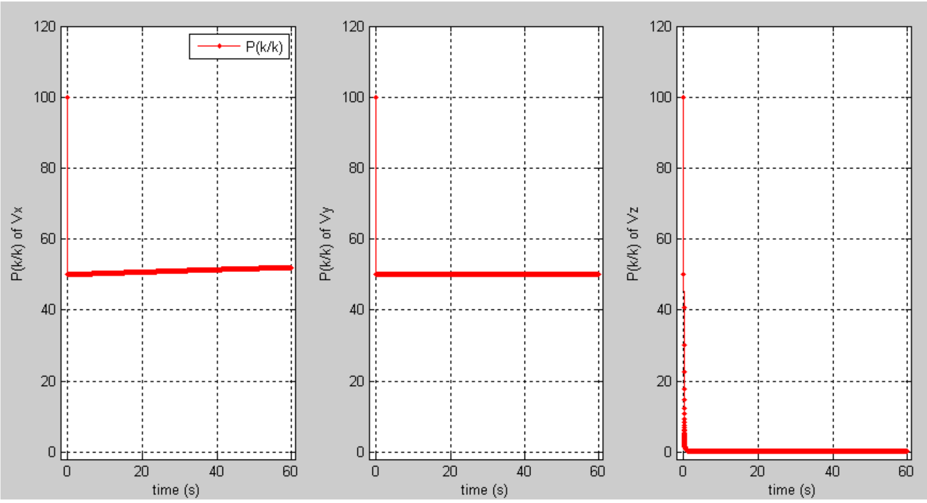

Figure 6.21 : Diagonal elements of covariance matrix for velocities.

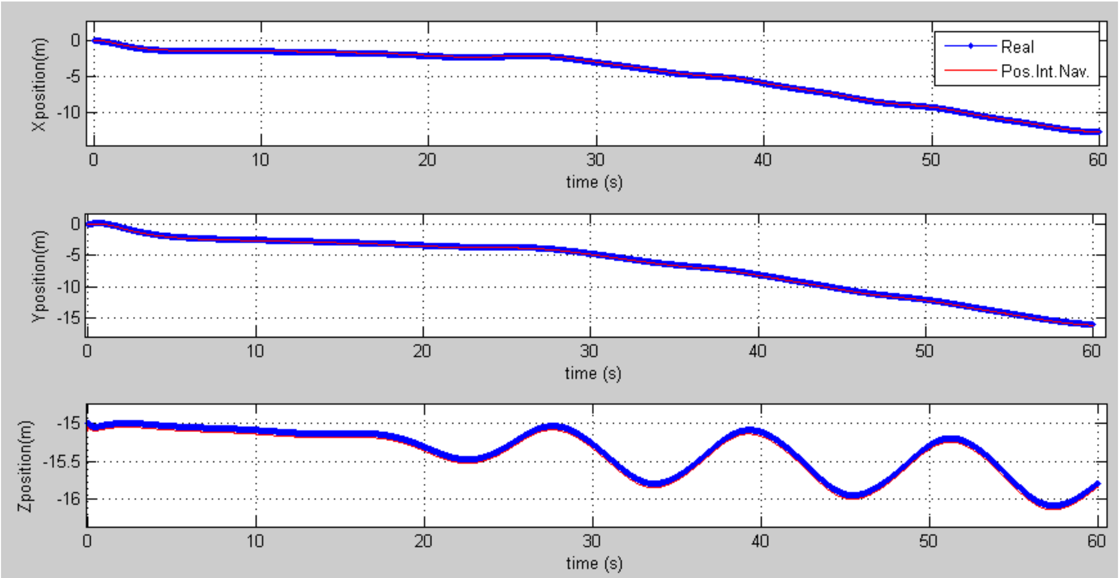

Figure 6.22 : Simulation results of AUV model & INS position estimation.

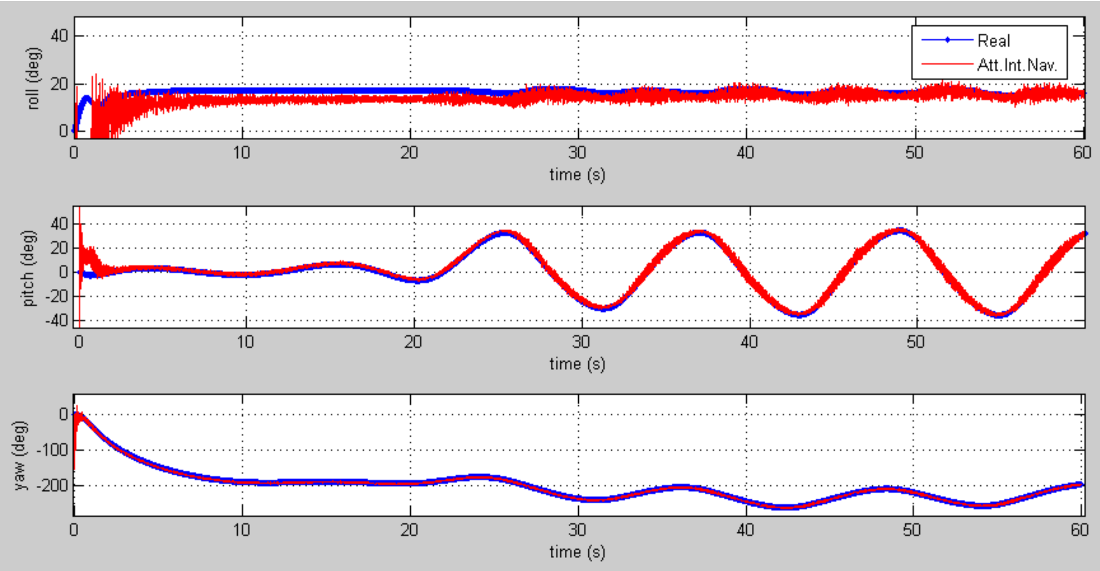

Figure 6.23 : Simulation results of AUV model & INS attitude estimation.

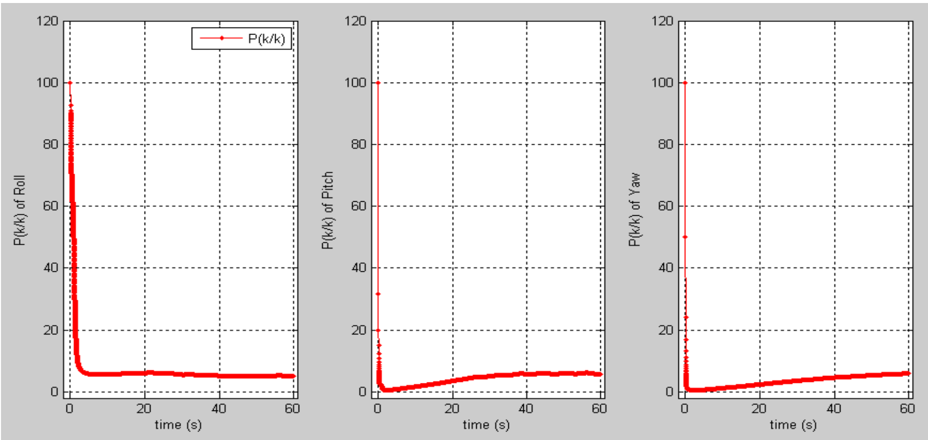

Figure 6.24 : Diagonal elements of covariance matrix for attitude anlges.

6.3.4 Comparison of integrated navigavigation systems

In this section, we compare three different types of integrated navigation systems which are INS calibration, integration of INS with accelometers and gyros calibration, and integration of INS with DVL, compass and depth sensor calibration, based on absolute error values. In Table 6.2 – 6.4, absolute error values of velocities, postions and attitude angles for those calibration methods are given during 60 seconds with 5 second time intervals. In the tables, INS calibration has superiority to the others with the minimum absolute errors becouse of lower number of state variables (n=9). Integration of INS with DVL, compass and depth sensor calibration has better performance than with gyro and accelometer calibration on all velocity, positon Y, roll, pitch and yaw angles. However, the integration of INS with accelometers and gyros calibration has better performance than with DVL, compass and depth sensor calibration on positions X and Z. On the other hand, the integration of INS with accelometers and gyros calibration has the worst performance on attitude angles in comparsion with the other integration metods.

Table 6.2 : Coparision of absolute velocity errors.

	Absolute Error of Velocity X (m/sec)			Absolute Error of Velocity Y (m/sec)			Absolute Error of Velocity Z (m/sec)		
Time (sec)	INS Only	with Gyro & Accelometer	with DVL, Compass, & Depth Sensor	INS Only	with Gyro & Accelometer	with DVL, Compass, & Depth Sensor	INS Only	with Gyro & Accelometer	with DVL, Compass, & Depth Sensor
0	2,0000	1,0000	1,0250	2,0100	1,0500	0,0150	2,2100	1,0500	0,0680
5	0,0015	0,0187	0,0179	0,0024	0,0040	0,0091	0,0005	0,0132	0,0028
10	0,0008	0,0102	0,0129	0,0018	0,0144	0,0109	0,0008	0,0038	0,0016
15	0,0027	0,0135	0,0163	0,0010	0,0064	0,0075	0,0009	0,0123	0,0002
20	0,0036	0,0141	0,0086	0,0010	0,0107	0,0075	0,0014	0,0069	0,0032
25	0,0011	0,0060	0,0143	0,0018	0,0090	0,0078	0,0013	0,0074	0,0005
30	0,0026	0,0085	0,0081	0,0019	0,0127	0,0114	0,0012	0,0071	0,0006
35	0,0031	0,0200	0,0171	0,0026	0,0129	0,0085	0,0008	0,0057	0,0028
40	0,0010	0,0133	0,0098	0,0014	0,0122	0,0041	0,0014	0,0083	0,0072
45	0,0018	0,0120	0,0079	0,0023	0,0147	0,0089	0,0012	0,0049	0,0007
50	0,0045	0,0130	0,0153	0,0025	0,0154	0,0082	0,0012	0,0110	0,0018
55	0,0029	0,0169	0,0154	0,0023	0,0136	0,0093	0,0011	0,0075	0,0040
60	0,0032	0,0072	0,0125	0,0010	0,0090	0,0077	0,0012	0,0037	0,0046

Table 6.3 : Coparision of absolute position errors.

	Absolute Error of Position X (m)			Absolute Error of Position Y (m)			Absolute Error of Position Z (m)		
Time (sec)	INS Only	with Gyro & Accelometer	with DVL, Compass, & Depth Sensor	INS Only	with Gyro & Accelometer	with DVL, Compass, & Depth Sensor	INS Only	with Gyro & Accelometer	with DVL, Compass, & Depth Sensor
0	0,1366	0,0363	0,0697	0,0683	0,2017	0,0983	0,0750	0,0250	0,0917
5	0,1385	0,0386	0,0674	0,0697	0,2031	0,1000	0,0008	0,0009	0,0523
10	0,1406	0,0407	0,0655	0,0711	0,2045	0,1017	0,0008	0,0010	0,0523
15	0,1428	0,0429	0,0630	0,0725	0,2059	0,1028	0,0008	0,0008	0,0519
20	0,1450	0,0450	0,0618	0,0739	0,2074	0,1041	0,0005	0,0009	0,0523
25	0,1471	0,0472	0,0590	0,0753	0,2088	0,1055	0,0009	0,0008	0,0522
30	0,1493	0,0494	0,0581	0,0768	0,2102	0,1080	0,0010	0,0007	0,0522
35	0,1515	0,0516	0,0542	0,0782	0,2117	0,1085	0,0008	0,0008	0,0524
40	0,1536	0,0538	0,0540	0,0797	0,2132	0,1082	0,0008	0,0009	0,0519
45	0,1559	0,0560	0,0525	0,0811	0,2147	0,1113	0,0008	0,0011	0,0522
50	0,1580	0,0581	0,0481	0,0824	0,2161	0,1121	0,0008	0,0012	0,0525
55	0,1602	0,0603	0,0461	0,0839	0,2176	0,1145	0,0006	0,0008	0,0524
60	0,1619	0,0625	0,0453	0,0849	0,2190	0,1145	0,0060	0,0010	0,0523

Table 6.4 : Coparision of absolute errors of attitude angles.

	Absolute Error of Roll (deg)			Absolute Error of Pitch (deg)			Absolute Error of Yaw (deg)		
Time (sec)	INS Only	with Gyro & Accelometer	with DVL, Compass, & Depth Sensor	INS Only	with Gyro & Accelometer	with DVL, Compass, & Depth Sensor	INS Only	with Gyro & Accelometer	with DVL, Compass, & Depth Sensor
0	3,0000	0,0000	0,4500	0,2300	0,2300	0,1150	0,2000	0,8000	0,1000
5	4,7450	18,6121	3,6658	1,9447	6,8068	0,4280	4,1210	3,9269	0,4933
10	2,8087	9,7762	2,7003	0,9888	3,8476	0,0937	2,0190	5,9130	2,4854
15	0,9244	10,0079	2,8327	0,1506	5,1445	0,8685	3,1976	3,6111	2,3200
20	0,4174	9,8990	4,9493	1,4167	6,0118	1,8510	4,8400	2,1854	0,7132
25	2,0276	7,4079	3,6007	0,9900	6,1978	1,6078	1,8182	2,3094	0,5463
30	1,2120	4,8101	1,9784	4,6105	4,4019	2,8211	4,2057	4,4348	0,6920
35	1,4686	4,8610	2,3355	4,7632	3,6040	4,8420	0,6005	2,7959	0,5681
40	3,7283	5,0994	2,5111	5,3677	3,4966	2,9356	4,0208	0,5837	0,5294
45	4,2374	6,1384	2,7507	3,3716	1,1773	2,6994	0,2094	2,8602	0,1610
50	0,5008	0,7748	2,3062	4,8646	3,3240	0,2795	0,3886	3,7295	0,4047
55	1,4924	3,0005	0,2934	0,3968	5,2771	0,0296	1,6650	3,8827	0,1198
60	1,6811	2,9614	0,8089	1,7361	5,8955	1,2459	4,3712	1,3583	0,2105

6.4 Simulation Results of Parameter Identification

Numerical simulations are made to show the parameter identifications of the AUV. The hydrodynamic coefficients associated with horizontal and vertical motions are estimated by simulating the combined yaw and sway motion of the AUV.

We will describe how state-of-the art algorithms are used to find a dynamic model that enables accurate simulation of steering dynamics. Simulation is in fact much more than what is required by sensor fusion algorithms for integrated navigation, where only the predictive ability of the model is important.

In summary, the system identification task to estimate the parameters is:

$$\boldsymbol{\theta} = \left[Y_{vv}\ Y_{rr}\ Y_{uv}\ Y_{ur}\ Y_{wp}\ N_{vv}\ N_{rr}\ N_{uv}\ N_{ur}\ N_{wp}\ \right] \qquad \textbf{(6.5)}$$

In this study, we used two different simulation settings for parameter identification: one is with measurement bias and the other is with integrated navigational system.

6.4.1 Numerical simulation for measurement bias

The combined problem of state and parameter identification leads to a nonlinear filtering problem. Furthermore, many AUV systems are characterized by nonlinear models as well as noisy and biased sensor measurements. In Figure 6.25, parameter identification simulation setting is illustrated in the presence of measurement bias used in this study.

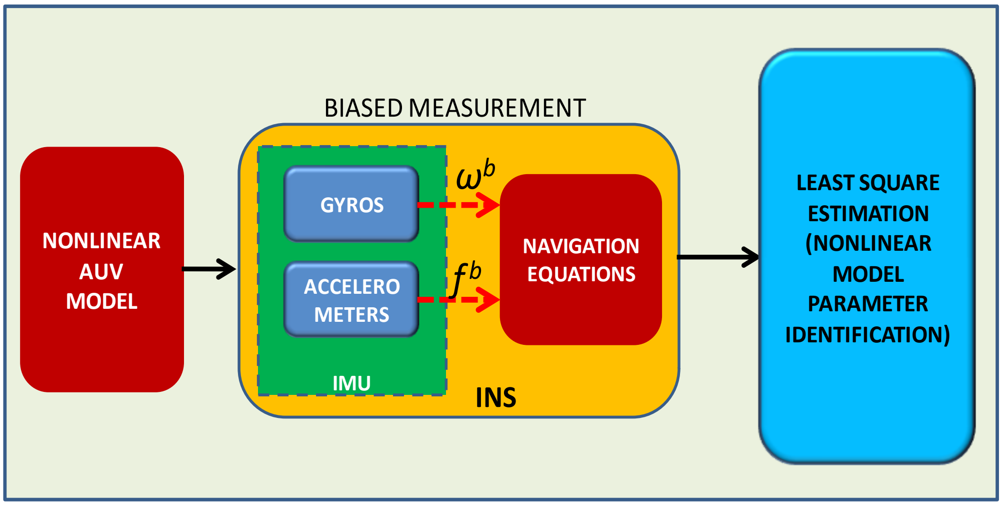

Figure 6.25 : Parameter identification in the presence of measurement biases.

Parameter identification was done by recording the rudder and elevator input angles and the AUV's yaw and pitch response during a closed-loop heading and depth maneuver. However, the AUV has to maintain constant speed and small roll angle during this maneuver. The Figures 6.26 – 6.28 show that the AUV had a surge velocity changed between 2.5 and 0 m/s and a heave velocity of 0.13 m/s. The depth changed between -15 m and -13.5 m. At the same time, the AUV pitched up and down between -40 deg and 0 deg in response to the changing elevator plane angle. The elevator was operated at the maximum deflection of 15 deg for most of the time and similarly the rudder deflection was operated at the maximum deflection of -11 deg. The iteration number N is chosen to be 5,000 and the sampling time is chosen to be 0.001 sec in this simulation.

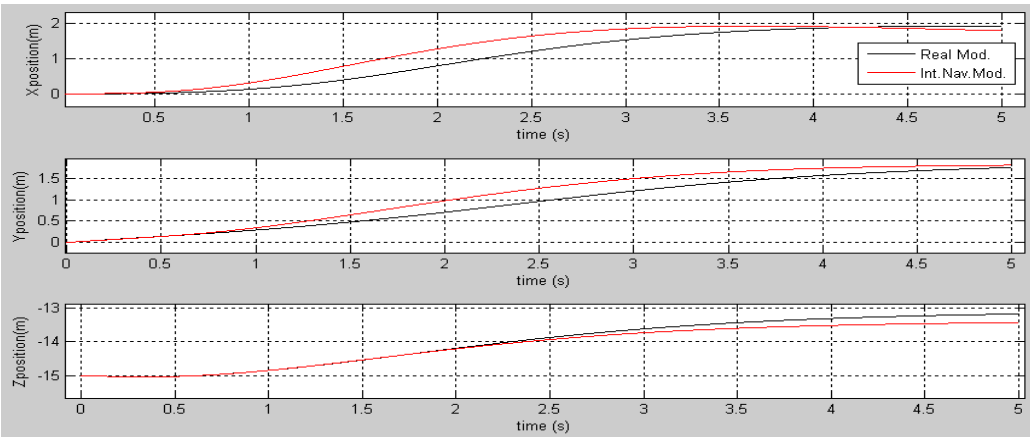

Figure 6.26 : Position results of real and identified model.

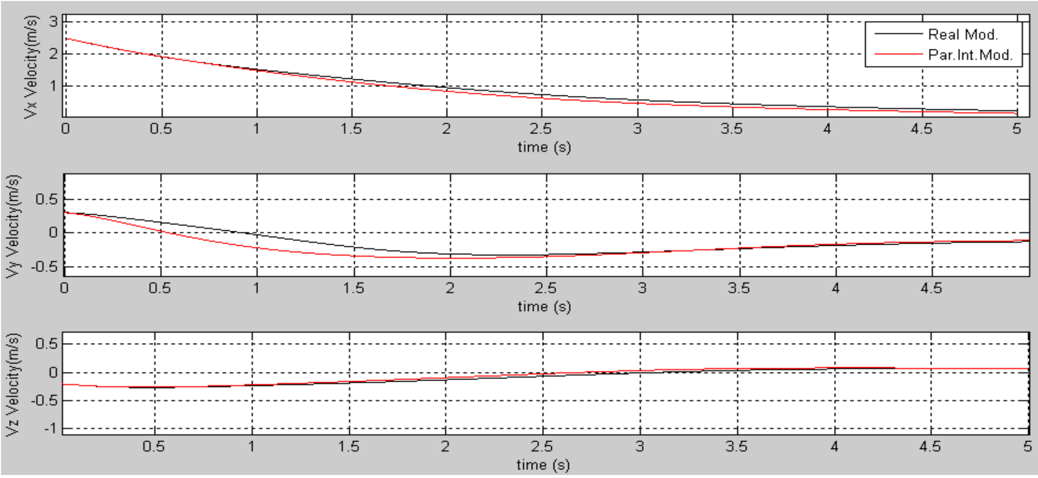

Figure 6.27 : Velocity results of real and identified model.

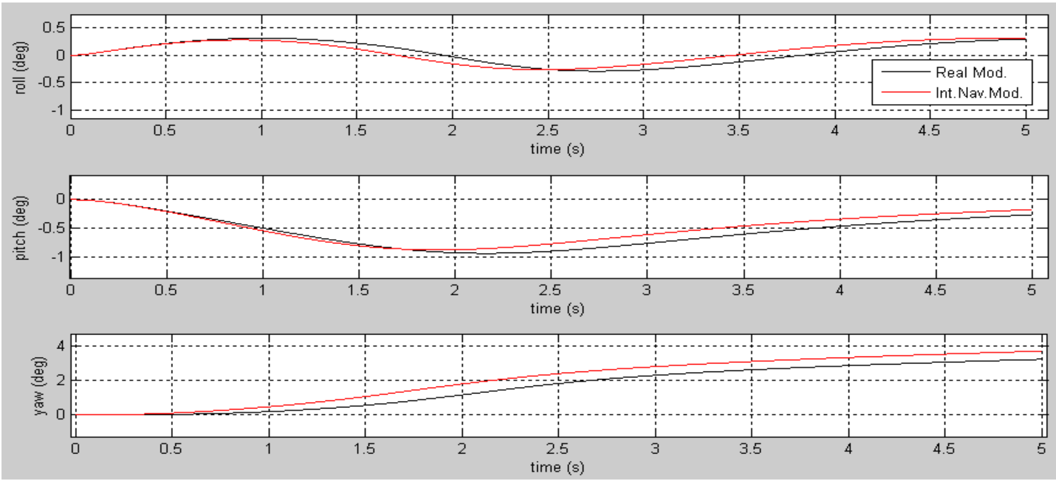

Figure 6.28 : Attitude results of real and identified model.

As seen in Figures 6.26 – 6.28, the difference between simulation results of real phsically based AUV model and identified model are shown. Most of the velocites are quite resonalable. However, there big difference in attitude and position response of the real and identified model as we expected.

The estimated values of the parameters and error differences are given in Table 6.5. This table also shows that iterated LSE has a performance under the condition of integration of navigational sensors with the maximum error difference of 172.42 % in Y_{rr} percent and the minimum error difference of 2.32% in Y_{ur}.

Table 6.5 : Parameter identification with measurement bias.

Parameters	Real Value	Est. Value with Bias	Percent %	Difference
Yvv	-196,26	-50,223	74,410	146,037
Yrr	8,30	22,611	172,419	14,311
Yuv	38,39	13,647	64,452	24,743
Yur	13,41	13,099	2,322	0,311
Ywp	35,50	95,156	168,046	59,656
Nvv	-7,95	-7,436	6,465	0,514
Nrr	-24,13	-18,457	23,511	5,673
Nuv	-21,89	-12,239	44,089	9,651
Nur	1,93	3,822	98,026	1,892
Nwp	-19,30	-3,489	81,922	15,811

For model verification, the sample variance-covariance matrix is calculated:

$$\boldsymbol{W} = \begin{bmatrix} 0.0065 & -0.0118 & 0.0229 & -0.0268 & -0.0002 \\ -0.0118 & 0.0284 & -0.0260 & 0.0499 & 0.0003 \\ 0.0229 & -0.0260 & 0.1159 & -0.0937 & -0.0008 \\ -0.0268 & 0.0499 & -0.0937 & 0.1210 & 0.0006 \\ -0.0002 & 0.0003 & -0.0008 & 0.0006 & 0.0000 \end{bmatrix}$$

Hotelling's T-square comes out to be:

$$\boldsymbol{T^2} = \mathbf{17318}$$

Similarly, the F-statistic is:

$$\boldsymbol{F} = \mathbf{3461} > 2.41 = \boldsymbol{F}_{\mathbf{10,4995,0.01}}$$

Using the statistical hypothesis test to evaluate the null hypothesis of the parameter identification model which was verified, the resulting test statistics is $\mathbf{17318}$. For an **0.01** level test, the critical $\boldsymbol{F}$ value is approximately found as **2.41** from the F-statistic table. Since $\mathbf{17318}$ is greater than this value, as a result we can reject the null hypothesis that the proposed model is not valid.

$$\mathbf{T^2} = \mathbf{17318};\ \mathbf{F} = \mathbf{3461};\ \mathbf{df} = \mathbf{10,4995};\mathbf{p} < 0.01$$

6.4.2 Numerical simulation for integrated navigation

The simulation setting of parameter identification after integrating the navigational systems are shown in Figure 6.28.

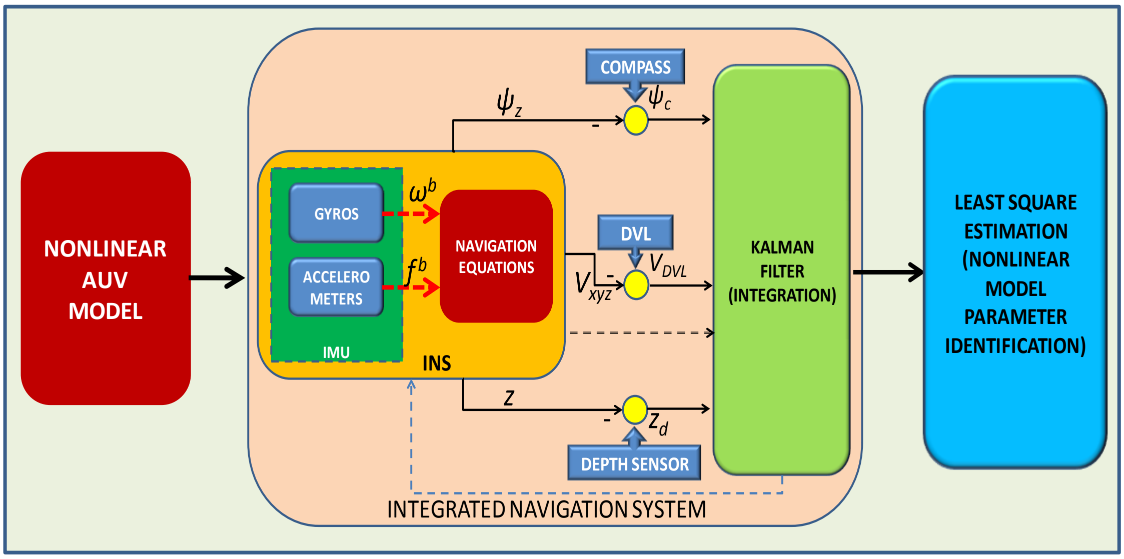

Figure 6.29 : Parameter identification after integration of navigational systems.

Parameter identification was done and the Figures 6.30 -6.32 show that the AUV had a surge velocity changed between 2.5 and 0 m/s. The depth changed between -15 m and -13.5 m. The elevator was operated at the maximum deflection of 15 deg for most of the time and similarly the rudder deflection operated at the maximum deflection of -11 deg. The iteration number N is chosen to be 5,000 and the sampling time is chosen to be 0.001 sec.

As seen from Figures 6.30 – 6.32 outputs of real and identified models are converged perfectly. Simulation results show that the proposed method works very well and iterated LSE has a better performance.

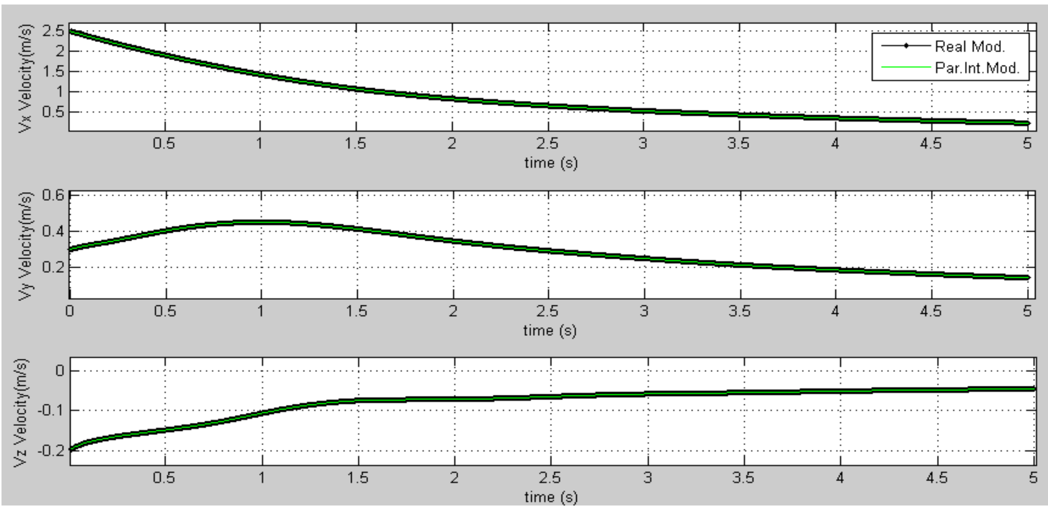

Figure 6.30 : Velocity simulation results of real and identified model.

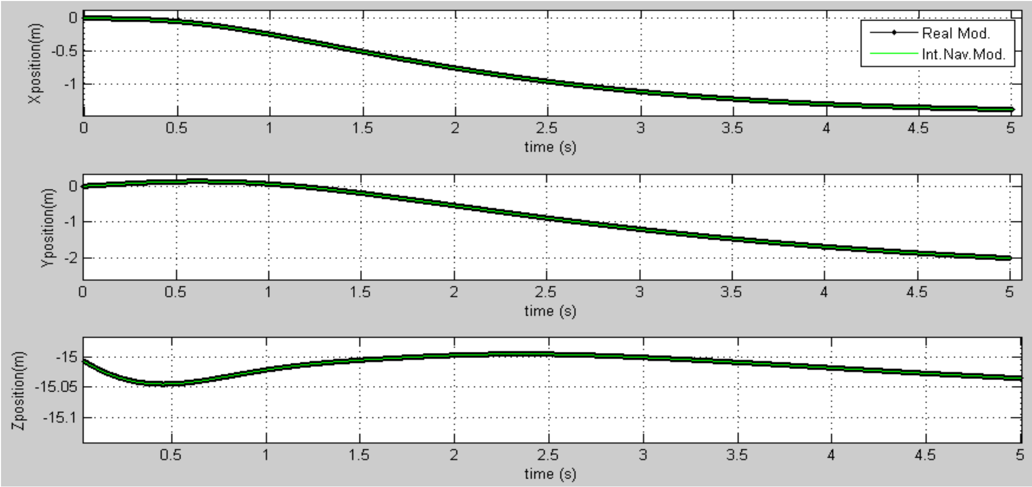

Figure 6.31 : Position simulation results of real and identified model.

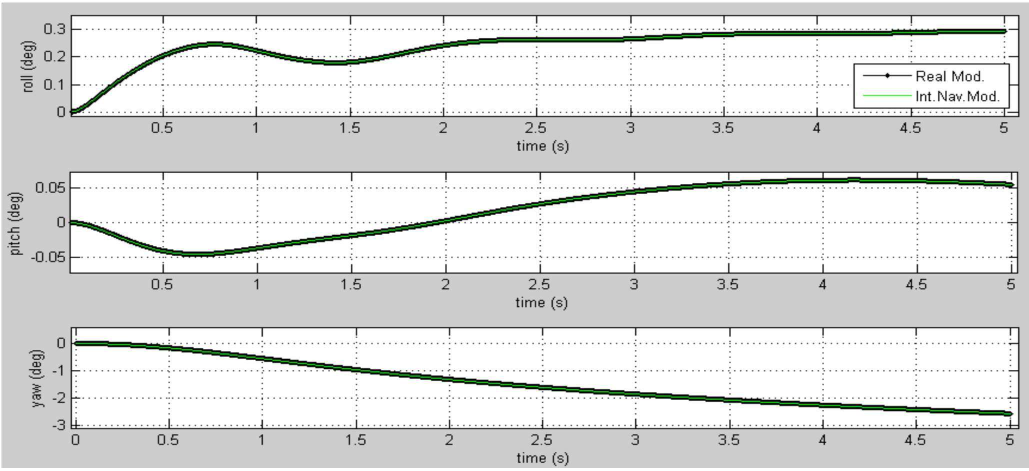

Figure 6.32 : Attitude simulation results of real and identified model.

In Table 6.6, parameter identification values for ten different hydrodynamic parameters are given. This table also shows that iterated LSE has a better performance under the condition of integration of navigational sensors with the maximum error difference of 3.37% in parameter Y_{rr} and the minimum error difference 0.22% in parameter N_{uv}.

Table 6.6 : Parameter identification after integrated navigation.

Parameters	Real Value	Est. Value with Int.Nav.	%	Difference
Yvv	-196,26	-192,650	1,839	3,610
Yrr	8,30	8,580	3,373	0,280
Yuv	38,39	38,277	0,295	0,113
Yur	13,41	13,320	0,674	0,090
Ywp	35,50	36,105	1,704	0,605
Nvv	-7,95	-7,733	2,736	0,218
Nrr	-24,13	-24,051	0,328	0,079
Nuv	-21,89	-21,843	0,216	0,047
Nur	1,93	1,922	0,435	0,008
Nwp	-19,30	-19,367	0,347	0,067

Numerical results demonstrated that the proposed method works very well in the case of using simulated data. It has been shown that the characteristic functions for LSE can be obtained in a stable way even in noisy environments.

For model verifation, the sample variance-covariance matrix is calculated as:

$$\boldsymbol{W} = \begin{bmatrix} 0.0031 & -0.0125 & 0.0118 & -0.0071 & -0.0004 \\ -0.0125 & 0.0913 & -0.0561 & 0.1112 & -0.0061 \\ 0.0118 & -0.0561 & 0.0576 & -0.0461 & -0.0019 \\ -0.0071 & 0.1112 & -0.0461 & 0.1969 & -0.0158 \\ -0.0004 & -0.0061 & -0.0019 & -0.0158 & 0.0022 \end{bmatrix}$$

Hotelling’s T-square comes out to be:

$$\boldsymbol{T^2} = \mathbf{5.27}$$

Similarly, the F-statistic is:

$$\boldsymbol{F} = \mathbf{1.054} < 2.41 = \boldsymbol{F}_{\mathbf{10,4995,0.01}}$$

Using the statistical hypothesis test to evaluate the null hypothesis of the parameter identification model verified, the resulting test statistics is $\mathbf{1.054}$. For an 0.01 level test, the critical ***F*** value is approximately found as **2.41.** Since $\mathbf{1.054}$ is smaller than this value, so we accept the null hypothesis that the proposed model is valid.

$$\boldsymbol{T^2} = \mathbf{5.27};\ \mathbf{F} = \mathbf{1.054};\ \mathbf{df} = \mathbf{10,4995};\mathbf{p} < 0.01$$

In conclusion, our results indicate that for AUV hydrodynamic parameter identification purposes, the LSE algorithm is a feasible tool, which consistently returns quality results and is the least costly in terms of computational demand.

.

7. CONCLUSIONS

The research on underwater systems has gained immense attention during the last two decades because of applications taking place in many fields. Therefore, the significant number of UUVs has been developed for solving the wide range of scientific and applied tasks of ocean research and development in the world. . The military, as well as civilian industary can see great potential uses of AUVs in the underwater environment.

Autonomous guidance, navigation, and control techniques are key research and development areas for success of the specific AUV missions. Moreover, further work is needed for in precision navigation, sensor development and integration, and improving the realiability and robustness of long term and complex mission completion.

This thesis is primarily concerned with implementing dynamic modeling of an AUV for different swimming conditions and then is to accomplish integration of navigational sensors to dynamic modeling of AUV based on sensor error models and Kalman filtering technique. This thesis has also given an insight and theoretical background about AUV kinematics, hydrodynamics and hydrostatic, as well as INS, and recent Kalman Filtering techniques. In addition, it has reported the current research interests on these subjects. However, the aim of this thesis does not directly involve the modeling of AUV systems from scratch since this is a different area of research interest alltogether. Because physically based mathematical modeling of AUV is an interdisciplinary study of kinematics, hydrostatics, and hydrodynamics and to achieve an accurate hydrodynamic model for AUV is extremely difficult at best. However, an INS framework is implemented in MATLAB Simulink environment since this INS module is used as a main navigational tool applied to AUV dynamic model.

Second, Based on dynamic nonlinear model, we develop three different types of low-cost Integrated Navigation System based on error models of INS and its aiding devices such as DVL, compass, and a pressure depth sensor. An INS error model and the corresponding measurement models of those aiding sources will be derived for the Kalman Filter (KF). The simulation results confirmed that low-cost IMU sensors produce a notable amount of noisy measurements but our Integrated Navigation System models for AUV based on KF can effectively mitigate those drawbacks. The simulation also shows that the method is satisfying and is preferable to the linear error models with linear KF.

It is found that the errors in the aided INS position, velocity and attitude estimates are significantly lower than that of the traditional INS during time. The aided INS also performs equally well or better than the traditional INS in cases with regular position updates.

This thesis also focused on the use of parameter identification methods to predict the hydrodynamic derivatives of the AUV based on the dynamic nonlinear modeling. LSE is used to tackle the problem of parameter identification of an AUV. This classical approach seems to have a better performance in cases where a specific parameter will be identified and the LSE results obtained are satisfactory. Therefore, numerical results demonstrate that the proposed method works very well, in both cases of using simulated data. It has been shown that the characteristic functions for LSE can be obtained in a stable way even in noisy environments.

Numerical simulations are made to show the parameter identifications of the AUV. The hydrodynamic coefficients associated with horizontal and vertical motions are estimated by simulating the combined yaw and sway motion of the AUV. The simulation results of this thesis indicate that for AUV hydrodynamic parameter identification purposes, the LSE algorithm remains a feasible tool, which constantly returns quality results.

In this study, *Hotelling's* T^2 distribution is used for model verification because it arises as the distribution of a set of statistics which are natural generalizations of the statistics. Test result indicates that the chosen model for parameter identification is verified.

Future work will concern on the identification of whole or faulty hydrodynamic parameters of the AUV, which involves a 6-DOF dynamics. Moreover, other approaches such as Extended KF, unscented KF is considered to be applied and compared alternatively.

REFERENCES

[1] **Acharya, T., Ray, A. K.** (2005). *Image Processing: Principles and Applications.* Hoboken. NJ : John Wiley & Sons Inc.

[2] **Antonelli, G., Fossen, T. I. and Yoerger, D.R.** (2007). *Underwater Robotics*. 989-996, USA.

[3] **Bekir, E.** (2007). *Introduction to Modern Navigation Systems.* Hackensack, NJ : World Scientific Publishing Co.Pte.Ltd.

[4] **Chatfield, A.B.** (1997). Fundamentals of High Accuracy Inertial Navigation. Reston, Virginia : AIAA.

[5] **Chowdhary, G., Jategaonkar, R.** (2010). Aerodynamic parameter estimation from flight data applying extended and unscented Kalman filter. *Aerospace Science and Technology,* 14(2), 106–117. <http://dx.doi.org/ 10.1016/j.ast.2009.10.003>.

[6] **Eun-Hwan Shin**. (2001). Accuracy Improvement of Low Cost INS/GPS for Land Applications (Master's Thesis). Available from <http://www.ucalgary.ca/engo_webdocs/NES/01.20156.EHShin.pdf>.

[7] **Faugstadmo, J.E.** (2007). Acoustic Positioning & INS. Kongsberg Maritime AS, Norway.

[8] **Fauske, K.M., Gustafsson, F., Hegrenæs, Ø. (**2007). *Estimation of AUV dynamics for Sensor Fusion.* Information Fusion, 2007 10th International Conference.

[9] **Fossen, I.T.** (1994). *Guidance and Control of Ocean Vehicles.* Chichester, John & Wiley Sons Ltd.

[10] **Frank, P. M., & Ding, X. (**1997). Survey of robust residual generation and evaluation methods in observer-based fault detection systems. *Journal of Process Control* 7(6), 403–424.

[11] **Gadzhiev, M. Ch. (**1995). Current Problems in Metrology and Measurement Techniques, Sequential Method for Verifying Adequacy of Mathematical Models for Multidimensional Dynamical Systems with Biased Measurement. *Journal of Measurement Techniques,* Vol. 38 No.10.

[12] **Gadzhiev, Ch. M.** (1996). *The Information Provision of Offshore Platform Supervision and Control*. Baku.

[13] **Geng, Y., Martins, R., Sousa, J.** (2010). Accuracy Analysis of DVL/IMU/Magnetometer Integrated Navigation System using Different IMUs in AUV. 8th *IEEE* International Conference on Control and Automation.

[14] **Geridönmez, F., Alemdaroğlu, N. (**2007). Control and Simulation of Motion of an Underwater Vehicle. *NATO RTO SCI-202-34*.

[15] **Gulmammadov, F.** (2009). Analysis, Modeling and Compensation of Bias Drift in MEMS Inertial Sensors. RAST 2009, *IEEE*.

[16] **Guo, Z., Hao, Y., Sun, F., Gao, W.** (2009). Design of seamless changing method for AUV integrated Navigation System. *IEEE Computer Society*, 160-165.

[17] **Haciyev, Ç.** (1999). *Radyo Navigasyon.*, İstanbul Technical University Pres, İstanbul.
[18] **Hajiyev, Ç.** (1994). Fault detection in multidimensional dynamic systems based on statistical analysis of Kalman Filter. IFAC Symposium on Fault Detection, *SAFEPROCESS'94*, C.1, p. 45-49.
[19] **Hajiyev, C., Soken, H.E. (**2009**).** Adaptive Kalman Filter with Multiple Fading Factors for UAV State Estimation. *7th IFAC Symposium* on Fault Detection.
[20] **Hajiyev, C., Soken, H.E. (**2012**).** Robust Estimation of UAV Dynamics in the Presence of Measurement Faults. Journal Of Aerospace Engineering *ASCE*.
[21] **Harris, M. M., Avera, W. E., Bibee, L. D.** (2002). Tow Vehicle Depth Verification. *OCEANS '02 MTS/IEEE*, 1119-1202.
[22] **Haykin, S.** (2001). *Kalman Filter and Neural Networks*. John Wiley & Sons, Inc.
[23] **Healey, A. J., & Good, M. R. (**1992). The NPS AUVII Autonomous Underwater Vehicle Testbed: Design and Experimental Verification. *Naval Engineers Journal*, 104, 191–202.
[24] **Healey, A. J., & Lienard, D.** (1993). Multivariable Sliding-Mode Control for Autonomous Diving and Steering of Unmanned Underwater Vehicles. *IEEE Journal of Oceanic Engineering*, Vol. 18, No. 3, 327-338.
[25] **Healey, A. J.** (1995). *Dynamics of Marine Vehicles* (MA-4823). Naval Post Graduate School, Monterey, CA.
[26] **Hegrenæs, Ø., Berglund, E., and Hallingstad, O.** (2008). Model-Aided Inertial Navigation for Underwater Vehicles. *IEEE International Conference on Robotics and Automation*.
[27] **Hemminger, D.L.** (2005). *Vertical Plane Obstacle Avoidance and Control of the REMUS AUV using Forward Look Sonar* (Master's Thesis), Naval Post Graduate School, Monterey, CA.
[28] **Hotelling, H.** (1931). The Generalization of Student's Ratio. *Annals of Mathematical Statistics* 2(3): p. 360–378.
[29] **Hwang, W. Y. (**1980). *Application of system identification to ship maneuvering* (Ph.D. Thesis). MIT, Cambridge, MA.
[30] **Inzartsev, A.V.** (2009). *Underwater Vehicles.* In-Tech Publication, Rijeka.
[31] **Jategaonkar, R. V. (**2006). *Flight Vehicle System Identification: A Time Domain Methodology*. Reston, VA.: AIAA**.**
[32] **Johnson, J.H.** (2001). *AUV Steering Parameter Identification for Improved Control Design* (Master's Thesis*)*. Naval Post Graduate School, Monterey, CA.
[33] **Kalman R. F.** (1961). New results in linear filtering and prediction theory. Trans. ASME, *Journal of Basic Engineering*, S. D, c 3, 95-108.
[34] **Kim, Kwangjin, Park, Chan G.** (2007). Feedforward Unscented Kalman Filter For INS/GPS Tightly Coupled Integration System. *Proceedings of the 2007 IFAC Conference*.
[35] **Klein, V., & Morelli, E. A. (**2006). *Aircraft System Identification Theory and Practice.* Reston, VA.: AIAA.
[36] **Kul, D.** (1995). *The Choice Criteria of Bow and Stern Planes of Submarine Related to Hydroplane Jams and Flooding* (Master's Thesis). Istanbul Technical University, İstanbul.

[37] **Lee, P.M, Jun, B.H.** (2007). Pseudo long base line navigation algorithm for underwater vehicles with inertial sensors and two acoustic range measurements. *Ocean Engineering* Vol. 34.

[38] **Lee, P.M., Jun, B.H., Kim, K., Lee, J., Aoki, T., and Hyakudome, T.** (2007). Simulation of an Inertial Acoustic Navigation System With Range Aiding for an Autonomous Underwater Vehicle. *IEEE Journal of Oceanic Engineering*, Vol. 32, No. 2.

[39] **Leonard, J., Bennett, A.** (1998). Autonomous Underwater Vehicle Navigation. *MIT Marine Robotic Laboratory Technical Memorandum,* 98-1.

[40] **Li, H., Tang, J., and Yuan, B.** (2009). The Integrated Navigation Underwater Used in SAS Motion Compensation. *IEEE*.

[41] **Marco, D. B., Martins, A., Healey, A.J. (**2005). *Surge Motion Parameter Identification for the NPS Phoenix AUV*. Naval Post Graduate School, Monterey, CA.

[42] **Mendel J. M.** (1995). *Lessons in Estimation Theory for Signal Processing, Communications And Control*. Prentice Hall PTR, Englewood Cliffs, NJ.

[43] **Mendenhall, M.R., and Perkins, S.C.** (1993). *Prediction of Vortex-Induced Fluid Mechanics of Maneuvering Submarines.* AIAA, Nielsen Engineering & Research, Inc.

[44] **Meng, L., Li, L., Veres, S.M. (**2010). Aerodynamic Parameter Estimation of an Unmanned Aerial Vehicle Based on Extended Kalman Filter and Its Higher Order Approach. *IEEE*.

[45] **Prestero T.** (2001). *Verification of a Six-Degree of Freedom Simulation Model for the REMUS Autonomous Underwater Vehicle* (Master's Thesis). MIT, Cambridge, MA.

[46] **Reet, A.R.** (2005). *Contour Tracking Control for the REMUS Autonomous Underwater Vehicle* (Master's Thesis). Naval Post Graduate School, Monterey, CA.

[47] **Report**. (2005). Surge *Motion Parameter Identification for the NPS Phoenix AUV.* Naval Postgraduate School, Monterey, CA.

[48] **Rogers, R.M.** (2003). *Applied Mathematics in Integrated Navigation Systems*. AIAA Inc. Education Series.

[49] **Schmidt, G.T.** (2007). INS/GPS Technology Trends. *NATO SET-104 Symposium*.

[50] **Sekhavat, P., Gong, Q., Ross, M.** (2007). NPSAT1 Parameter Estimation Using Unscented Kalman Filtering. *Proceedings of the 2007 American Control Conference*.

[51] **SNAME –Society of Naval Architects and Marine Engineers,** (1964). Nomenclature For Treating the Motion of a Submerged Body Through a Fluid. *Society of Naval Architects and Marine Engineers Technical and Research Bulletin*, No. 1-5.

[52] **Sotak, M., Sopata, M., Berezny, S.** (2007). Integrated Navigation System Using Sigma-Point Kalman Filter and Particle Filter. *Proceedings of the 2007 RTO SET-104 Symposium*.

[53] **Stutters, L., Liu, H., Tiltman, C., and Brown, D.J.** (2008). Navigation Technologies for Autonomous Underwater Vehicles. *IEEE* Transactions on Systems, Man, and Cybernetics —Part C: Applications and Reviews, Vol. 38, No. 4.

[54] **Thacker, B. H., Doebling, S. W., Hemez, F.M., Anderson, M.C., Pepin, J.E., Rodriguez, E.A.** (2004). *Concepts of Model Verification and Validation* (Report No. LA-14167-MS). Retrieved from U.S. Department of Energy OSTI website: <http://www.osti.gov/bridge/servlets/purl/835920-Yl8Ow3/native/835920.pdf>.

[55] **Titterton, D.H., and Weston, J.L.** (2004). Strapdown Inertial Navigation Technology. Progress in Astronautics and Aeronautics *MIT Lincoln Laboratory*, Vol. 207.

[56] **Volk, C., Lincoln, J., and Tazartes D.** (2008). *Northrop Grumman's Family of Fiber-Optic Based Inertial Navigation Systems*. USA. Date Received: January 19, 2012 Access Address: <*http://www.nsd.es.northropgrumman.com*>.

[57] **Wan, E.A., Menve, R.** (2001). The Unscented Kalman Filter for Nonlinear Estimation. *IEEE*.

[58] **Vandersteen, G., Rolain, Y., Schoukens, J., Pintelon, R. (**1996). On the Use of System Identification for Accurate Parametric Modeling of Nonlinear Systems Using Noisy Measurements. *IEEE* Transactions On Instrumentation And Measurement, Vol. 45, No. 2.

[59] **Welch, G., Bishop, G.** (2006). *An Introduction to the Kalman Filter*. TR 95-041 Department of Computer Science University of North Carolina Chapel Hill, NC.

[60] **Buoyancy, (**2012**).** *Wikipedia***.** Date Received: May 18, 2012. Access Address: <*http://en.wikipedia.org/wiki/Buoyancy*>.

[61] **Hotelling T-Square Distribution, (**2012**).** *Wikipedia***.** Date Received: July 19, 2012, Access Address: <*http://en.wikipedia.org/wiki/Hotelling's_T-squared_ distribution*>.

[62] **Sliding Mode Control, (**2012**).** *Wikipedia***.** Date Received: November 25, 2012, Access Address: <*http://en.wikipedia.org/wiki Sliding_mode _control*>.

[63] **Yalçin, L., Ilgaz, M., and Erdem, B.** (2007). Hydrodynamic Analysis of DARPA SUBOFF Model. *SubSeaTech'2007*.

[64] **Yanling, H., Jing, G., Wei, G., Liang, L.** (2008). Research on the Dynamic Error of Strapdown Inertial Navigation System. Proceedings of 2008 *IEEE* International Conference on Mechatronics and Automation, 815-818.

[65] **Yoshitomi, S., Takewaki, I.** (2009). Noise-bias compensation in physical-parameter system identification under microtremor input. *Elsevier*, Engineering Structures 31, 580-590.

[66] **Zhanxin, Z., Yanan, G., and Jiabin, C.** (2006). Unscented Kalman filter for SINS alignment. *Science Direct Journal of Systems Engineering and Electronics* Vol. 18, No. 2.

[67] **Zhao, L., Gao,W.** (2004). *The Experimental Study on GPS/INS/DVL Integration for AUV*. Harbin Engineering University, Harbin.

APPENDICES

APPENDIX A : Coordinate Systems

APPENDIX A.1 : ECEF Coordinate System

The Cartesian coordinate frame of reference used in GPS is called Earth-Centered, Earth-Fixed (ECEF). ECEF uses three-dimensional XYZ coor-dinates (in meters) to describe the location of a GPS user or satellite. The term "Earth-Centered" comes from the fact that the origin of the axis (0,0,0) is located at the mass center of gravity (determined through years of tracking satellite trajectories). The term "Earth-Fixed" implies that the axes are fixed with respect to the earth (that is, they rotate with the earth). The Z-axis pierces the North Pole, and the XY-axis defines the equatorial plane. ECEF coordinates are expressed in a reference system that is related to mapping representations.

Because the earth has a complex shape, a simple yet accurate, method to approximate the earth's shape is required. The use of a reference ellipsoid allows for the conversion of the ECEF coordinates to the more commonly used geodetic-mapping coordinates of Latitude, Longitude, and Altitude (LLA).

A reference ellipsoid can be described by a series of parameters that define its shape and which include a semi-major axis (a), a semi-minor axis (b) and its first eccentricity e) and its second eccentricity (e') as shown in Figure A.2. Depending on the formulation used, ellipsoid flattening (f) may be required.

WGS84 Parameters:

$$a = 6378137$$
$$b = a(1 - f) = 6356752.31424518$$
$$f = \frac{1}{298.257223563}$$

$$e = \sqrt{\frac{a^2 - b^2}{a^2}}$$

For global applications, the geodetic reference (datum) used for GPS is the World Geodetic System 1984 (WGS84). This ellipsoid has its origin coincident with the ECEF origin. The X-axis pierces the Greenwich meridian and the XY plane make up the equatorial plane. Altitude is described as the perpendicular distance above the ellipsoid surface (which should not to be confused with the mean sea level datum).

APPENDIX A.2 : Conversion between ECEF and Local Tangential Plane (LTP)

The conversion between the two reference coordinate systems can be performed using closed formulas (although iteration methods also exist). The conversion from LLA to ECEF (in meters) is shown in Figure A.1.

$$X = (N + h)\cos\varphi\cos\lambda$$
$$Y = (N + h)\cos\varphi\cos\lambda$$
$$Z = (\frac{b^2}{a^2} N + h)\sin\varphi$$

where

$\varphi =$ Latitude
$\lambda =$ Longitude
$h =$ height above ellipsoid(meters)
$N =$ Radius of Curvature(meters),defined as:

$$N = \frac{a}{\sqrt{1 - e^2 \sin^2 \phi}}$$

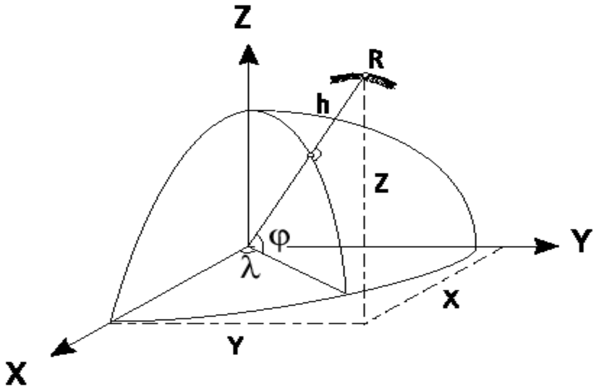

Figure A.1: ECEF and reference ellipsoid [10].

APPENDIX B : Simulation Trials of Parameter Identification

n_steps=10000;
time_step=0.001;
delta_e = 0.5*pi/180;
delta_r = -5.0*pi/180;
theta_1 = [Yvv, Yrr, Yuv, Yur, Ywp]
theta_est = [-197.5817 7.9543 38.5746 13.4362 35.6808]
theta_real = [**-196.26 8.3 38.39 13.41 35.5**]

n_steps=13000;
time_step=0.001;
delta_e = 0.5*pi/180;
delta_r = -5.0*pi/180;
theta1 = [Yvv, Yrr, Yuv, Yur, Ywp]
theta_est = [-197.1223 8.0780 38.5232 13.4306 35.7777]
theta_real = [**-196.26 8.3 38.39 13.41 35.5**]

n_steps=20000;
time_step=0.001;
delta_e = 0.5*pi/180;
delta_r = -5.0*pi/180;
theta1 = [Yvv, Yrr, Yuv, Yur, Ywp]
theta_est = [-196.8926 8.1415 38.4958 13.4260 35.8205]
theta_real = [**-196.26 8.3 38.39 13.41 35.5**]

n_steps=30000;
theta_est = [-196.4287 8.2659 38.4319 13.4134 35.8343]

n_steps=9000;
time_step=0.001;
theta2 = [Nvv, Nrr, Nuv, Nur, Nwp]
theta_est = [-4.5817 -23.4772 -21.9566 2.1652 -16.9166]
theta_real = **[-7.95 -24.13 -21.89 1.93 -19.3]**

n_steps=20000;
time_step=0.001;
theta_est = [-5.2085 -23.6097 -21.8947 2.1577 -17.0834]

n_steps=30000;
time_step=0.001;
theta_est = [-6.1476 -23.8145 -21.8453 2.1247 -17.6819]

n_steps=20000;
time_step=0.001;
delta_e = -1.5*pi/180;
delta_r = -12.0*pi/180;
theta_est = [-8.0435 -24.1785 -21.9281 1.9454 -19.4908

n_steps=20000;
time_step=0.001;
delta_e = -1.5*pi/180;
delta_r = -10.0*pi/180;
theta_est = [-7.7011 -24.0868 -21.8873 1.9214 -18.9961]
theta_real = **[-7.95 -24.13 -21.89 1.93 -19.3]**

n_steps=20000;
time_step=0.001;
delta_e = -1.5*pi/180;
delta_r = -11.0*pi/180;
theta_est = [-7.9699   -24.1509   -21.9053   1.9402   -19.3280]

<u>Measurement Bias</u>
n = 10000
theta = [-8.0048 -24.1617 -21.9051   1.9443 -19.3432]
theta1_est = [11.3830 -21.3121 -16.0633   4.9128   1.0230]
Theta_real = [-7.95   -24.13   -21.89   1.93   -19.3]
----
n = 15000
dr = -11 deg
est = [-8.0036 -24.1614 -21.9051   1.9442 -19.3426]
est1= [-11.8132 -18.9949 -11.8354 3.7643   -1.4132]

----
n = 5000
dr = -15 deg
est = [-8.3023 -24.3042 -21.9941   1.9875 -19.7561]
est1 = [-16.2704 -19.1578 -11.8048 3.0637   -3.2743]
----
n = 10000
est= [-8.3028 -24.3011 -21.9923   1.9860 -19.7559]
est1 = [-11.8029 -19.2546 -12.5286 3.1299   -2.9808]

----
n = 3000
est= [-8.2272 -24.2895 -22.0473   1.9613 -20.2272]
est1= [-16.5333 -19.1425 -11.7635   3.0577   -3.3742]

APPENDIX C : Simulation Results of Integrated Navigation System

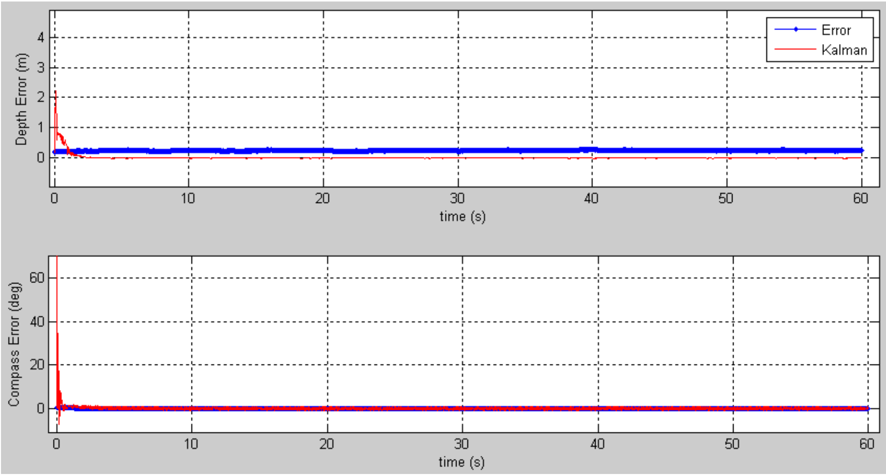

Figure C.1: Simulation results of compass and pressure depth senors.

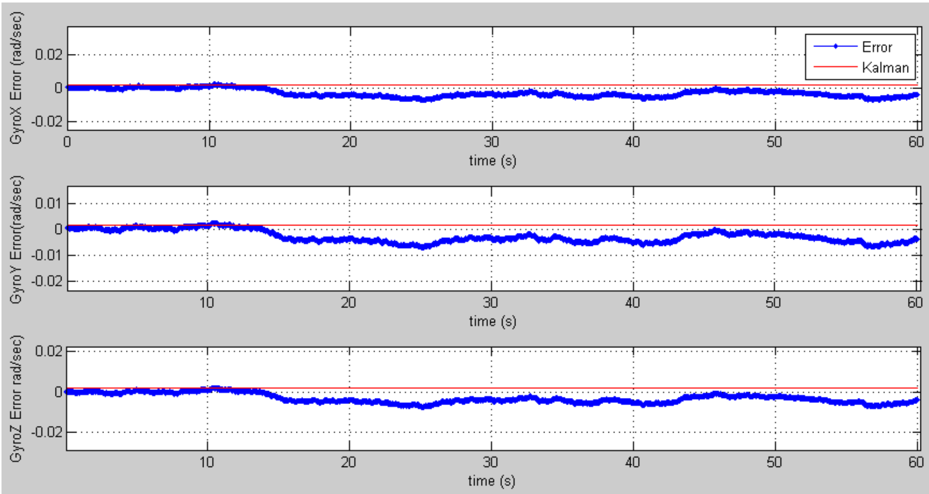

Figure C.2: Simulation results of gyros.

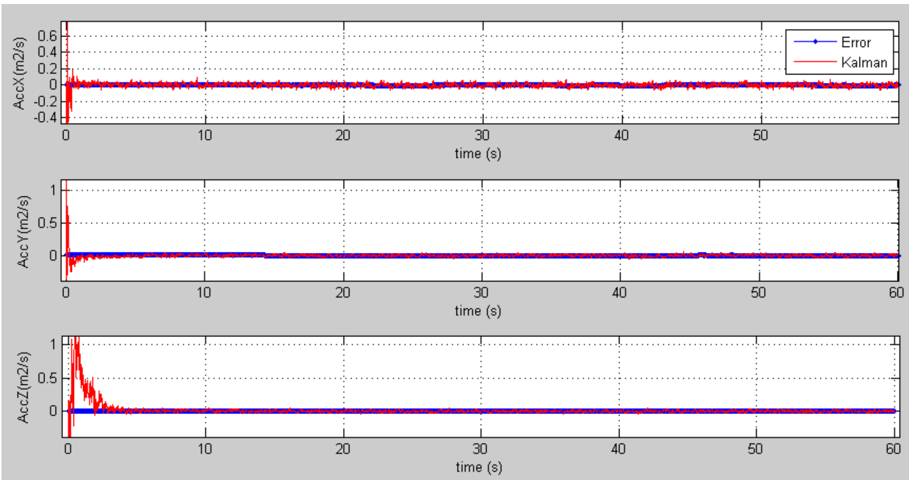

Figure C.3: Simulation results of accelometers.

APPENDIX D : MATLAB Source Code

AUVSIM.M

```
disp(sprintf('\n\n AUV Simulation begins....')) ;

getInputs;
n_steps=6000;
time_step=0.01;

% Initial Conditions
x  = [u0 v0 w0 p0 q0 r0 x0 y0 z0 phi0 theta0 psi0]';
ui=[delta_e delta_r u0];

% -----------------------------------------------------------------
% MM matrisi oluştur
%acc = [udot vdot wdot pdot qdot rdot]'
MM = [m-Xudot    0        0          0        m*zg       -m*yg;
       0      m-Yvdot     0        -m*zg        0      m*xg-Yrdot;
       0        0      m-Zwdot      m*yg   -m*xg-Zqdot     0;
       0      -m*zg       m*yg     Ixx-Kpdot     0          0;
     m*zg       0     -m*xg-Mwdot     0      Iyy-Mqdot      0;
    -m*yg   m*xg-Nvdot     0          0          0      Izz-Nrdot];

Minv=inv(MM);

xout(:,1)=x;
time(1)=time_step;
kuvvet(:,1)=[0 0 0 0 0 0];
Xdot(:,1)=[0 0 0 0 0 0 0 0 0 0 0 0 ];

%AUV Model Itereation
for i = 1:n_steps,

   % Calculate forces, accelerations
   [xdot,forces] = states(x,ui,Minv);

  % RUNGE-KUTTA
   k1_vec = xdot;
   k2_vec = states(x+(0.5.*time_step.*k1_vec),ui,Minv);
   k3_vec = states(x+(0.5.*time_step.*k2_vec),ui,Minv);
   k4_vec = states(x+(time_step.*k3_vec),ui,Minv);
   x = x + time_step/6.*(k1_vec + 2.*k2_vec + 2.*k3_vec + k4_vec);
   xout(:,i+1) = x;
   time(i+1) = (i+1)*time_step;
   kuvvet(:,i+1) = forces;
   Xdot(:,i+1) = xdot;
end

Fy = kuvvet(2,:)';
Mz = kuvvet(6,:)';
v_dot = Xdot(2,:);
p_dot = Xdot(4,:);
r_dot = Xdot(6,:);
u = xout(1,:)';
v = xout(2,:)';
```

```
w = xout(3,:)';
p = xout(4,:)';
q = xout(5,:)';
r = xout(6,:)';
thet = xout(11,:)';
% theta1 = [Yvv, Yrr, Yuv, Yur, Ywp ]
% theta2 = [Nvv, Nrr, Nuv, Nur, Nwp ]

% [theta] = AUVPI(Fy, Mz, v_dot, p_dot, r_dot, u, v, w, p, q, r, thet, W, delta_r);

%------------------Error Model başlıyor---------------------------
% erX = [Delta_x_ins, Delta_y_ins, Delta_z_ins, Delta_Vx_ins, Delta_Vy_ins, Delta_Vz_ins, ...
%        Phi_x_ins,   Phi_y_ins,   Phi_z_ins]';

 glb_var = [g R omega_ie lat Beta_xdvl Beta_ydvl Beta_zdvl Alfa_gyro Beta_acc sigma_acc ...
          sigma_gyro sigma_Vdvl sigma_depth  sigma_smag  ];
%-------------------------------------------------------------

% errOut(:,1)=[Delta_x_ins, Delta_y_ins, Delta_z_ins, Delta_Vx_ins, Delta_Vy_ins, Delta_Vz_ins,
Phi_x_ins,...
%            Phi_y_ins,   Phi_z_ins    Bias_Vx_dvl, Bias_Vy_dvl, Bias_Vz_dvl,  Bias_zd,  Bias_mag]';

errOut(:,1)=[Delta_x_ins, Delta_y_ins, Delta_z_ins, Delta_Vx_ins, Delta_Vy_ins, Delta_Vz_ins,
Phi_x_ins,...
           Phi_y_ins,   Phi_z_ins    Epsilon_x    Epsilon_y     Epsilon_z     Grad_x       Grad_y
Grad_z]';

% errOut(:,1)=[Delta_x_ins, Delta_y_ins, Delta_z_ins, Delta_Vx_ins, Delta_Vy_ins, Delta_Vz_ins,
Phi_x_ins,...
%            Phi_y_ins,   Phi_z_ins]';
erX = errOut(:,1);
% Kalman State (14) Initialization
% Xk1(:,1) = [ -2, 3, 3.5, Delta_Vx_ins*1.05, Delta_Vy_ins*1.02, Delta_Vz_ins*1.08, Phi_x_ins*1.3,
Phi_y_ins*1.05, ...
%           Phi_z_ins*0.9, Bias_Vx_dvl, Bias_Vy_dvl, Bias_Vz_dvl, Bias_zd*0.9, Bias_mag*1.2]';

% Kalman State (15) Initialization
Xk1(:,1) = [ -1, -6, 1.5, 1.5, 1.8, 1.9, Phi_x_ins*1.2, Phi_y_ins*1.2, Phi_z_ins*1.1, ...
          0.042, 0.00061, 0.00083, 0.11*pi/180, 0.12*pi/180, 0.15*pi/180]';
% Kalman State (9) Initialization
% Xk1(:,1) = [ -4, -2, -1.5, 10.5, 10.8, 11.9, -Phi_x_ins*1.0, Phi_y_ins*1.1, Phi_z_ins*1.2]';
Pk1(:,:,1) = P;
Pk11(:,1)= diag(Pk1(:,:,1));
s = 1;

for i = 1:n_steps,
%   Error Model
%   Calculate forces, accelerations
   Vx = xout(1,i);
   Vy = xout(2,i);
   Vz = xout(3,i);
   a_x = Xdot(1,i);%kuvvet(i,1);
   a_y = Xdot(2,i);%kuvvet(i,2);
   a_z = Xdot(3,i);%kuvvet(i,3);

   [Xout,A, F] = error_model(erX,Vx,Vy,Vz,a_x,a_y,a_z,glb_var,time_step);
   if i == 1
       erXdot(:,i) = A*erX;
   end
```

```
    erX = Xout;
    erXdot(:,i+1) = A*erX;

    errOut(:,i+1) = Xout;
    % Kalman Measurements;%
    z(1,i) = errOut(3,i)- sigma_mdepth*rand(1,1)-0.2*rand(1,1); % INS_Z-Z_dept
    z(2,i) = errOut(4,i)- sigma_Vmdvl*rand(1,1)-0.21*rand(1,1); % INS_Vx-DVL_Vx
    z(3,i) = errOut(5,i)- sigma_Vmdvl*rand(1,1)-0.12*rand(1,1); % INS_Vy-DVL_Vy
    z(4,i) = errOut(6,i)- sigma_Vmdvl*rand(1,1)-0.1*rand(1,1);  % INS_Vz-DVL_Vz
    z(5,i) = errOut(9,i)- sigma_mag*rand(1,1)-0.1*rand(1,1);    % INS_Phi_z-Phi_mag
%
    % Kalman Filter Algorithm
    %-----------------------------------------------

    Pk = F*Pk1(:,:,i)*F'+G*Q*G';
%    diag(Pk)
    Sk = H*Pk*H'+s*KalR; %s is adaptive parameter
    K = Pk*H'*inv(Sk);
    Pk1(:,:,i+1) =(eye(15)-K*H)*Pk;
    Pk11(:,i+1)= diag(Pk1(:,:,i+1));
    Xk = F*Xk1(:,i);
    Delta = z(:,i)-H*Xk;
    Xk1(:,i+1)=Xk + K*Delta;
end

%Measurement Bias
%-------------------------------------
% uEr = xout(1,:)'+ errOut(4,:)'/5;
% vEr = xout(2,:)'+ errOut(5,:)'/5;
% wEr = xout(3,:)'+ errOut(6,:)'/5;
% thetEr = xout(11,:)'+ errOut(8,:)'*3;
%
% pEr = xout(4,:)'+ erXdot(7,:)'*3;
% qEr = xout(5,:)'+ erXdot(8,:)'*3;
% rEr = xout(6,:)'+ erXdot(9,:)'*3;
%
% % theta1 = [Yvv, Yrr, Yuv, Yur, Ywp ]
% % theta2 = [Nvv, Nrr, Nuv, Nur, Nwp ]
%
% [theta1] = AUVPI(Fy, Mz, v_dot, p_dot, r_dot, uEr, vEr, wEr, pEr, qEr, rEr, thetEr, W, delta_r);
%
% %Integrated Navigation
% %-----------------------------------------------
% uIN = xout(1,:)'+ errOut(4,:)'/5-Xk1(4,:)'/5;
% vIN = xout(2,:)'+ errOut(5,:)'/5-Xk1(5,:)'/5;
% wIN = xout(3,:)'+ errOut(6,:)'/5-Xk1(6,:)'/5;
% thetIN = xout(11,:)'+ errOut(8,:)'*3-Xk1(8,:)'*3;
%
% pIN = xout(4,:)'+ erXdot(7,:)'*3;
% qIN = xout(5,:)'+ erXdot(8,:)'*3;
% rIN = xout(6,:)'+ erXdot(9,:)'*3;
%
% % theta1 = [Yvv, Yrr, Yuv, Yur, Ywp ]
% % theta2 = [Nvv, Nrr, Nuv, Nur, Nwp ]
%
% [theta2] = AUVPI(Fy, Mz, v_dot, p_dot, r_dot, uIN, vIN, wIN, pIN, qIN, rIN, thetIN, W, delta_r);

disp(sprintf('\n\n AUV Simulation ends ...')) ;
```

STATES.M

```matlab
function [ACCELERATIONS,FORCES] = states(x,ui,Minv)
% ---------------------------------------------------------------
% STATE VECTOR:
% x = [u v w p q r xpos ypos zpos phi theta psi]’
% INPUT VECTOR
% ui = [delta_e delta_r]’
getInputs;

% Get state variables
u = x(1); v = x(2) ; w = x(3) ; p = x(4) ; q = x(5) ;
r = x(6) ; phi = x(10); theta = x(11) ; psi = x(12) ;
delta_e = ui(1) ; delta_r = ui(2);

%trigonometrik kısaltmalar
% ---------------------------------------------------------------
c1 = cos(phi); c2 = cos(theta); c3 = cos(psi); s1 = sin(phi); s2 = sin(theta);
s3 = sin(psi); t2 = tan(theta);

%A local lever North-East-Down frame is defined as navigation frame.
%Transformation matrix from body to navigation frame
C_bn = [ c2*c3  -c1*s3+s1*s2*c3     s1*s3+c1*s2*c3;
        c2*s3   c1*c3+s1*s2*s3    -s1*c3+c1*s2*c3;
        -s2       s1*c2              c1*c2      ];

% AUV a etkiyen toplam kuvvet hesaplanır
% ---------------------------------------------------------------
X = -(W-B)*sin(theta) + Xuu*u*abs(u) + (Xwq-m)*w*q + (Xqq + m*xg)*q^2     ...
   +(Xvr+m)*v*r + (Xrr + m*xg)*r^2 - m*yg*p*q - m*zg*p*r + Xprop ;

Y = (W-B)*cos(theta)*sin(phi)+ Yuv*u*v + (Ywp+m)*w*p + (Yur-m)*u*r        ...
   - (m*zg)*q*r + (Ypq - m*xg)*p*q + Yvv*v*abs(v) + Yrr*r*abs(r)         ...
   + Yuudr*u^2*delta_r;

Z = (W-B)*cos(theta)*cos(phi) + (Zuq+m)*u*q + (Zvp-m)*v*p + (m*zg)*p^2  ...
   + Zuw*u*w + (m*zg)*q^2 + (Zrp - m*xg)*r*p +Zww*w*abs(w) + Zqq*q*abs(q) ...
   + Zuude*u^2*delta_e;

K = -(yg*W-yb*B)*cos(theta)*cos(phi) - (zg*W-zb*B)*cos(theta)*sin(phi) ...
   -(Izz-Iyy)*q*r - (m*zg)*w*p + (m*zg)*u*r +Kpp*p*abs(p) + Kprop ;

M = -(zg*W-zb*B)*sin(theta) - (xg*W-xb*B)*cos(theta)*cos(phi) +  ...
   (Mrp - (Ixx-Izz))*r*p + (m*zg)*v*r - (m*zg)*w*q + (Muq - m*xg)*u*q +   ...
   + Muw*u*w + (Mvp + m*xg)*v*p + Mqq*q*abs(q)+Mww*w*abs(w)+ Muude*u^2*delta_e;

N = (xg*W-xb*B)*cos(theta)*sin(phi) + (yg*W-yb*B)*sin(theta)+ ...
   (Npq - (Iyy-Ixx))*p*q + (Nwp-m*xg)*w*p + (Nur + m*xg)*u*r ...
   +  Nuv*u*v + Nrr*r*abs(r) +  Nvv*v*abs(v) + Nuudr*u^2*delta_r;

% x = [u v w p q r xpos ypos zpos phi theta psi]’
% Kalman Fu matrix
FORCES = [X Y Z K M N]' ;

%-------------------------------------------------% MMdot

Mvindot=Minv*FORCES;
```

```
ACCELERATIONS =[ Mvindot;        %ax,ay,az,pdot,qdot,rdot
   s3*c2*u + (c3*s2*s1-s3*c1)*v + (s3*s1+c3*c1*s2)*w;  %Xdot=u
   s3*c2*u + (c1*c3+s1*s2*s3)*v + (c1*s2*s3-c3*s1)*w;  %Ydot=v
   -s2*u + c2*s1*v + c1*c2*w;                  %Zdot=w
     p + s1*t2*q + c1*t2*r;                   %Phidot
             c1*q - s1*r;                     %Thetadot
          s1/c2*q + c1/c2*r   ];              %Psidot
```

ERRORMODEL.M

```
function [Xdot,A,Fy] = error_model(X,Vx,Vy,Vz,a_x,a_y,a_z,glb_var,time_step)

g = glb_var(1);
R = glb_var(2);
omega_ie = glb_var(3);
lat = glb_var(4);
Beta_xdvl = glb_var(5);
Beta_ydvl = glb_var(6);
Beta_zdvl = glb_var(7);

M_ins = [      Vx/R          Vx*tan(lat)/R        0         1        0   0                    0                  0              0;
    -Vx*tan(lat)/R + Vx/R           0              0         0        1        0                  0                  0              0;
    -Vy*tan(lat)/R + Vx/R           0              0         0        0        1                    0                  0              0;
   -g/R      0      0        0  2*omega_ie*sin(lat)+ Vx*tan(lat)/R   2*omega_ie*cos(lat)+Vx/R ...      0      a_z   -
a_y;
     0      -g/R     0  -2*omega_ie*sin(lat)-Vx*tan(lat)/R    0                Vy/R        ...     -a_z      0     a_x;
     0       0    2*g/R -(2*omega_ie*cos(lat)+Vx/R)        -Vy/R                0          ...     a_y     -a_x     0;
         0                      0                   0           0       0       0        0      omega_ie*sin(lat)+Vx*tan(lat)/R
omega_ie*cos(lat)+Vx/R;
     0                          0                   0            0       0       0  (omega_ie*sin(lat)+Vx*tan(lat)/R)   0
Vy/R;
     0                          0                   0            0       0       0   (omega_ie*cos(lat)+Vx/R)        Vz/R    0  ];
```

AUVPI.M

```
function [Theta] = AUVPI(Fy, Mz, v_dot, p_dot, r_dot, u, v, w, p, q, r, thet, W, delta_r)

%% MOMENT CARPANLARININ HESAPLANMASI
Nvv_mult   = v.*abs(v) ;
Nrr_mult   = r.*abs(r) ;
Nuv_mult   = u.*v;
Nur_mult   = u.*r;
Npq_mult   = p.*q;
Nwp_mult   = w.*p;
Nuud_r_mult = u.^2.*delta_r ;

Iyy = 3.45;
Ixx = 1.77e-01;
Nuudr = -13.92;
Npq = -4.86;
% zg = 1.96e-2;
yg = -0.8e-2; %m
% xg = 0;
% xb = 0;

parameter_cell = {
   'Nvv'        'Nvv_mult'
   'Nrr'       'Nrr_mult'
   'Nuv'        'Nuv_mult'
   'Nur'       'Nur_mult'
   'Nwp'        'Nwp_mult'  };
```

```
z_olcum = Mz - Nuudr*Nuud_r_mult - yg*W*sin(thet) - (Npq - (Iyy-Ixx))*Npq_mult;

%% REGRESSION ANALYSIS
X_reg = [] ;
for i = 1:length(parameter_cell)
    eval( ['X_reg = [X_reg ' parameter_cell{i,2} ']; '] )
end
NDP = size(X_reg,1);
np = size(X_reg,2);                    % Number of normal equations
cr = corrcoef(X_reg) ;                 % Regressor correlation coefficients
Theta = inv(X_reg'*X_reg)*X_reg'*z_olcum % Ordinary Least Squares Estimation
check = inv(X_reg'*X_reg)*X_reg'*X_reg;
y_est = X_reg*Theta;                             % Model equation
v_err = z_olcum - y_est;                         % Residuals
x_m = mean(X_reg);
W_cov = cov(X_reg)
invW = iwishrnd(W_cov,np);
T_sqr = NDP*(x_m' - Theta)'*invW*(x_m' - Theta)
F_stat = (NDP - np)/(np*(NDP-1))*T_sqr
```

CURRICULUM VITAE

Name Surname:	Mustafa DİNÇ
Place and Date of Birth:	Sivas - 13 February 1972
Address:	Kardelen Mah. Güvenç 1. Sitesi Nu.63 Yenimahalle/ANKARA
E-Mail:	mdinc1972@gmail.com
B.Sc.:	Electrical and Electronics Engineering, Naval Academy/İSTANABUL
M.Sc.:	Modeling and Simulation, Naval Postgraduate School/USA

Conference Proceedings

Dinç, M., Anlı, E., Hajiyev, C., Özkol, İ. (2011). Development of Integrated INS/GPS Navigation System for Unmanned Air Vehicle Based on Kalman Filtering Technique. *Recent Advances in Space Technologies*, İstanbul.

PUBLICATIONS/PRESENTATIONS ON THE THESIS

▪ **Dinç, M.** 2001. *Modeling Bluetooth Radio Technology Simulation Using Multi-Agent Based System and Genetic Algorithm Design Paradigm*. (Master's Thesis) Naval Postgraduate School, Monterey, CA.

▪ **Dinç, M.,** Hajiyev, C. (2010). Development of Autonomous Underwater Vehicle Navigation System Based on Kalman Filtering Technique. *International Unmanned Vehicles Workshop UVW2010*, İstanbul.

▪ **Dinç, M.,** Hajiyev, C. (2011). Development Of Autonomous Underwater Vehicle Navigation System Based on Kalman Filtering Technique. *RAST 2011*, İstanbul,

▪ **Dinç, M.,** Hajiyev, C. (2011). Development Of Autonomous Underwater Vehicle Navigation System Based on Kalman Filtering Technique. *ICINS18,* Saint Petersburg.